8-2000

Crystallization and melting studies of branched isotactic polypropylenes

Michael J. Trapp

To the Graduate Council:

I am submitting herewith a thesis written by Michael J. Trapp entitled "Crystallization and melting studies of branched isotactic polypropylenes." I have examined the final electronic copy of this thesis for form and content and recommend that it be accepted in partial fulfillment of the requirements for the degree of Master of Science, with a major in Polymer Engineering.

Paul J. Phillips, Major Professor

We have read this thesis and recommend its acceptance:

Kevin Kit, Roberto Benson

Accepted for the Council:
Carolyn R. Hodges

Vice Provost and Dean of the Graduate School

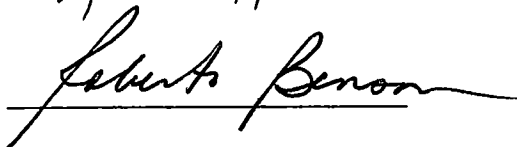(Original signatures are on file with official student records.)
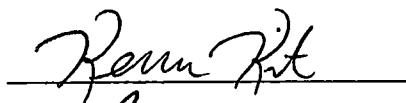
To the Graduate Council:

I am submitting herewith a thesis written by Michael J. Trapp entitled "Crystallization and Melting Studies of Branched Isotactic Polypropylenes" I have examined the final copy of this thesis for form and content and recommend that it be accepted in partial fulfillment of the requirements for the degree of Master of Science, with a major in Polymer Engineering

Paul J. Phillips, Major Professor

We have read this thesis
and recommend its acceptance·

Accepted for the Council

Associate Vice Chancellor and
Dean of the Graduate School

Crystallization and Melting Studies of
Branched Isotactic Polypropylenes

A Thesis
Presented for the
Master of Science
Degree
The University of Tennessee, Knoxville

Michael J. Trapp
August 2000

Dedication

I would first and foremost like to dedicate this thesis to the Lord Jesus Christ in order that I might glorify His name. Secondly, I wish to express my total gratitude to my wonderful wife, Kristie, for all the love and support she has given me and for helping me become a better person. To my newborn son, Solomon O'Brien, I dedicate this manuscript. I look forward to seeing him mature and I thank him for making my life complete. I would also like to include Mika and Poppy.

I would be remiss if I did not include my mother and father, siblings and their families in this dedication. Through all my life they have given me unconditional love and unwavering support I thank God for placing me into this family

Lastly, I would also like to dedicate this thesis to all loved ones, past and present, and to the memory of Bertha.

Acknowledgements

I would like to express my sincere thanks to my major professor, Dr. Paul J. Phillips I am grateful for his guidance and the confidence he has shown in my abilities. I would also like to thank the other professors on my committee, Dr. Roberto Benson and Dr Kevin Kit I have learned a great deal about polymer science from all these committee members. I wish to thank Dr J E. Spruiell for answering questions about wide-angle x-ray procedures I would also like to thank all the graduate students, faculty and staff in the Materials Science and Engineering department for their help and companionship

I wish to acknowledge Montell Polyolefins, USA and FINA Oil and Chemical Company for iPP samples used in these studies. Special thanks go to Dr. Roger Phillips for answering questions concerning the high melt strength iPP from Montell

I would also like to acknowledge the support given to me by the administration, faculty and staff of Pellissippi State Technical Community College. Special thanks go to the faculty and staff of the Natural Sciences Department, department head Dr. James Kelley, for their support and patience Without this I would not have been able to obtain this graduate degree, therefore, I am forever grateful

Abstract

Crystallization, melting and structural studies were conducted on iostactic polypropylenes treated with varying dosages of electron beam radiation and an untreated iPP. Through FTIR methods, all specimens were found to be greater than 99% isotactic. Crystallization and melting studies were performed using light depolarizing microscopy (LDM) and other melting experiments were conducted using differential scanning calorimetry (DSC). Structural studies were conducted by use of a wide-angle x-ray diffractometer (WAXD). Through isothermal crystallization studies it was found that at the highest supercoolings all specimens had approximately the same half-time of crystallization values, $t_{1/2}$, attributed to increased nucleation by increased supercooling. At higher temperatures of crystallization, T_c, it was observed that $t_{1/2}$ varied for the specimens. This was attributed to the effects of branching on primary nucleation and to the size of the spherulites. All specimens were observed to nucleate in the heterogeneous mode, meaning that nuclei density stayed constant throughout the isothermal crystallization process. Average spherulite growth geometry (Avrami) exponent, n, values were in the range of 2.2 and 2.5. These low values were a consequence of the amount of branching and stereoregularity of the polymer chains and secondary crystallization. The spherulite growth rates, k, for all the samples decreased with decreasing supercooling, resulting from the decrease in the number of nuclei forming into spherulites. Through x-ray studies the predominant crystal form was found to be of the α modification, with some β and

γ modifications observed. No structural changes at the crystal lattice level were detected. The degree of crystallization was seen to decrease as a result of increased branching in the treated specimens and attributed to thermal degradation in the untreated one. From the DSC endotherms small melting peaks in the range of 140 °C to approximately 145 °C was noticed in some of the specimens and attributed to the β modification as a consequence of nucleating agent(s) and stresses induced during sample film preparations. The equilibrium melting points taken from the highest peak and the return to baseline of the endothermic curves showed that the treated samples had lower points than the untreated one This was due to branching and degradation from the irradiation process. The melting ranges of the treated specimens were shifted to lower values as compared to the untreated specimen, as a consequence of branching and degradation The temperature ranges for the irradiated specimens were broader than the melt range of the untreated sample The α peak also showed broadening as a result of branching.

Table of Contents

ı

List of Tables

List of Figures

List of Abbreviations

iPP   Isotactic Polypropylene

FTIR   Fourier Transform Infrared Spectrometer

LDM   Light Depolarizing Microscopy

DSC   Differential Scanning Calorimetry

WAXD   Wide Angle X-Ray Diffractometer

LDPE   Low Density Polyethylene

LLDPE   Linear Low Density Polyethylene

Chapter 1

Introduction

Isotactic polypropylene commonly found in industry is generally of the linear type. It has many desirable properties, such as high melt temperatures, chemical resistivity, and high tensile modulus. These properties have made the polymer a widely used thermoplastic. However, the uses for this material are relatively narrow compared to other polymers, such as LDPE, because of its poor melt strength and low elongational viscosity (Bradley and Phillips, 1991). Therefore, processes are being devised to enhance these properties by grafting branches onto the linear backbone of the chain

One method employed is to irradiate the material with electron beams in a low oxygen atmosphere, preventing oxidative degradation. The dosages used are less than that to cause gelation. The irradiation results in initial chain scission, recombination of some chain fragments to reform the chain, and joining of other fragments to the chains to form branches. In this way the polypropylene will be able to retain its properties, while acquiring the melt strength properties of LDPE or LLDPE.

A polymer that has high melt strength often exhibits strain hardening in the molten state. Strain hardening is that property that allows a molten polymer to increase resistance to elongation when a stress is applied. These types of materials are excellent for processes such as extrusion coating, sheet extrusion and blow molding (Montell Polyolefins, 1997). Materials such as LDPE have

these properties because of the non-linearity, or natural branching of the macromolecular chains. The addition of long chain branching to polypropylene enables the material to exhibit an elongational viscosity, which tends to increase over longer distances than linear iPP (Scheve et. al., 1990). Because of the long chain branching, these high melt strength polymers are finding wider areas of usage, including in the manufacture of low-density foams for the packaging and automotive industries (Yoshii, et. al., 1996).

Irradiating iPP with low dosages of radiation is known to initiate chain scissions and branching when carried out in certain atmospheres. The structural changes produced by this method often depress physical properties such as melting temperatures and crystallinity. The effects of branching are known to lower linear growth rates of spherulites, while chain scission increases the nucleation density, leading to much faster growth rates.

Another effect attributed to low level irradiation of these polymers can be seen through viscosity studies. One such study has been performed by DeNicola and his colleagues (1992) and shows that simultaneous scission and branching produces rather complicated responses from the viscosity and, subsequently, molecular weight. These investigators irradiated isotactic polypropylenes of various weight-average molecular weights with increasing doses of electron beams, under a nitrogen environment. They found that as the dose increased, the intrinsic viscosity decreased monotonically, while the weight-average molecular weight decreased at the lower doses but began increasing at the higher ones. The degree of branching resulting from the radiation was found by the ratio of the

branched specimens' intrinsic viscosity to the intrinsic viscosity of a linear iPP of equivalent molecular weight. Through this they determined that, although the viscosity values continued to decrease with dose, the branching index also decreased. This was evidence that increased branching was taking place as with the dose. Adding branches to linear polymer chains will increase molecular weight, therefore an increase in intrinsic viscosity should be observed, resulting in higher branching index values. However, it seems that the branches actually lowered the viscosity while increasing the weight-average molecular weight and gave lower branching index values. The equation used by DeNicola gives lower values for greater degrees of branching, in that the viscosity of the branched specimen will be lower than the linear one. This effect will be discussed later in this thesis

This research studies the crystallization and melting behavior of three isotactic polypropylenes each irradiated by different doses of electron beams Structural studies are also conducted to determine any morphological affects generated by the radiation. An untreated iPP is studied as a comparison. Specimens are isothermally crystallized within the range of 115 °C to 140 °C, the range of temperatures where iPP is known to nucleate heterogeneously By running experiments within an array of temperatures the changes in the properties of each sample are tracked.

Light depolarizing microscopy is used to track the crystallization and melting behavior of each specimen. Through this method the half-times of crystallization are determined, making analyses of growth rates and mode of

spherulitic growth possible. In some specimens the process of secondary crystallization is observed. It is shown that the degrees of chain scission and branching have an effect on growth values, with the former tending to produce shorter crystallization times than the latter.

Wide-angle x-ray analyses are conducted to determine the structural integrity and the percent crystallinity of each specimen. It is observed that the predominant structure for all samples is of the alpha modification However, some beta and possibly gamma crystals are observed in a few of the specimens. Percent crystallinity studies show that as the melt flow rate increases, a consequence of increasing irradiation dose, the amorphous phase of the specimens increase

The use of a differential scanning calorimeter is employed to determine the equilibrium and return-to-baseline melting points, along with the onset of melting points. It is observed that the effects of radiation decrease these values as compared to the untreated specimen. The range of melting, as determined by the temperature difference between the onset and return-to-baseline melting points, increases as a consequence of increasing irradiation.

Very little, if any, melting, crystallization and structural studies of high molecular weight iPPs treated with electron beams have been performed. Therefore this thesis may serve as a basis for further studies A thorough understanding of these new materials is useful for industrial purposes, in that all polymer processes depend on the morphology of the material Methods of production and the selection of materials are decided by factors such as

crystallinity, melting temperature, density, and other properties   Therefore, this study is of great benefit to iPP production and manufacturing processes. Materials can be characterized, thereby determining if they are suitable for a given application

Chapter 2

Theoretical Background and Literature Review

Polypropylene can exist in three different forms, isotactic, syndiotactic and atactic. The isotactic form has all its methyl groups positioned in the same plane about each chiral carbon. The degree of isotacticity of a polymer chain is given as a percentage. Isotactic polypropylenes produced presently may have degrees of isotacticity greater than 99%. The syndiotactic form has methyl groups alternately positioned in two opposing planes, while there is no systematic pattern of group positioning within the atactic macromolecule. Figure 1 is a diagram of the three forms as described by Natta and Corradini. The samples used in this research were of the isotactic form therefore only this type will be discussed.

2.1   Structure of Isotactic Polypropylene

Isotactic polymers are macromolecules consisting of successive head-to-tail repeating units, referred to as monomers, showing the same configuration along the length, or a very long segment, of the polymer chain. Therefore an isotactic polymer will be the *cis* stereoisomer of a vinyl head-to-tail chain (Natta and Corradini, 1959). This will allow the long chain to assume a helix type structure.

In the latter part of the 1950's Natta and Corradini investigated the structure of isotactic polypropylene. They confirmed that the chain configuration
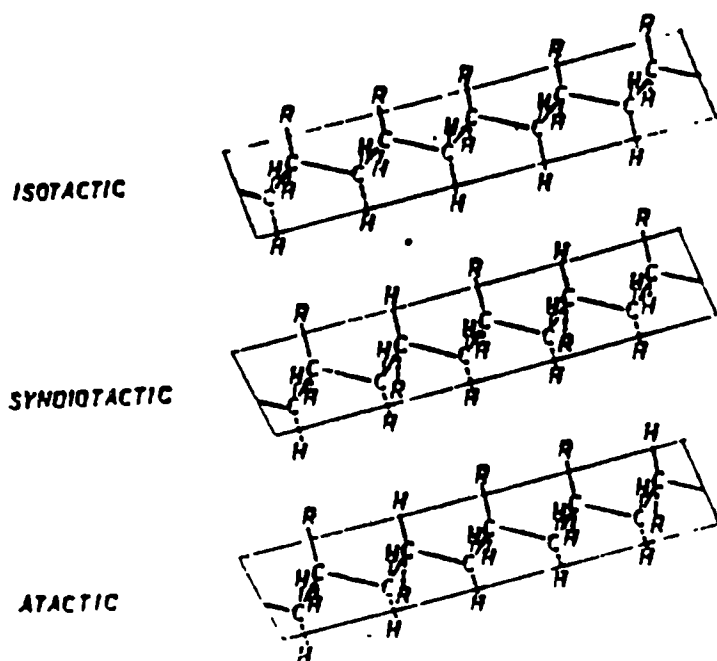
Figure 1: The three forms of isotactic polypropylene as described by Natta and Corradini (Natta G. and Corradini P., *Nuovo Cimento, Suppl.*, 15 (1960) 9). R is any substituent group.

is indeed a threefold (3_1) helix, having a periodicity of 6.50 Å Also, the helices can be either right or left-handed, with the position of the methyl groups up or down with respect to the chain axis (Mezghani and Phillips, 1996). Figure 2 is a diagram of the four chain configurations Isotactic polypropylene can be further subdivided according to differences in structure at the unit cell level These polymorphs are referred to as the alpha, beta, gamma, and smectic forms.

2.1.1 α Modification

The monoclinic α form is considered the predominant crystal structure of pure isotactic polypropylene obtained at atmospheric pressure. As early as 1959, Natta and Corradini calculated its cell parameters listed below·

$$a = 6 65 \text{ Å}$$
$$b = 20.96 \text{ Å}$$
$$c = 6.50 \text{ Å}$$
$$\alpha = \gamma = 90°$$
$$\beta = 99°20'$$

They also determined the space group to be either C2/c or Cc, depending on whether the chains within the unit cell were anticlined (C2/c) or isoclined (Cc) to each other. This classification was based on the assumption that the unit cell encompassed four separate polymer chains and that the cell was a base centered monoclinic structure. No extensive packing alterations were found to exist between these two space groups (Natta and Corradini, 1960) Turner-Jones et. al. found slight variations in the cell parameters for different unit cell densities (Turner-Jones et. al. 1964).

L dw   R dw   L up   R up
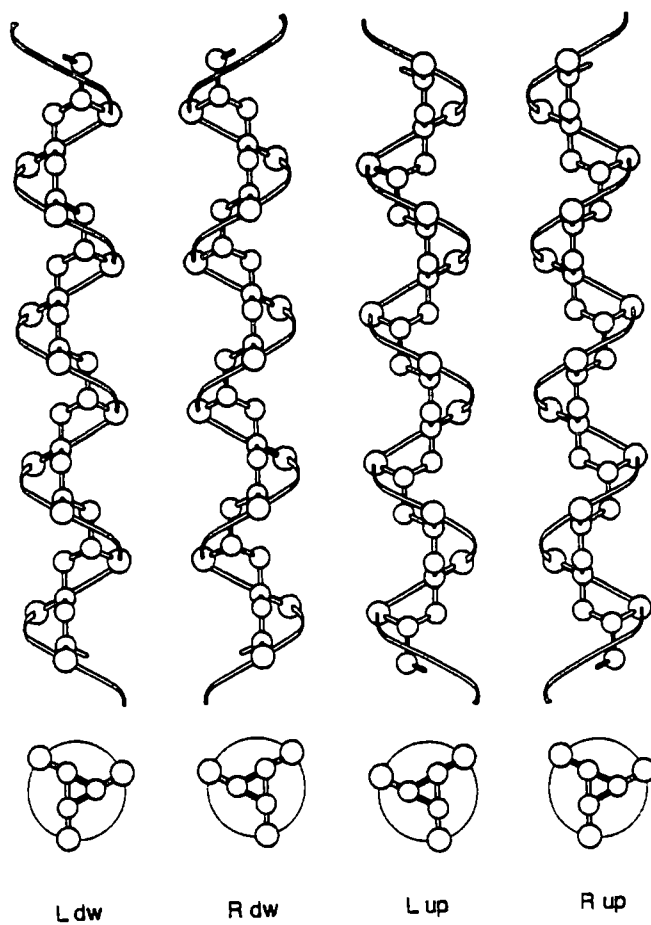
Figure 2: The four helical configurations of isotactic polypropylene (Phillips P J. and Mezghani K., in "Polymeric Materials Encyclopedia", Salamone J. C. (ed.), CRC Press, Inc., Boca Raton (1996)).

According to x-ray diffraction extinction rules a base centered cubic structure must not have reflections where the sum of $h + k$ is an odd integer. Work performed by Mencik and others did show some reflections where $h + k$ was indeed an odd sum (Mencik, 1972) Since these reflections could not be accounted for using the base centered model, he proposed a model assuming a primitive cubic space group $P2_1/c$. With no restrictions of systematic absences of reflections this structure would explain the existence of "odd" reflections.

Even though the observed intensities of the odd reflections were weaker than calculations indicated, this was explained by the unit cell having a certain disorder in distribution of chains having the arrangement of methyl groups in either the "up" or "down" position. In an ideal $P2_1/c$ crystal structure the placement of chains would be ordered as in figure 3 (Mencik, 1972) and the $h + k$ = odd reflections would be observed In Natta's model the chains were placed in the unit cell at random, resulting in a lack of the $h + k$ = odd reflections in the crystal structure Therefore the lower than expected intensities observed in Mencik's work could be explained by some disordered chains appearing in the lattice "masking" otherwise strong odd reflections.

Using x-ray diffraction methods, Hikosaka and Seto investigated iPP samples annealed at different temperatures to show that a structural model for the disorder-order transition was related to ordering of the molecular chain arrangement within the unit cell (Hikosaka and Seto, 1973) They observed that the once systematically absent $h + k$ = odd reflections increased both in occurrence and intensity as the annealing temperature was raised. The samples
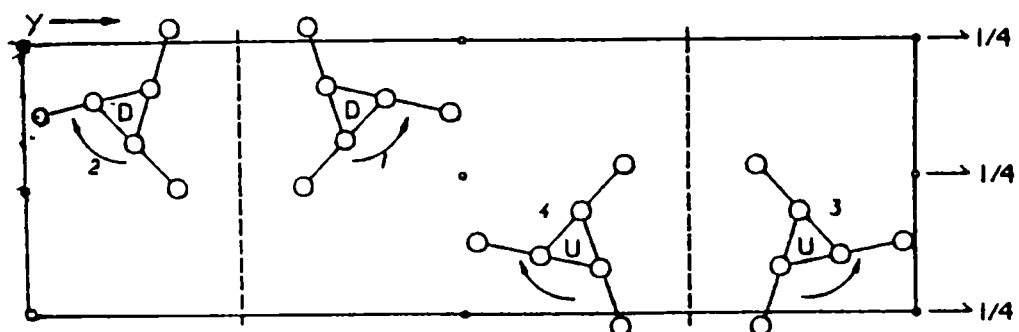
Figure 3: Diagram of the placement of chains in an ideal P2₁/c crystal (Mencık Z., *J Macromol. Scı , Phys* , B6 (1972) 101)

with the odd reflections extinct were distinguished as α1 while the ones where the reflections reached maximum intensity were called α2 All states in between were referred to as intermediate forms and assumed to be a mixture of the two Therefore Natta's disordered C2/c model was consistent with the α1 form while the α2 was described by Mencik's $P2_1/c$ ordered structure.

2 1.2 β Modification

Hexagonal iPP is the usual name given to the beta modification of isotactic polypropylene It was first identified by Padden and Keith in 1959 and was sub-classified as either Type III or IV, with the latter having a ringed structure when viewed under a polarizing microscope These spherulites were formed in the crystallization temperature range of 128-132 °C (Padden and Keith, 1959) The x-ray diffraction patterns revealed two reflections at d-spacings of 5.53 Å and 4 173 Å, and the hexagonal symmetry of the inner arcs of the pattern suggested a hexagonal type structure (Keith et al , 1959) Addink and Beintema investigated this form and indexed the reflections with d=5 35 Å and 4 127 Å as from the (100) and (101) planes, respectively They assumed a hexagonal, or trigonal, structure with the a-axis parallel to the radius of the spherulite. After closer inspection of the structure proposed by Keith and his co-workers, it was concluded that their structure was actually orthorhombic (Addink and Beintema, 1962) Geil investigated individual spherulites of the β form by electron

diffraction and microscopy. From the electron diffraction pattern and the shape of the spiral growths of the crystal, he concluded that the unit cell was hexagonal (Geil, 1962)

The x-ray diffraction studies of Turner-Jones et al on iPP samples crystallized in the β temperature range produced reflections of medium intensities at d-spacings of 3 85 Å and 3.61 Å (Turner-Jones et. al , 1964) As these two reflections did not fit the models proposed earlier, they proposed and investigated four new unit cell models, labeled A through D The parameters of these models, along with the Addink/Beintema and Keith/Padden cells, are given in table 1. Due to discrepancies between observed and calculated d-space values of models A, B and D, they concluded that cell C, with true trigonal symmetry $P3_1$, was the preferred unit cell.

The conclusion that the unit cell C model was the preferred structure was based on x-ray photographs of unoriented specimens with some α form present and that the reflection at d = 3 61 Å was not equatorial. In a later study, Turner-Jones and Cobbold prepared specimens by using dyestuff Permanent Red E2B (Leugering, 1967, Jacoby et al., 1986) as a nucleating agent The resulting hexagonal β–iPP differed from the specimens obtained from Geil, the material used in their previous study (Turner-Jones and Cobbold, 1968) By electron diffraction they showed that the reflection at d = 3 61 Å was indeed equatorial and fit cell B with nine polymer chains passing through the cell.

Table 1: Unit cell parameters for the different models of the β modification of isotactic polypropylene (Turner-Jones A, Aizlewood J. M , and Beckett D R., *Makromol Chem*, 75 (1964) 134).

Cell	Hexagonal (Å)	Chains/ Cell	Orthorhombic (Å)	Chains/ Cell
Addink/ Beintema	a = 6 36	1		
Keith/ Padden	a = 12 72	4	a = 6 36, b = 11 01	2
Turner-Jones (A)	a = 11.01	3		
Turner-Jones (B)	a = 19.08	9		
Turner-Jones (C)	a = 22 03	12	a = 19.08; b = 11 01	6
Turner-Jones (D)	a = 25 43	16	a = 12 72; b = 22 03	8

Samuels and Yee studied the beta spherulite modification type III and concluded the structure to be hexagonal with the a-axis positioned in the radial direction. The unit cell present was the aforementioned B cell, with reflection planes (210), (300), (130), and (301). It was concluded that the type III and IV spherulites could not be differentiated by d-spacing measurements alone (Samuels and Yee, 1972).

2 1 3   γ Modification

During some X-ray diffraction studies of low molecular weight fractions of iPP, Addink and Beintema discovered reflections that could not be explained by the crystal structure proposed by Natta (Addink and Beintema, 1961) Those odd reflections were the first reported observations of the gamma form of isotactic polypropylene.

Turner-Jones et. al. studied γ–iPP specimens cooled from the melt and noted that the form could be characterized by strong d-spacing reflections of 6 37 Å, 5 29 Å, 4 42 Å, 4 19 Å, and 4 05 Å lying closely to four out of five alpha form spacings (Turner-Jones et al 1964). The α form reflection at d = 4.77 Å was replaced by d = 4 42 Å in the γ phase. Assuming the chain repeat unit to be 6 49 Å and the structure of the unit cell to be triclinic, they suggested the reflections were from ($hk0$) planes parallel to the c-axis It was also deduced that the density ($\rho \cong 0.93$ g/cm^3) must be close to that of the alpha form

Awaya studied isotactic polypropylene samples that had been decomposed at 300 °C under a nitrogen environment. He found peaks on X-ray diffraction patterns at (CuKα) 2θ = 14.8° and 19.8°, corresponding to d-spacings of 6 0 Å and 4 5 Å, respectively It was concluded that these peaks were indicative of the gamma modification and resulted from the slight displacement of the molecular chains in the packing scheme of the alpha modification

Morrow and Newman used selected area electron diffraction to study fractions of iPP with increasing molecular weight (Morrow and Newman, 1968) They found the α form to be predominant in the lowest and highest molecular weight fractions while the intermediate fractions consisted of a mixture of the α/γ phases. Based on the assumption that the crystal structure was triclinic, they proposed unit cell parameters given in table 2.   Through these studies they concluded that the γ phase could be derived by a simple shear along the a-axis of the α form   These investigators also concluded that the α/γ phase mixing occurred in individual crystals of specimens of mixed forms   In their detailed investigation of the gamma modification, Lotz et al. also came to the conclusion that the γ form arose from a simple shear along the a-axis of the monoclinic α structure (Lotz et al , 1986)

Bruckner et al (Brückner and Meille, 1989; Brückner et. al , 1990, Meille et. al., 1990) studied the structure of γ-iPP using lattice models of differing unit cell parameters. These were designated cells I, II and III   Cell I was the triclinic

Table 2: Unit cell parameters of the different models of the γ modification of isotactic polypropylene (Brückner S. and Meille S. V , *Nature*, 340 (1989) 455; Phillips P. J. and Mezghani K., in "Polymeric Materials Encyclopedia", Salamone J C (ed), CRC Press, Inc., Boca Raton (1996))

Cell	Triclinic (Å)	Chains/ Cell	Orthorhombic (Å)	Chains/ Cell
I	a = 6.54 b = 21 40 c = 6 50 α = 89.0° β = 99.6° γ = 99 0°	12		
II	a = 6.55 b = 21.57 c = 6 55 α = 97 4° β = 98 8° γ = 97 4°	12		
III (Fddd; Fdd2)			a = 8.54 b = 9.93 c = 42 41	48

model reported by Morrow and Newman (1968) and cell II a refined model based on the same crystallographic structure. Cell III was a face- centered orthorhombic proposal with an assigned space group of Fddd. The particulars of the three models are given in table 2. The cell I model could not account for the reflection at $2\theta = 24.35°$ while reflections in the $2\theta = 18-24°$ were not adequately reproduced. However, their data was consistent with the proposed orthorhombic structure.

2 1.4   Smectic Modification

The smectic form of isotactic polypropylene has been described using Hosemann's model of a paracrystalline structure (Hosemann, 1951)   This model can be visualized as a deformation of an ideally crystalline unit cell by replacing the constant cell edges with vectors varying in length and direction.   Figure 4 shows a diagram of this model.

Natta and coworkers studied this metastable form, originally referred to it as "modification II", and eventually labeled it the smectic form, to distinguish it from the α phase (Natta et. al , 1959). They found the density to be 0 88 g/cm^3, which was lower than the highly crystalline and higher than amorphous forms. Infrared studies of this sample showed a remarkable resemblance to the spectrum of the alpha form. It was thus concluded long segments of the polymer chain were oriented in a threefold helix configuration.   X-ray studies revealed a broad halo with a maximum at d = 5 85 Å and a less intense and broad peak at approximately $2\theta = 21°$ They therefore described the structure as one with right and left-handed
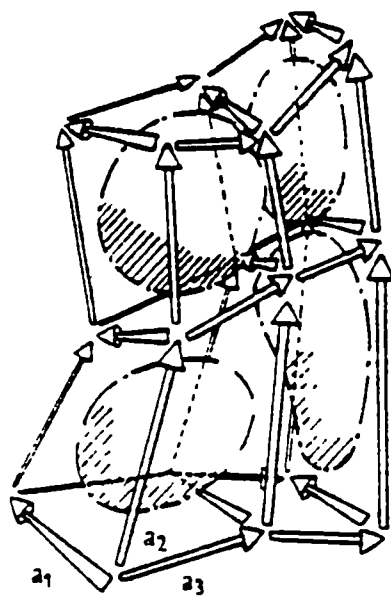
Figure 4: Hosemann's model of a paracrystalline structure (Hosemann R , *Acta Cryst* , 4 (1951) 520)

3_1 helices distributed perpendicularly to the chain axis in a disorderly fashion. These macromolecules, appearing in small bundles, could become parallel upon stretching Miller's studies of this modification were in good agreement with Natta's results (Miller, 1959). X-ray diffraction studies performed by other investigators (Boye et al., 1959, McAllister et al , 1978, Gomez et al , 1987, Corradini et al., 1989, and Vittoria et al, 1989) revealed peaks at $2\theta = 14 8^\circ$ and $21 3^\circ$, but also found less intense maxima at positions of $2\theta = 28 8^\circ$ and $42 6^\circ$.

2.2   Crystallization of Isotactic Polypropylene from the Melt

The different polymorphs of isotactic polypropylene obtained from the melt result from specific procedures used during crystallization   Each form can be obtained by isothermally crystallizing a molten specimen at a certain temperature, by quenching a sample from well above its melting point into ice water, crystallizing a degraded sample from the melt, or by using an array of nucleating agents.

2 2 1   General Crystallization Concepts

Since Keller's isolation of a single polyethylene crystal and conclusion that the macromolecules must be folded upon themselves, much research of folded-chain polymer spherulites and the method of crystallization from the bulk state have been performed. As a result a wealth of knowledge can be found in

books and review articles (Geil, 1973; Wunderlich, 1973, Lambert, 1988, Phillips, 1990; Sperling, 1992). Figure 5 is a diagram of edge-on and flat-on views of chain-folded spherulite evolution.

2 2.1 1 Kinetic Theories of Melt Crystallization and Growth Rates

When polymers crystallize from the molten state they form lamellae which in turn are organized into spherulitic structures. It has been shown that the rate of radial growth of spherulites is linear in time until they impinge upon one another Also, this growth rate goes through a maximum as the crystallization temperature is decreased. Theories by Avrami and Hoffman and Lauritzen were developed to explain the kinetics of spherulitic growth

Avrami (1939, 1940, 1941) based his theory on the Poisson equation which was derived for the probability of wave fronts crossing a certain point. These wave fronts can be imagined to be the product of the action of raindrops falling into a puddle This model can be described by the equation.

$$p_x = \frac{e^{-E} E^x}{x^!} \qquad \text{(equation 1)}$$

where p_x is the probability that a point is crossed by the x number of fronts E represents the average number of points of the system This equation can be reconciled to the polymeric system by imagining the expanding circular waves being the spherulite growth fronts and impact points made by the raindrops in the puddle as the crystallite nuclei If the point has not been crossed by the
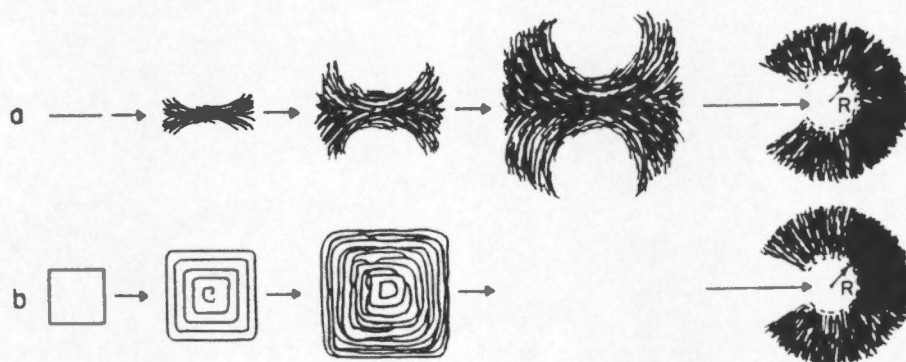
Figure 5: The edge-on (a) and flat-on (b) views of chain-folded spherulite evolution (Sperling L. H., "Introduction to Physical Polymer Science, 2nd ed.", John Wiley and Sons, Inc., New York (1992)).

crystallization fronts, then the material remains amorphous and is given by the equation.

$$p_o = e^{-E} \qquad \text{(equation 2)}$$

The variable p_o can be equated to $1 - X_t$, with X_t being the degree of crystallinity of the polymer specimen. For specimens with low degrees of crystallinity, X_t is equivalent to the exponential term E, and, in bulk crystallization, could be considered the volume of material in crystalline form, V_t. Upon evaluation of the crystallization volume variable, the familiar form of the Avrami equation results.

$$1 - X_t = e^{-kt^n} \qquad \text{(equation 3)}$$

or in the logarithmic form.

$$\ln(1 - X_t) = -kt^n \qquad \text{(equation 4)}$$

where k and n are Avrami constants and t is a certain time variable. k and n are variables indicative of the crystallization mechanism n generally decreases as crystallization proceeds.

In a paper published in 1961, Hoffman and Lauritzen (1961) presented their theory of radial growth rate for different crystallizing mechanisms in polymer systems. They proposed an equation to describe the radial growth of spherulites considering the dimensions of the crystal and their corresponding surface energies This general equation is given below

$$G = G_o \exp\left(-\Delta F/kT\right)\exp\left(-\Delta \phi_s/kT\right) \qquad \text{(equation 5)}$$

where k is Boltzmann's constant, and ΔF is the bulk free energy of fusion, equivalent to $\Delta H - T\Delta S$. $\Delta\phi_s$ is given by the equation below

$$\Delta\phi_s = 4xl\sigma + 2x^2\sigma_e - x^2l(\Delta F) \qquad \text{(equation 6)}$$

where x and l are the large and thin crystal dimensions, respectively Figure 6 presents the model for this equation σ_e and σ are the fold surface and lateral surface free energies, respectively.

2 2.1 2 Secondary Nucleation and Regime Theory

Spherulite growth rates are affected by the degree of undercooling from the melt Secondary nucleation theory states that a crystal grows by the deposition of polymer chains onto a substrate Therefore, the greater the undercooling, the greater the amount of chains being deposited The regime theory, postulated by Lauritzen and Hoffman (1973), attempts to explain crystal growth in terms of two competing processes These processes were referred to as secondary nucleation and lateral spreading of the nuclei, the rates thereof being designated i and g, respectively

Regime I will usually occur in temperature ranges where the undercooling is small. It has also been observed that low molecular weight fractions of certain polymers exhibit this pattern In this process a nucleus is deposited onto a substrate and the lateral face of the crystal is completed before another layer is initiated. Therefore g is much greater than i, and the overall growth rate is nucleation controlled. At higher undercoolings regime II occurs This regime has
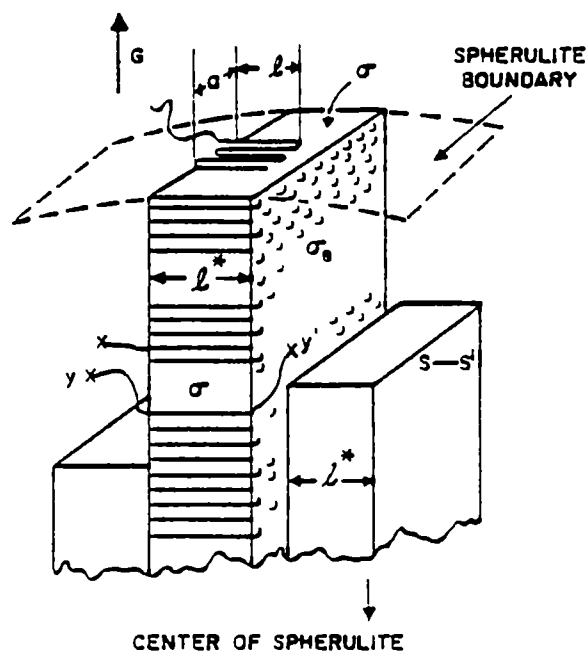
Figure 6: The model for the Launtzen-Hoffman theory of radial growth rate (Hoffman J. D. and Launtzen J. L., Jr., *J Res NBS*, 65A (1961) 297)

been observed in higher molecular weight polymer fractions In this process multiple nucleation sites are initiated on the substrate, since the rate of nucleation and the rate of lateral spreading are similar. As a consequence, nucleation can occur on partially completed crystal faces, with the growth rate being proportional to the square root of ig

Phillips (1979) proposed a third regime in which the nucleation rate exceeded the rate of lateral spreading Hoffman (1983) published this theory in 1983. This model, designated regime III, appears at even greater undercoolings than those of regime II and in high molecular weight specimens Due to the rapid nature of nucleation, the growth rate of the crystal, as in regime I, is proportional to i Figure 7 is a diagram of the three regime models.

2 2.2   Melt Crystallization of α Modification

Employing optical miscroscopy, Padden and Keith (1959) classified spherulites of melt crystallized isotactic polypropylene with respect to their birefringence The birefringence of these spherulites was determined by the change in relative amounts of tangential to radial branches inside the structure. The equation used is given below·

$$\Delta n = n_r - n_t \qquad \text{(equation 7)}$$

where n_r and n_t are the spherulitic refractive indices in the radial and tangential directions, respectively. Their studies found that α-iPP exists in three forms, designated α_I, α_{II} and α_m

Polymer crystals
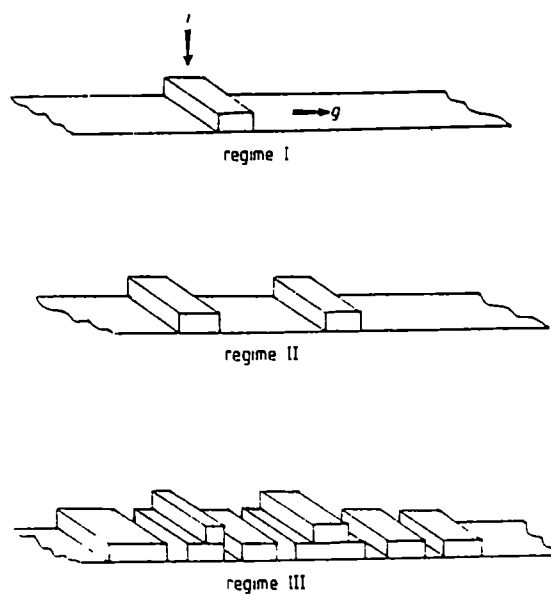
Figure 7: Diagram of the three regime models (Phillips P J , *Rep Prog Phys* , 53 (1990) 549).

The predominant form of the alpha modification was found to be α_I This structure was obtained at an isothermal crystallization temperature below 134 °C The spherulite had a positive birefringence around 0.003 and exhibited a simple Maltese cross extinction pattern. At temperatures greater than 138 °C, a negatively birefringent structure, α_{II}, was observed. The value of the birefringence was reported to be approximately –0 002 In the temperature range of 134-138 °C, and temperatures above 150 °C, the most common structure was the mixed alpha spherulite, designated α_m This spherulite consisted of intermingled areas of positive and negative birefringence and presented no distinct Maltese cross extinction pattern.

Khoury (1965) studied isotactic polypropylene crystallized from moderately concentrated solutions. He showed that the angle subtended between the daughter and parent branches in the crosshatched pattern was 80°40'. This mode of branching was responsible for the lower birefringence exhibited in the alpha modification. He also speculated that formation of new branches was by epitaxial accretion

Norton and Keller (1985) observed a reduction in the degree of crosshatching as the temperature was increased to a limiting point at 160 °C This crosshatching phenomenon was observed in all subclasses of the alpha modification They were able to show that the radial lamellae were responsible for the negative birefringence, with the tangential lamellae being positive It was also shown that the radial lathlike lamellar crystals were slightly thicker than their tangential counterparts, with thicknesses of 50 nm and 40 nm, respectively

2 2 3   Melt Crystallization of β Modification

In the same study mentioned in the last section, Padden and Keith also studied the negatively birefringent spherulites formed in the temperature range below 128 °C to about 132 °C They referred to these crystalline structures as types III and IV, distinguishable only by the characteristic extinction rings of type IV that were visible through optical microscopy Type III spherulites appeared at temperatures below 128 °C and their formation was seemingly favored by rapid cooling from the melt.   The birefringence was observed to be negative and approximately 0 007 in magnitude   Type IV spherulites were formed in the temperature range of 128-132 °C and, like type III, are highly negative in birefringence and appeared sporadically amongst spherulites of the alpha form As mentioned above, the distinguishable characteristic between the two was the appearance of ringed extinction patterns.   These investigators concluded that the rings were formed by lamellar twists along the radial growth direction.

Geil (1962, 1973) studied the beta modification spherulites he obtained by melting and slow cooling of thin films of iPP. He found that this structure was composed of approximately 150 Å thick lamellae, crystallizing in the hexagonal form It was also observed that growth of type III spherulites could be enhanced by rapid cooling from the melt He also concluded that the band spacing of the type IV spherulites was temperature dependent.   Other investigators, such as Samuels and Yee, and Norton and Keller arrived at the same conclusions as the ones above (Samuels and Yee, 1972; Norton and Keller, 1985)

2.2.4 <u>Melt Crystallization of γ Modification</u>

The seemingly most effective way to obtain the gamma modification of isotactic polypropylene is the method of crystallizing the unfractionated polymer from the melt employing high pressures (Kardos et al.,1966, Pae, 1966, Morrow, 1969). It has been observed that these specimens do not revert to the alpha form when cooled to room temperature, the reverse being true for the ones crystallized at normal atmospheric pressures (Sauer and Pae, 1968).

Morrow and Newman (1968) studied fractions with a number-average molecular weight of 1260 that was crystallized under pressure They found that the specimen crystallized predominantly in the γ form and no distinct morphological boundaries existed between the α and γ phases appearing in the same needle-like single crystal structures It was also postulated that due to the short chain lengths of the fractions, ~100 Å, the crystallization was of the extended chain fashion of high pressure, melt-crystallized polyethylene observed by Wunderlich (1973). Based on studies of decomposed iPP fractions, Kojima (1967, 1968) estimated the lamellar crystals to be 100-150 Å thick.

Padden and Keith (1973) studied thin films of iPP and suggested that branching in specimens containing both α and γ phases involve epitaxy similar to that described by Khoury. They proposed that branching was initiated by the γ form being deposited onto the alpha branches on its (010) lateral surface Lotz et al (Lotz, Graff and Wittmann, 1986) undertook a detailed study of the morphology of the gamma phase and confirmed the orientation to the α crystal was approximately 40° and the chain axes of the two structures were identical.

Figure 8 represents the various branching occurring on the alpha lamella

Through low-angle electron diffraction studies of gold decorated specimens, they

concluded the thickness of the γ lamellae to be approximately 75 Å

2.2.5   Melt Crystallization of Smectic Modification

In the paper presented by Natta (Natta et al., 1959) the procedure used to

obtain the smectic form of iPP from the melt was discussed   This method

consisted of melting films a few tenths of a millimeter thick above approximately

176 °C and rapidly quenching them into cold water.

The exact structure of the smectic form has been a subject of considerable

debate   Bodor (1964) concluded that this form was composed of microscopic

crystals of monoclinic α-iPP, while Gailey and Ralston (1964) proposed the form

to consist of the hexagonal, β form crystals.

The x-ray work of McAllister et al. (1978) revealed the smectic structure

to consist of 40% quenched phase and 60% amorphous form and concluded that

the model put forth by Bodor was not valid   By using Scherrer's line broadening

method, they calculated the crystallite size of the quenched constituent to be

approximately 30 Å   Studies by Gomez et al (1987) disproved Bodor's theory

and suggested that the crystalline phase of the smectic modification was indeed

composed of small β crystallites.   Corradini et al. (1989) concluded, through x-

ray studies, that the mesomorphic form consisted of neither the α or β form, but

rather of disordered bundles of chains
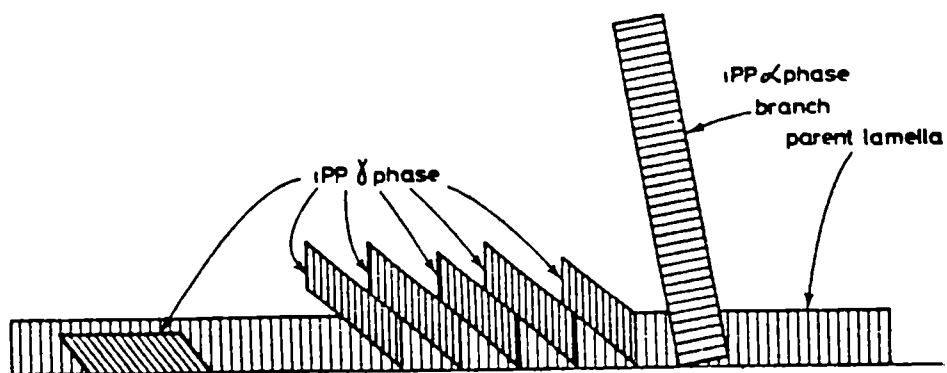
Figure 8: Representation of the α and γ branching occurring on an α parent branch (Lotz B , Graff S , and Wittmann J. C , *J Polym. Sci* , B24 (1986) 2017)

2.3   Melting Behavior of Isotactic Polypropylene

The melting of polymer crystals is a thermodynamic process in which an ordered crystal structure transforms into a molten disordered amorphous form There is no distinct point where this transformation occurs, but rather the crystal gradually degrades over a temperature range   This is due to imperfections residing in the crystal structure, chain branching, lamellar thickening, and surface energies, among others   In regards to isotactic polypropylene, the individual polymorphs will have different "melting points" primarily due to structural differences of each phase

2 3.1   General Concept of Melting

At the point where a polymer crystal is totally transformed into the disordered state, the free energy of formation is essentially zero. Therefore, the melting temperature can be calculated by the equation

$$T_m = T_m^o \left[1 - \left(\frac{2\sigma_e}{\Delta H_f l} \right) \right]$$ (equation 8)

where T_m^o is the equilibrium melting point, discussed in the next section, and l is the thickness of the lamella of the crystal   The other variables are either self-explanatory or have been discussed previously

2 3 1.1 Equilibrium Melting Point

The concept of an equilibrium melting point of a polymer was conceived on the basis that a polymer crystal transforms gradually into a disordered species

over a given range of temperatures. Therefore this point of transition can be defined for a crystal with large dimensions as that point where the crystalline polymer is in equilibrium with the molten state. A generally accepted method to obtain this point was introduced by Hoffman and Weeks (1961) The procedure is basically an extrapolation of the straight line of a plot of observed melting temperature versus crystallization temperature to the line obtained where the observed melting temperature is equal to the crystallization temperature

Many investigators have studied the melting behavior of isotactic polypropylene and values for the equilibrium melting points usually fall into two categories Krigbaum and Miller (Krigbaum and Uematsu, 1965, Miller and Seeley, 1982) determined T_m^o of bulk iPP to be in the region of 186 °C At the other extreme, Fatou and Monnasse (Fatou, 1971, Monnasse and Haudin, 1985) found T_m^o to lie close to 208 °C. Mezghani and Phillips (Mezghani et al , 1994) showed that lamellar thickening can occur during heating of specimens if sufficiently slow rates of melting are used They proved that this thickening led to high extrapolations, thus disproving the equilibrium melting point of 208 °C

2.3 2   Melting Behavior of α Modification

The melting behavior of the alpha form of isotactic polypropylene is a complicated process that arises from crystallization of the thinner tangential branches positioned roughly 80° onto the parent crystal During the heating cycle

these daughter lamellae will obviously melt before the radially aligned parent, causing the positive or mixed spherulites to become more negative as the temperature is increased.

Padden and Keith (1959) studied the melting points of this modification using a polarizing microscope and hot stage By slowly melting the specimen, they found that type α_I showed no visible change until around 157 °C Beyond this point the birefringence begins to diminish and the sign changes gradually from positive to negative. At an approximate temperature of 162 °C, the birefringence is negative and small in magnitude. Approaching still higher temperatures, the birefringence begins to disappear until, at 168 °C, it disappears altogether. Therefore, the observed melting point of α_I was taken to be around 157 °C, while the α_m and α_{II} types melted in the ranges of 157-162 °C and 162-168 °C, respectively.

2 3 3   Melting Behavior of β Modification

Using the same procedure for studying the melting behavior of the alpha modification, Padden and Keith (1959) observed the β form to melt in the 141-150 °C temperature range. The negative birefringence of the type III β spherulites begins to decrease at 141 °C until it completely disappears The negative birefringence of the type IV β spherulites was observed to begin decreasing at 145 °C and became very dark at roughly 150 °C Therefore the melting ranges of types III and IV were taken as 141-145 °C and 145-150 °C, respectively

2.3.4 Melting Behavior of γ Modification

Upon annealing at a certain temperature, the gamma modification of isotactic polypropylene can be transformed into the α phase. Padden and Keith (1973) presented evidence that this transformation occurred at temperatures around 147 °C DSC studies performed by Sauer and Pae (Sauer and Pae, 1968; Pae, 1968) revealed endothermic peaks in the range of 151-152 2 °C This was taken as the melting temperature of the γ form A second observed peak, at 159 °C, was attributed to the material converted from the gamma phase

2 3 5 Melting Behavior of the Smectic Modification

During the study of the smectic form, Natta and coworkers (Natta et. al., 1959) found that when heating these samples close to the point where the melting process begins, 140-150 °C, the structure was transformed into the alpha modification. Gomez et. al. (1987) not only obtained α-iPP from the smectic form by annealing at 160 °C, but also isolated β form crystals by using a unidirectional crystallization method

2.4   Ionizing Radiation and Isotactic Polypropylene

The many types of radiation can be categorized into three basic groups To the first group belong electromagnetic waves, including x-rays and gamma rays, that are the result of energy emitted from changes within the atomic nucleus and electron shell. The second group is composed of streams of neutral particles such as fast and slow neutrons. Due to the lack of electrical charge of these

particles, their interaction with the electrons is extremely small and the ionizing effect is negligible (Friedlander et. al., 1981). Streams of negatively and positively charged particles comprise the third group. Electrons, protons, α-particles, etc., belong in this category.

The effect of radiation on a macromolecule is generally not determined by the type of radiation used but by the chemical structure of the irradiated molecule and the quantity of energy it absorbs. Only at high doses and long exposure times does the type of radiation become a factor (Nikitina et. al., 1963) Because the specimens that are the subject of this research were treated with electron beams and, since the largest amount of research on irradiation of isotactic polypropylene employs the use of gamma rays, only these two types will be discussed

2.4 1   Gamma Rays

Gamma rays are electromagnetic waves similar in nature to visible and ultraviolet light, but with much shorter wavelengths. This type of radiation is emitted from a number of isotopes, the most common being ^{60}Co The intensity of radiation produced by this element can be reduced to $\frac{1}{10}$ its initial value by passing through 43 2 cm of water or 4 1 cm of lead Other important gamma emitting isotopes are radium and ^{137}Cs (Chapiro, 1962, Nikitina et al., 1963)

2.4 2 <u>Electron Beams</u>

As the name suggests, electron beams are comprised of high-energy electrons produced by an electron accelerator The impact of the electron beam, or e-beam for short, on polymeric materials is similar to that produced by gamma rays (Calhoun et. al , 1999) A number of apparatuses have been devised to produce beams of energies in the range of 0 5 to 100 MeV (mega-electron volts). The penetrating power of the electrons is much smaller than that of γ-rays. As an example, a 2 MeV e-beam is completely absorbed by 1 cm of water (Chapiro, 1962).   This effect is a consequence of the electrical charge carried by the particles, making them easily absorbed by matter. The radio-chemical effect from e-beam radiation is therefore primarily observed on the irradiated material's surface.   In contrast, γ-rays have a lack of electrical charge, increasing their penetrating power.   The gamma irradiation effect is usually observed to be uniform throughout the target material (Nikitina et al., 1963)

2.5   **Energy Dissipation of Ionizing Radiation in Matter**

Both γ-rays and electrons dissipate their energies when passing through matter. This is usually caused by the particles interacting with electrons of atoms in the material.

2.5.1 Dissipation of the Energy of Gamma Rays

Gamma rays deposit their energies by three major processes The first is by the photoelectric effect, which involves electromagnetic radiation of very low quantum energy In this process all energy of the incident beam is relinquished to the electrons of the irradiated substance The second mechanism is known as the Compton effect, where only a large portion of the incident energy is given to either a bound or free electron. As a consequence of this action an energetically degraded photon emerges, traveling in a direction differing from the original photon by an angle θ A third way electromagnetic energy is dissipated by matter is by the production of electron pairs This involves the creation of a positron-negatron pair through conversion of a photon of electromagnetic radiation equal to or greater than 1 02 MeV ($=2mc^2$). All of the above processes produce fast moving electrons that are responsible for most of the chemical changes taking place within the treated material (Chapiro, 1962).

2 5 2 Dissipation of the Energy of Electron Beams

When a charged particle moves within a certain distance of a macromolecule, it will lose all or a large sum of its energy by interaction with electrons of the target material (Chapiro, 1962). This process will lead to either dissociation or ionization of the target's molecules (Friedlander et al , 1981). If the energy of the incident electron is not of the extent to cause ionization, it may

still have the energy needed to cause the target electron to be displaced to a higher energy level, leaving the molecule in an excited state (Chapiro, 1962; Charlesby, 1967).

2.6   Radiation Induced Reaction Mechanisms

The first events following the interaction of ionizing radiation with matter are considered to be either the formation of positive ions or excitation of the irradiated molecule.

$$AB \rightsquigarrow \Rightarrow AB^+ + e^- \qquad\qquad \text{(reaction 1)}$$

$$AB \rightsquigarrow \Rightarrow AB^* \qquad\qquad \text{(reaction 2)}$$

In the above scheme, AB is the molecule being bombarded with radiation. AB^+ and AB^* are the molecular ion and the excited molecule, respectively

2 6.1   Ionic Reactions

According to Chapiro (1962, 1967), equal amounts of positive and negative ions are produced by a steady stream of radiation. The recombination of these ions results in charge neutralization. Three different neutralization processes are considered.

1)   ion-electron recombination
2)   positive (+) ion, negative (-) ion interaction
3)   ion-molecule reactions.

2 6.1.1 Ion-Electron Recombination

During this process a liberated electron nears the vicinity of a positive ion. The result is the production of a highly excited molecule that will probably undergo further dissociation:

$$AB^+ + e^- \rightarrow AB^*$$
(reaction 3)

2 6 1.2 Positive-Ion, Negative-Ion Interaction

This reaction involves two oppositely charged molecular ions, either of the same or different molecule(s)   Like reaction 3, excited molecular structures result·

$$AB^+ + CD^- \rightarrow AB^* + CD^*$$
(reaction 4)
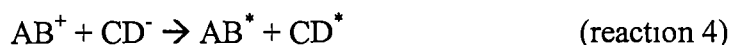
2 6.1.3 Ion-Molecule Reactions

This mechanism can be divided into two groups. hydrogen transfer and condensation reactions

a)   Hydrogen transfer reactions
$$RH^+ + RH \rightarrow RH_2^+ + R ,$$
(reaction 5)
RH represents an olefin chain and R the derived free radical

b)   Condensation reactions:
$$A^+ + CD \rightarrow AC^+ + D,$$
(reaction 6)
AC^+ represents the condensation product and D, a stable molecule.

2.6 2   Reactions of Excited Molecules

It has been observed that cross-linking, a molecular chemical change that will be discussed later, occurs in dilute aqueous polymer solutions, an environment where the chances of ionic species being in the position to bond with one another is slim. Therefore, Charlesby (1967) opined that the ionic contribution to the cross-linking reactions is minimal Chapiro (1962) has outlined three processes determining the fate of the excited molecule

2 6 2 1 Dissociation into Free Radicals

Due to the high amount of energy imparted to an excited molecule, dissociation of the structure is the predominant reaction, believed to be the most important production path of the reactive free radical species (Chapiro, 1962, 1967; Nikitina et al., 1963; Rånby et al., 1967).

$$AB^* \rightarrow A^{\cdot} + B \qquad\qquad \text{(reaction 7)}$$

If the excited molecule possesses an amount of energy much larger in magnitude than the dissociation energy of the broken bond(s), the products may have enough kinetic energy to escape the confines of the surrounding molecular environment, making recombination unlikely

2 6.2 2 <u>Dissociation into Other Molecular Products</u>

These type of reactions are believed to occur in molecules of a highly excited state:

$$AB^* \rightarrow C + D \qquad\qquad (\text{reaction } 8)$$

In this scheme, C and D are saturated or unsaturated molecules

2 6 2 3 <u>Reactions with Different Molecules</u>

These reactions occur between the excited molecule and another, non-excited molecular structure:

$$AB^* + CD \rightarrow \text{various products} \qquad (\text{reaction } 9)$$
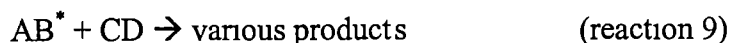
This process could transfer enough energy from the originally excited molecule to "excite" another species

2.7 **Reactions of Free Radicals**

The reactions of free radicals are responsible for most of the chemical changes in irradiated polymeric systems   Three basic free radical reactions are the exchange (transfer), addition and destruction reactions (Chapiro, 1962, 1967, Nikitina et al , 1963).

1) Exchange reactions
$$R_1 + XR_2 \rightarrow R_1X + R_2 , \qquad (\text{reaction } 10)$$
where X is H^+, Cl^-, Br^-, Na^+, etc
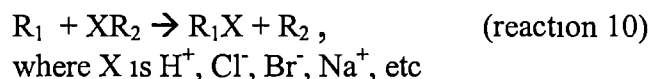
2) Addition to an unsaturated molecule (propagation step).
$$R_2 + H_2C= CH_2 \rightarrow R_2CH_2CH_2\text{-} \qquad (\text{reaction } 11)$$
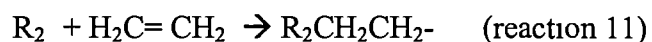
3) Reactions destroying the free radical (termination step). This can only happen by reaction with another radical

a) Combination·

$R_1^{\cdot} + R_2 \rightarrow R_1R_2$ (reaction 12)

A chemical bond is formed by both radicals sharing one another's unshared electron

b) Disproportionation.   (reaction 13)

$R_1 + R_2CH_2CH_2 \rightarrow R_1H + R_2CH=CH_2$
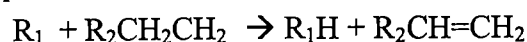
This leaves a double bond and usually proceeds at higher temperatures due to higher activation energies involved in forming the bond

2.7.1   Free Radical Reactions Involving Isotactic Polypropylene

The free radical reactions involving isotactic polypropylene essentially follow the same scheme as for other macromolecules. The cycle of radical reactions encompasses three stages initiation, propagation and termination, as alluded to above The initiation step may take place at random sites on the iPP chain and leads to the propagation step, where abstraction of a neighboring hydrogen atom transfers the radical produced in the first step to another chain or to a position further down the same chain (Tidjani and Watanabe, 1996). Rånby and Carstensen (1967) used electron spin resonance (ESR) spectroscopy to identify six radical structures formed by ionizing radiation on the iPP structure. These are shown in figure 9

$$-CH_2-\overset{\bullet}{C}H-CH_2-$$

$$-CH_2-\overset{\bullet}{C}-CH_2-$$
$$|$$
$$CH_3$$

$$-CH_2-\overset{}{C}H-CH_2-$$
$$|$$
$$CH_2$$

$$-\overset{}{C}H-\overset{\bullet}{C}H-\overset{}{C}H-$$
$$|\qquad\ \ |$$
$$CH_3\quad CH_3$$

$$-\overset{}{C}H-\overset{}{C}H-\overset{\bullet}{C}=CH-\overset{}{C}H-$$
$$|\qquad\ |\qquad\ \ |$$
$$CH_3\quad CH_3\quad CH_3$$

$$-CH_2-\overset{\bullet}{C}H-CH_3$$
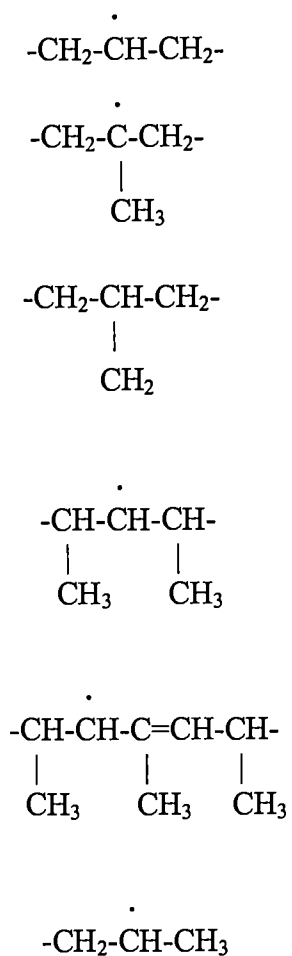
Figure 9: Six possible radical structures formed by ionizing radiation on isotactic polypropylene. These were identified by the ESR method (Rånby B and Carstensen P., in "Irradiation of Polymers", Gould R F (ed), ACS Publications, Washington, D C (1967))

The radical reactions will proceed in two different ways depending on the environment in which the polymer is irradiated If the polymer is irradiated in vacuum, reactions will involve species produced from the macromolecule itself. On the other hand, if the material rests in a gaseous environment, such as air, or in a slurry containing other reactants, reactions will occur with the other species. The reaction schemes of iPP irradiated in vacuum and in oxygen will be used as examples.

2 7 1 1 <u>Reaction Scheme of iPP Irradiated in Vacuum</u>

Sarcinelli and his colleagues (Sarcinelli et al , 1996) studied the effects of gamma irradiation on iPP in vacuum and concluded that not only degradation but also chain-branching and cross-linking occurred They hypothesized that the rate of radical generation was proportional to the dose rate (I) and that free radicals stemmed from C-H bond cleavage The free radicals formed through main-chain scission generally underwent recombination due to low mobility of the chain residing in the solid state, while the ones formed by side group scission diffused to radical partners The reactions they considered dominant are as follows·

1)   Initiation.
$$R\text{-}H \rightarrow R + H,$$ (reaction 14)
where R is the iPP chain

2) Propagation:

$$
\begin{array}{cccc}
CH_3 & CH_3 & CH_3 & CH_3 \\
| & | & | & | \\
\end{array}
$$

$-CH_2-C-CH_2-CH- \rightarrow -CH_2-C=CH_2 + CH-$ (reaction 15)
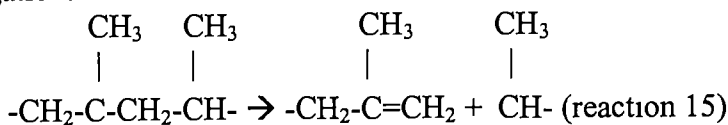
This is referred to as β-scission, resulting in chain length reduction and lower molecular weight.

$R + CH_2=CH_2 \rightarrow R-CH_2-CH_2-$ (reaction 16)
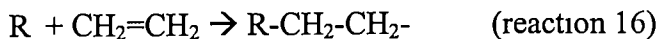
This is the addition of free radicals to double bonds and results in chain branching, increasing the molecular weight

3) Termination

$R + R \rightarrow R-R$ (reaction 17)

This results in a cross-linked molecule, also increasing the molecular weight.

$R + R \rightarrow R + R^=$ (reaction 18)

This is an electron transfer reaction, resulting with one ion having a valence number of -2 and one neutral molecule.

2 7 1.2 <u>Reaction Scheme of iPP Irradiated in the Presence of Oxygen</u>

There exists many studies on iPP irradiated in an environment with high concentrations of oxygen (Williams et al , 1977, Williams et al , 1982, Williams and Dunn, 1983; Klee et al , 1985, Nishimoto et. al , 1991, Lacoste et al , 1993; Yoshii et. al , 1995, Tidjani and Watanabe, 1996). It was found that isotactic polypropylene readily degrades, causing the polymer to discolor and become brittle These effects can be minimized with the use of antioxidants to stabilize the product during and after irradiation (Horng and Klemchuk, 1984) The

introduction of mobilizing additives into the material will increase the main chain mobility, leading to reactions among the radicals and lessening the extent of environmental reactions (Williams and Dunn, 1983)

The mechanism of iPP degradation in air is auto-oxidative in nature, meaning every free radical formed will react with oxygen unless prevented (Williams et. al., 1977) The predominant species resulting from degradation are hydroperoxides, and, to a lesser extent, chains containing carbonyl groups (Nishimoto et al., 1991; Lacoste et. al , 1993, Tidjani and Watanabe, 1996) The auto-oxidative reaction scheme is given below (Williams et al , 1982, Williams and Dunn, 1983):

1) Initiation:
$$R \rightsquigarrow 2R^{\cdot}$$ (reaction 19)

2) Propagation.
$$R + O_2 \rightarrow RO_2$$ (reaction 20)

3) Auto-oxidative process:
$$RO_2 + RH \rightarrow ROOH + R$$ (reaction 21)
$$RO_2 + R \rightarrow ROOR$$ (reaction 22)
$$RO_2 + RO_2 \rightarrow ROOR + O_2$$ (reaction 23)

4) Termination·
$$R + R \rightarrow R\text{-}R$$ (reaction 24)

2.8 Effects of Ionizing Radiation on Vinyl Polymers

Many polymers, as in the case of isotactic polypropylene, will simultaneously undergo cross-linking and chain scission upon irradiation (Kondo and Dole, 1966) A major determinant of a polymer chain's fate is the structure of

the monomer comprising the macromolecule   Although much disagreement on theories postulated to explain the predominance of either cross-linking or scission on a specific polymer exists, an empirical rule can be applied, placing the emphasis on the structure of the species. This rule states that if a vinyl polymer has at least one hydrogen atom on its main chain, it will predominantly cross-link and be classified structurally as a group I polymer·

$$-(CH_2-C)_n- \quad \begin{array}{c} H \\ | \\ \\ | \\ R \end{array}$$
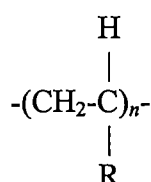
Figure 10: General structure of a cross-linking polymer

If the polymer has a structure similar to figure 11, it will generally degrade by chain scission

$$-(CH_2-C-)_n- \quad \begin{array}{c} R_1 \\ | \\ \\ | \\ R_2 \end{array}$$
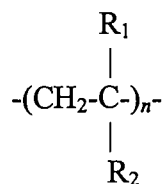
Figure 11: General structure of a polymer that will undergo chain scission.

R, R_1 and R_2, of course, stand for any substituent other than hydrogen (Chapiro, 1962; Wilson, 1974)

2 8 1   Radiation Induced Cross-linking

Although thermal and chemical techniques have been used extensively to produce cross-links between individual polymer chains, another method being

utilized is irradiation by ionizing radiation Bonds between polymer molecules consist of weak van der Waals forces, permanent dipoles or hydrogen bonds. Cross-linking of the macromolecules involves replacing these bonds with stronger covalent ones, creating a three dimensional structure with chains rigidly fixed in positions relative to one another. This is commonly referred to as the gel phase and will essentially become one large molecule when, on average, one cross-link per every polymer chain has been produced. Up to a limiting value, increasing the radiation dosage will increase gel formation, thus increasing molecular weight As a result, the solubility of the polymer in its normal solvents decreases, while the melting and softening points increase considerably (Chapiro, 1962; Nikitina et al , 1963; Billmeyer, 1971, Wilson, 1974; Moore and Kline, 1984)

2.8.2 Radiation Induced Degradation

As mentioned earlier, isotactic polypropylene readily degrades when irradiated in air unless additives such as antioxidants or chain mobilizers are included into the material Figure 11 shows the basic structure of a polymer that will follow a degradation path. It is theorized that the substitution of hydrogen atoms with larger groups adds to the steric strain on the polymer chain bonds, making them weaker and more likely to cleave This is the reason polymers with increasing degrees of branching become increasingly susceptible to β scission. A decrease in the weight average molecular weight is one result of this degradation (Chapiro, 1962, Nikitina, 1963, Billmeyer, 1971, Wilson, 1974)

Tidjani and Watanabe (1996) observed that at low dose rates of γ radiation, products associated with degradation reactions appeared at higher concentrations than when iPP was irradiated with the higher dose rates used in cross-linking reactions They also observed that iPP having a lower degree of crystallinity produced a higher percentage of degradation products, confirmation that chain scission reactions take place in the amorphous part of a semi-crystalline polymer. Sarcinelli et al. (1996) found that when irradiating iPP with low doses (D) of gamma radiation in vacuum the main effect is β scission The explanation for this is found in reactions 15 and 16 above The concentration of the double bonds needed for addition reactions (reaction 16) was proved to be very low at the lower doses used. Therefore, addition reactions became negligible and scission dominated. As dose increased, so did the double bond concentration, leading to greater competition between reactions 15 and 16, with addition reactions dominating at the higher doses It was also observed that decreasing the dose rate lowered degradation

2 8 3   Radiation Induced Branching

Branching of a linear polymer chain is achieved by adding a monomer or scission fragment of another chain to an active center, i e a free radical site serving as a branch point. The addition of methyl or phenyl groups to a chain backbone is not considered branching Long-chain branching results when polymer species are added to this site, while short-chain branching involves the abstraction of an atom from the same chain The result is a structure with an

increased molecular weight and no gel fraction, still retaining solubility in its original solvents. The latter property is a consequence of neighboring chains not being rigidly attached to one another, thus producing no three dimensional structure associated with cross-linking (Seymour, 1971, Wilson, 1974, Hiemenz, 1984)

Recalling reaction 16, Sarcinelli and his co-workers postulated that there were certain levels of absorbed dose at fixed dose rates where chain branching was enhanced as a consequence of increased concentrations of double bonds (Sarcinelli et. al, 1996). Also, the decreasing of I, at fixed D, lowered degradation, increasing the molecular weight. This produced a species that was neither considered cross-linked, due to its being under the gel point threshold, nor degraded. This suggested that at radiation doses of higher levels and lower dose rates than those used in scission reactions could be utilized to produce branched isotactic polypropylene chains. The studies by DeNicola (1992), mentioned previously, showed that at the lower dose levels scission dominated, while as dose increased, so did branching. Figure 12 is the data they obtained by irradiating an iPP of weight-average molecular weight 875 x 10^3 with increasing doses of electron beams. It can be seen from the plot that at the lower doses, scission reactions dominate as evidenced by the decrease in molecular weight Chain scissions produce species with lower weight-average molecular weights As the

doses increase, so does the amount of branching, causing an increase in the molecular weight. This is seen in the molecular weight curve as it tends upward at the higher doses. The branching index continues to decrease, meaning that branching is increasing.

Chapter 3

<u>Experimental</u>

3.1   <u>Bulk Material</u>

High melt-strength isotactic polypropylene was obtained in pellet form from Montell Polyolefins, USA. The branching in these samples was achieved via electron beam irradiation technology. Each sample received different doses of radiation These samples were designated X1 (XA11654-36-1), X2 (XA11654-36-2), and X3 (XA11654-36-3). Melt flow rate (MFR) information provided by the company is given in table 3. An unirradiated isotactic polypropylene designated FINA (9170-70A) was used as a comparison to the irradiated ones and was obtained from FINA Oil and Chemical Company The MFR value for this specimen is also given in table 3 The degree of isotacticity was determined by use of a Nicolet Impact 410 Fourier Transform Infrared Spectrometer (FTIR). The absorption peaks were analyzed by applying the method devised by Luongo (1960). Samples used in this method were thin films of the bulk samples heat compressed at approximately 180 °C and five tons of force. A Wabash heating press was used for this purpose. All samples were determined to have isotacticities greater than 99 %

Table 3 MFR values for the specimens studied

Sample	MFR before treatment (dg/10 mm)	MFR after treatment (dg/10 mm)
X1	0 62	5 5
X2	0 27	2 8
X3	higher MFR feedstock than X1/X2	30-35
FINA	8.0	NA

3.2   Specimen Preparation

The samples used in this research were first converted to a powder and melt-pressed into thin films using the Wabash press mentioned above   To obtain specimens free of any processing orientations, a powder form of the material was made by placing approximately 5 grams of bulk sample into approximately 75 milliliters of boiling xylene   After all visible signs of solid polymer disappeared, usually around 30 minutes, this solution was dumped into a container of 0 °C methanol (Phillips, 1999, Spruiell, 1999)   This solution was subsequently suction filtered. The residue was scraped from the filter paper unto a glass petri dish and placed in a 100 °C oven overnight to drive off the excess xylene/methanol   The samples now in powder form were placed in the Wabash heating press and formed into thin films   The temperature and pressure used was the same as mentioned above.

3.3   Light Depolarizing Microscopy (LDM)

The isothermal crystallization studies and melting studies were performed by the light depolarizing method described by McGill (1960, 1961)   In this method a section of the thin film of the powder sample was placed on a hot stage set at 200 °C under a nitrogen atmosphere. The films were melted for 10 minutes to ensure complete melting of the crystals and removal of any stresses introduced during sample preparation   These samples were immediately transferred to another nitrogen flushed hot stage set at the desired crystallization temperature   This hot stage sat directly under a 20 X objective of a Nikon polarizing

microscope that was connected to a photomultiplier, itself connected to a x-y chart recorder. The chart recorder was used to plot the change in light intensity versus time for both the crystallization and melting studies. The hot stages were calibrated by a thermocouple connected to a digital thermometer that was itself calibrated using boiling water to measure accuracy of temperature to within ± 0.4 °C. Figure 13 is a schematic diagram of the apparatus. After crystallization was completed, these specimens were quenched by rapidly transferring them into ice water. This effectively ended any further crystallization. Specimens used in the melting studies were discarded

3.4   Wide Angle X-Ray Diffraction (WAXD)

The isothermally crystallized specimens obtained from the procedure mentioned in section 3.3 were used in the WAXD studies. A Rigaku Denki diffractometer using CuKα radiation (λ=1.542 Å) and a Ni filter was utilized for all experiments. The instrument was calibrated using the diffraction peak at $2\theta = 28.465°$ of a Si standard. The diffraction patterns were taken in both reflection and transmission modes in the $2\theta = 10°$ to $30°$ range. Operating voltage and x-ray tube current were set at 35 kV and 25 mA, respectively. Degree of crystallinity was determined using the method developed by Hermans and Weidinger (1960). Peaks obtained through the reflection mode were used to determine the crystallinity of each specimen by separation of the crystalline peaks
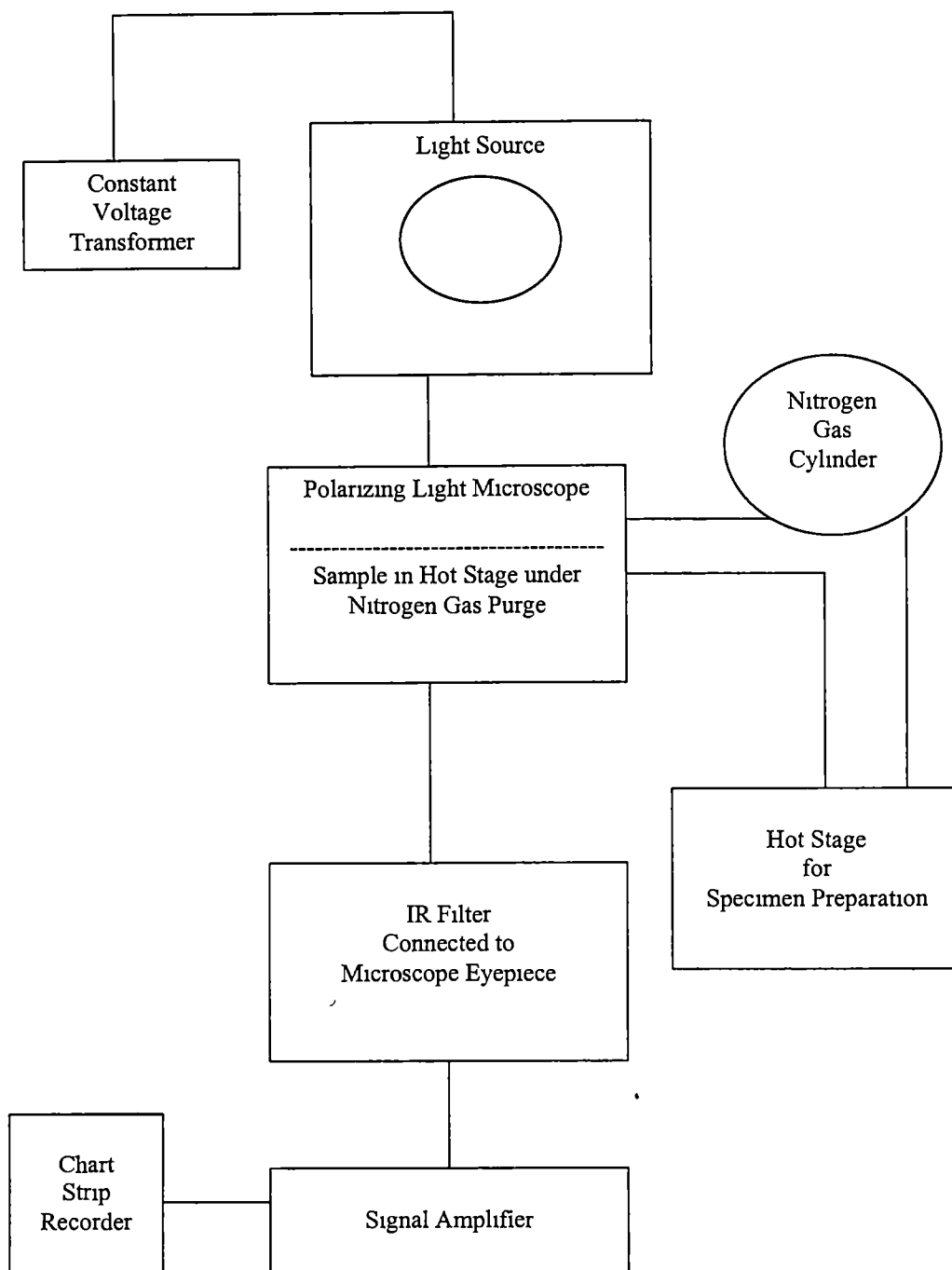
Figure 13: Schematic diagram of the apparatus used in LDM studies

from the amorphous halo and measuring the areas   The crystalline peak area was

divided by the total area to determine percent crystallinity   The transmission

mode was employed to determine if any surface orientation was present

3.5   Differential Scanning Calorimetry (DSC)

The specimens of section 3 4 were used to run melting experiments on a

Perkin-Elmer DSC-7 instrument   The instrument was calibrated using an Indium

standard, melting peak equal to 156 6 °C   Samples, ranging from 3 to 7 mg, were

accurately weighed and sealed in sample pans by "crimping" the lids tightly

These specimens were then placed under a nitrogen atmosphere and heated from

100 °C to 180 °C at a heating rate of 10 °C per minute   The initial onset of

melting was taken at that point where the heating plot began to deviate from the

baseline   The extrapolated onset of melting of the alpha modification was

obtained as per the procedure outlined in figure 14, and will be discussed later.

The return to baseline was taken as that temperature where the heating plot

returns to the baseline. The onset of melting and return to baseline temperatures

made the determination of the melting range of the complete sample and the alpha

modification possible   The apparent melting point of each specimen was taken as

the peak height of the endothermic curve and the return to baseline temperature.

Both values were used to determine the equilibrium melting point, as some

controversy exists between the usage of the two procedures.
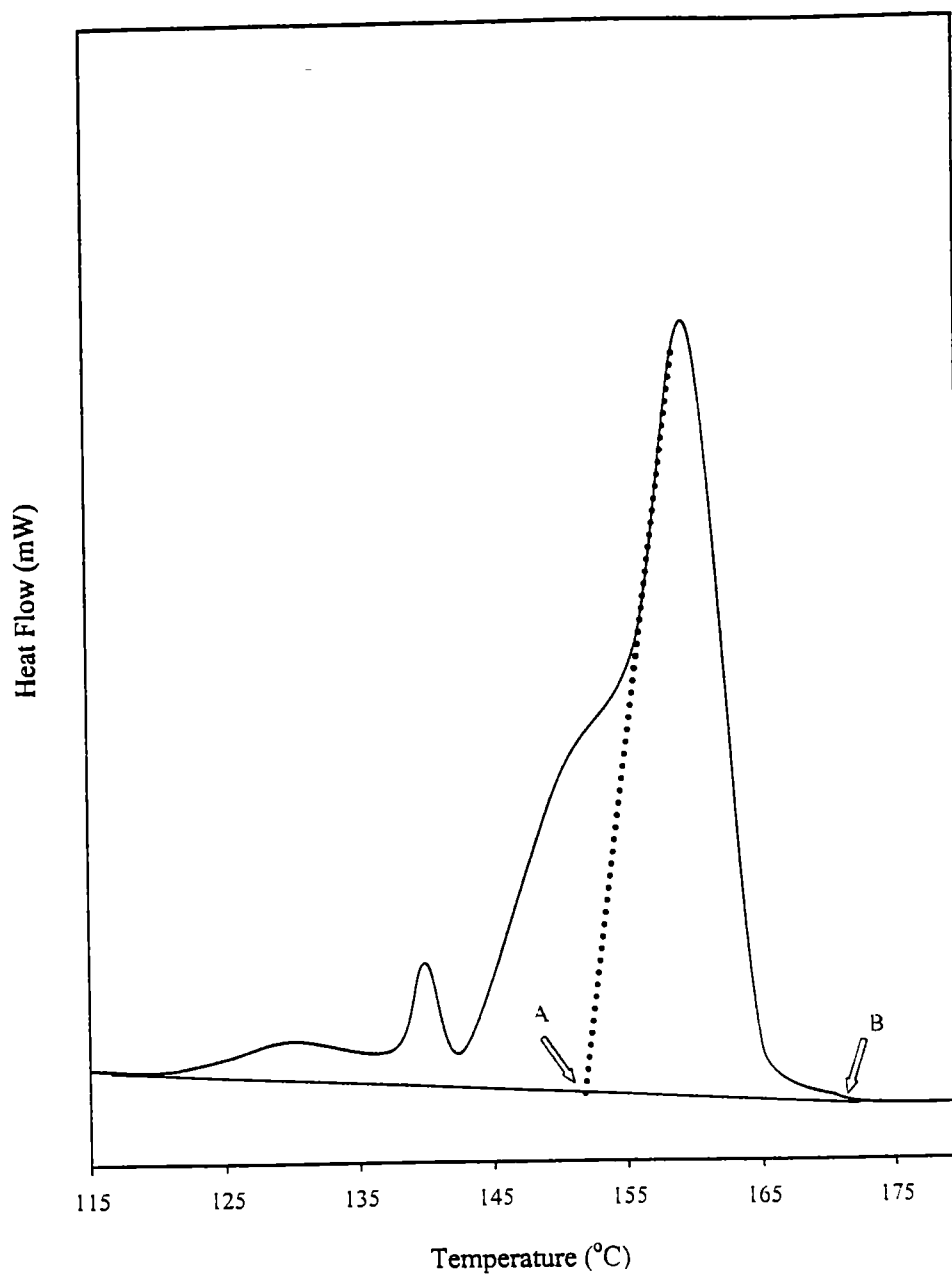
Figure 14: Procedure determining the melting range from a DSC thermogram. Point A is the extrapolated onset of melting point. Point B is the return to baseline (end of melting) point.

Chapter 4

Results

4.1 Results of Crystallization Studies Obtained from LDM

The Avrami equation (equation 4) is the basis for Magill's light depolarizing method used in the crystallization studies. This method utilizes the increase of light intensity observed as crystallization proceeds Equation 9 is used to reconcile this effect with the Avrami equation·

$$\ln\left(1 - \frac{I}{I_\infty}\right) = -kt^n \qquad \text{(equation 9)}$$

where I is the intensity of light at a point in time and I_∞ is taken as the light intensity at the observed point of complete crystallization. When the polymer is in the molten state the field of view under a light depolarizing microscope is dark. As crystallization proceeds, the field becomes increasingly brighter until a limiting value of intensity is obtained This is taken as the observed point of complete crystallization and can be detected when the linearly rising graph begins to curve, eventually reaching a plateau where no increase in the graph takes place. Figures 15 through 18 are plots of crystallization curves obtained for samples X1, X2, X3, and FINA, respectively

The ultimate goal in Avrami analyses is to attain the spherulite growth rate constant, k, and the exponent, n These two variables describe how fast the crystallization proceeds and the geometry of the growing crystal, respectively, at a predetermined temperature. To obtain values for k equation 10 was utilized.
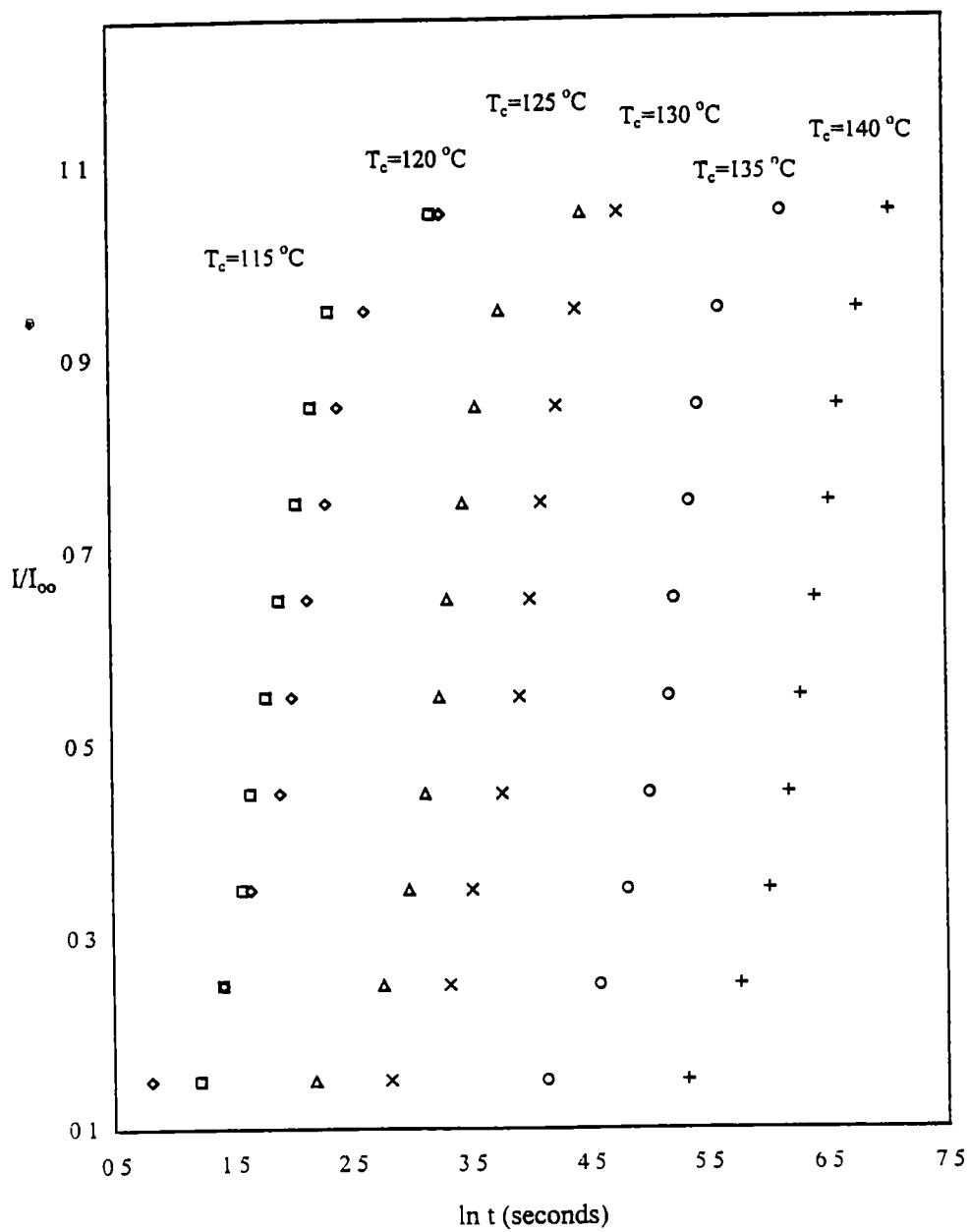
Figure 15. Crystallization curves of specimen X1 obtained by LDM.
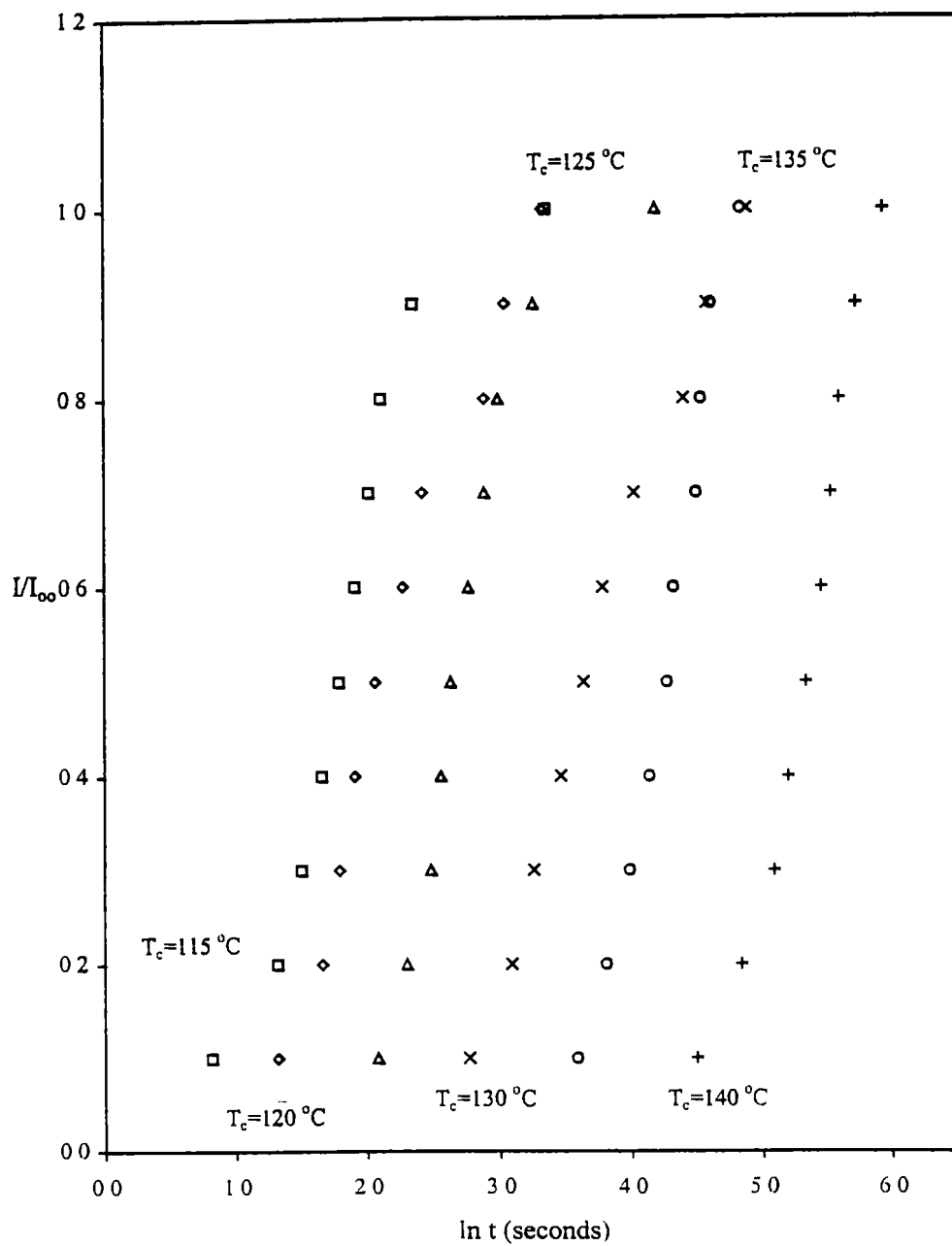
Figure 16 Crystallization curves of specimen X2 obtained by LDM

Figure 17 Crystallization curves of specimen X3 obtained by LDM
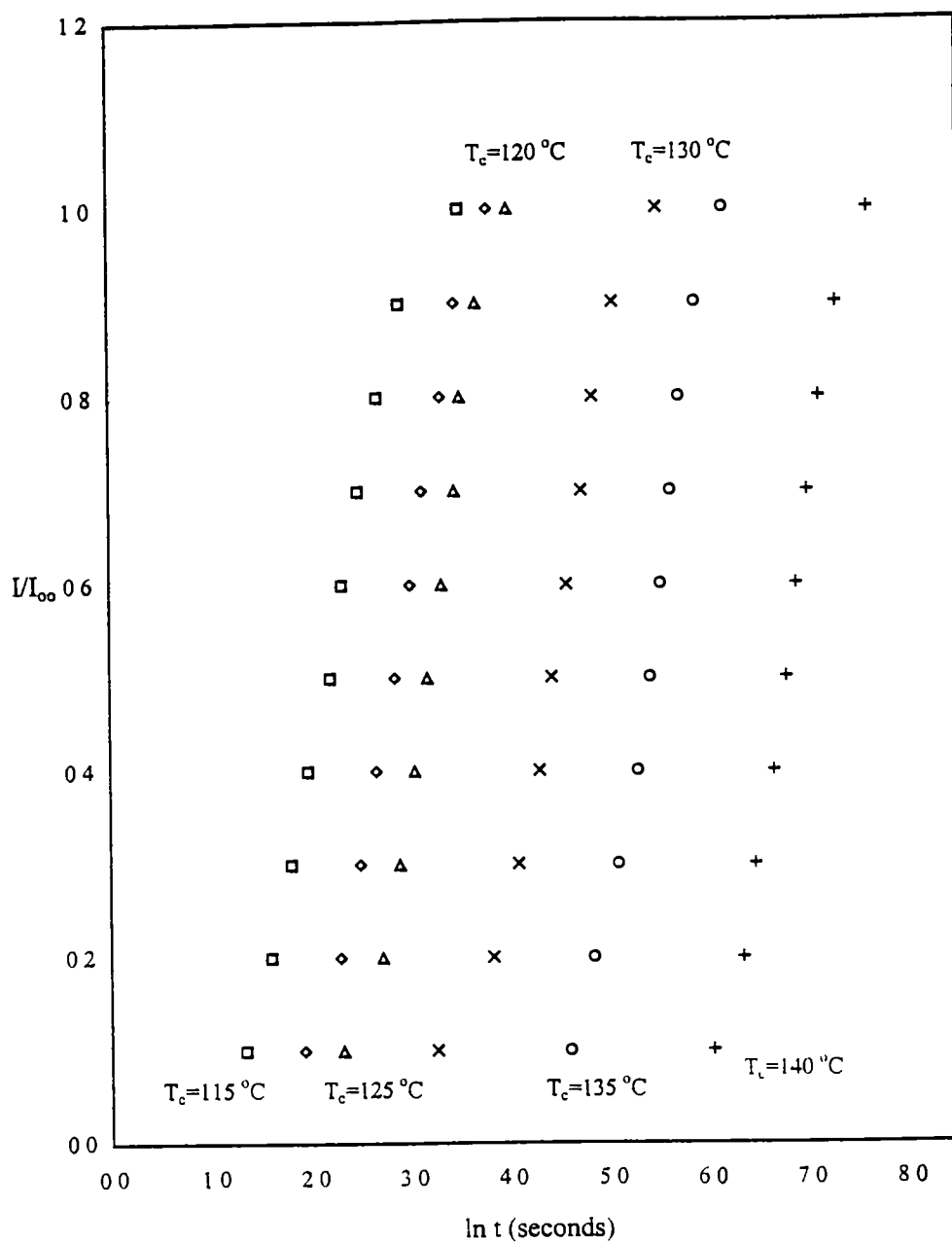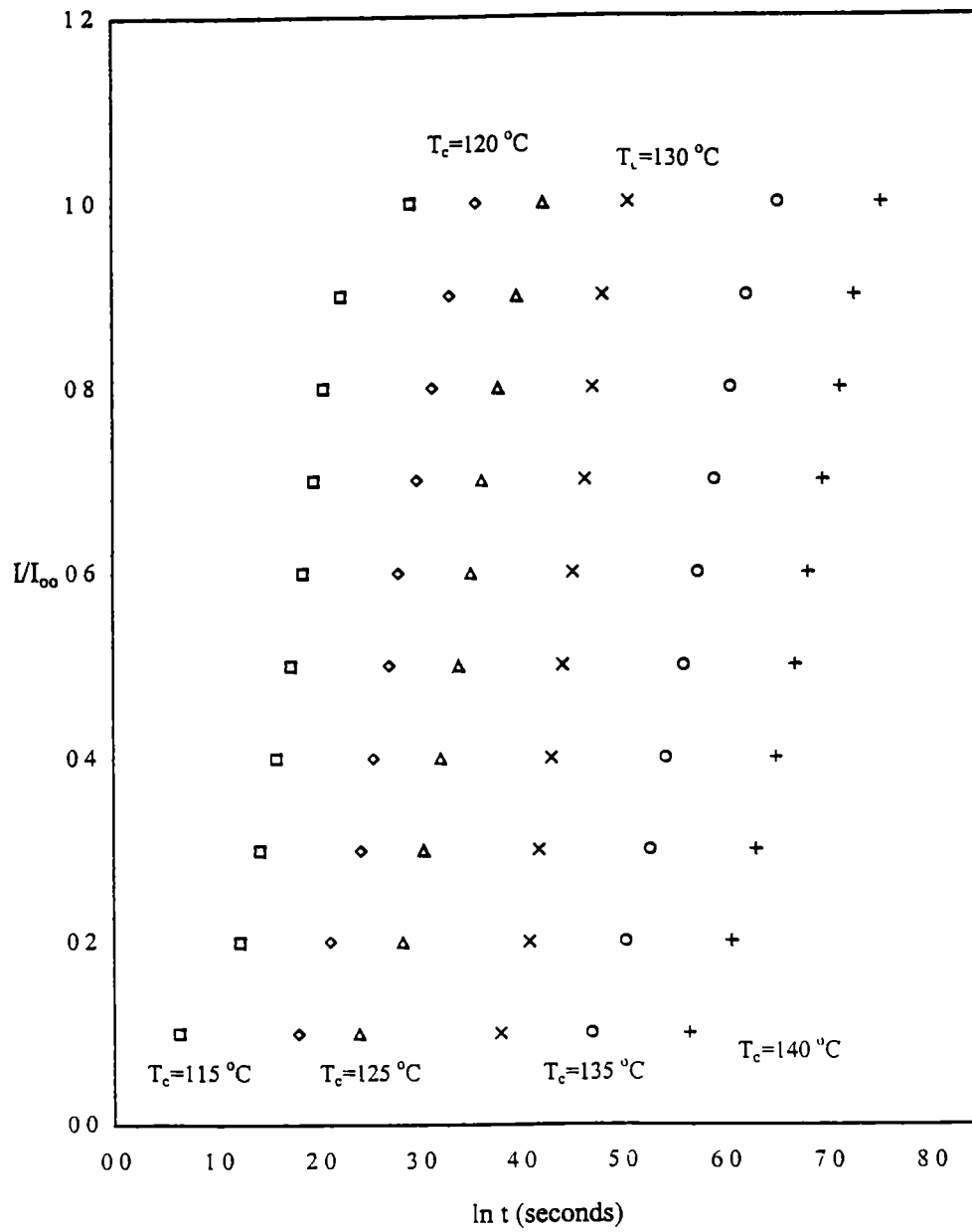
Figure 18 Crystallization curves for specimen FINA obtained by LDM

$$k = \frac{\ln(2)}{(t_{1/2})^n} \qquad \text{(equation 10)}$$

where $t_{1/2}$ is that elapsed time at which one half of the specimen has been crystallized. Figure 19 demonstrates how the half-time value is obtained and table 4 presents values for the half-times of crystallization for all specimens at different crystallization temperatures.

Although the half-time of crystallization term in equation 10 has been resolved, the exponent n has to be attained. By graphical analysis, this is found to be the slope of a plot of $\log\left[\ln\left(\frac{1}{1-X(t)}\right)\right]$ versus $\log(t)$, where t is the crystallization time in seconds (Magill, 1960, Wunderlich, 1976). Figures 20 through 23 are these plots of the specimens and table 5 presents the values for the exponents at different temperatures. A drastic change in slope can be observed involving points at the higher values of some curves in figures 16 and 21. This is attributed to secondary crystallization and will be discussed later. Having obtained the half-time and n values, the rate constant, k, can finally be calculated using equation 10. These values are also given in table 5.

One last bit of information about the nucleation process was obtained by plotting $\ln\left(\frac{1}{t_{1/2}}\right)$ versus either $\frac{1}{T\Delta T}$ or $\frac{1}{T\Delta T^2}$, where T is the crystallization temperature in degrees Celsius, and ΔT is the degree of supercooling. A linear plot of $\ln\left(\frac{1}{t_{1/2}}\right)$ versus either $\frac{1}{T\Delta T}$ or $\frac{1}{T\Delta T^2}$ implies that the nucleation process
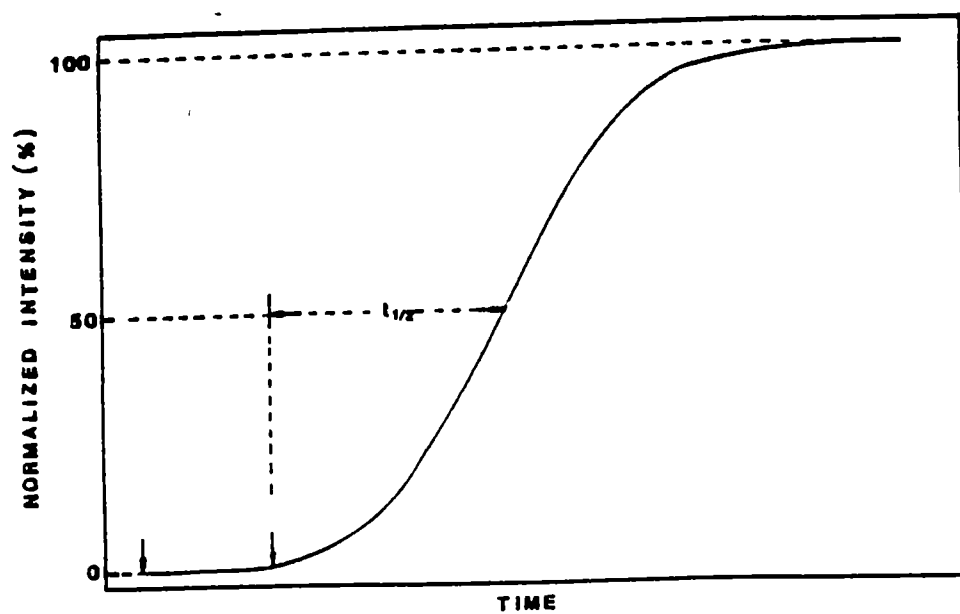
Figure 19: Obtaining the crystallization half-time value from a LDM graph (Lambert W. S., M S. Thesis, University of Tennessee, Knoxville (1988))

Table 4: Half-time of crystallization values for the specimens at different crystallization temperatures

T_c (°C)	X1 (sec.)	X2 (sec.)	X3 (sec.)	FINA (sec)
115	6 0	6 0	9 0	5 7
120	7 5	7.9	17 3	15 0
125	26 0	14.0	24 0	30 0
130	51.0	38 0	84 0	84 0
135	180 0	72 0	225 0	276 0
140	540 0	207 0	891 0	810 0
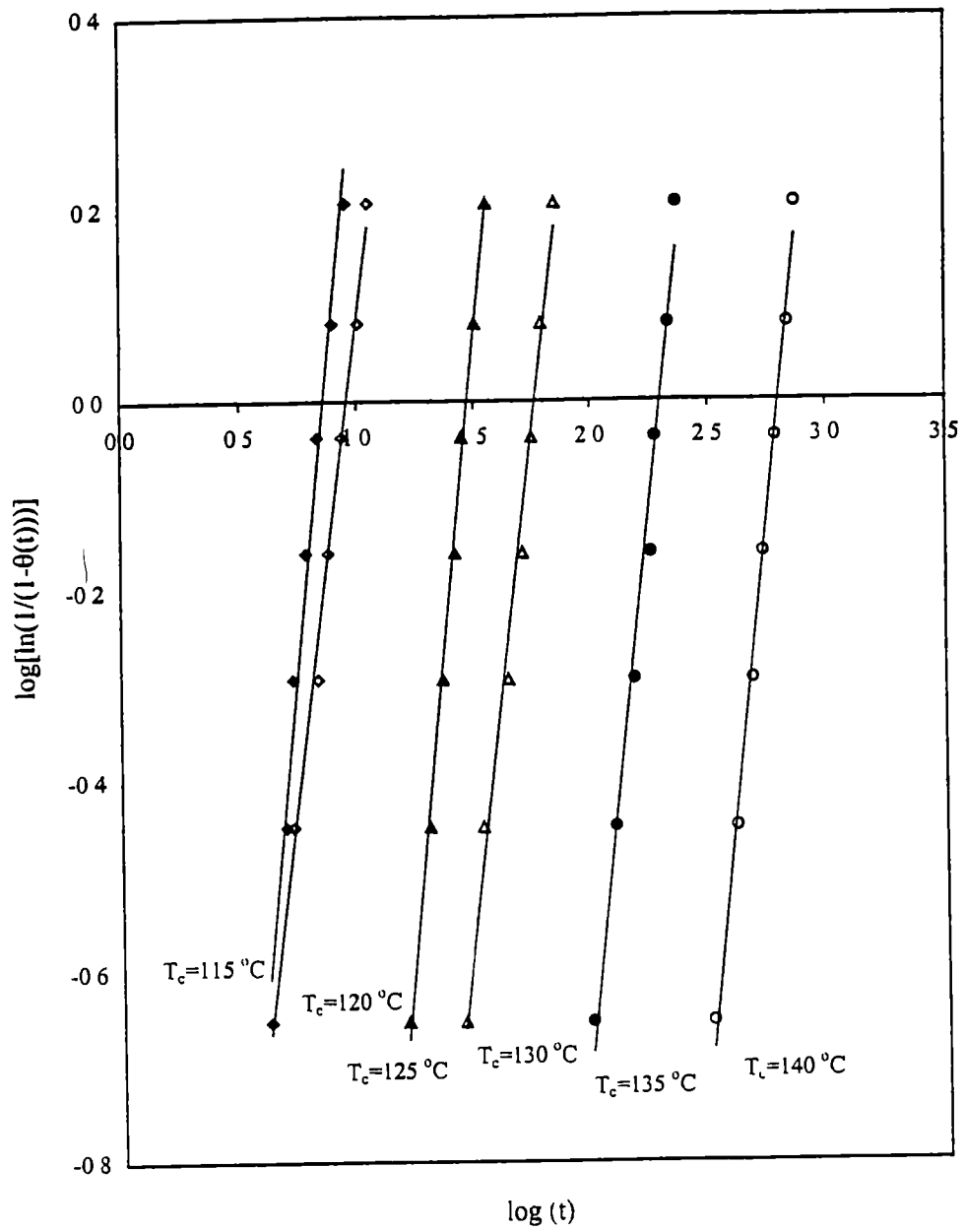
Figure 20: Plot of $\log\left[\ln\left(\dfrac{1}{1-X(t)}\right)\right]$ versus $\log(t)$ for specimen X1
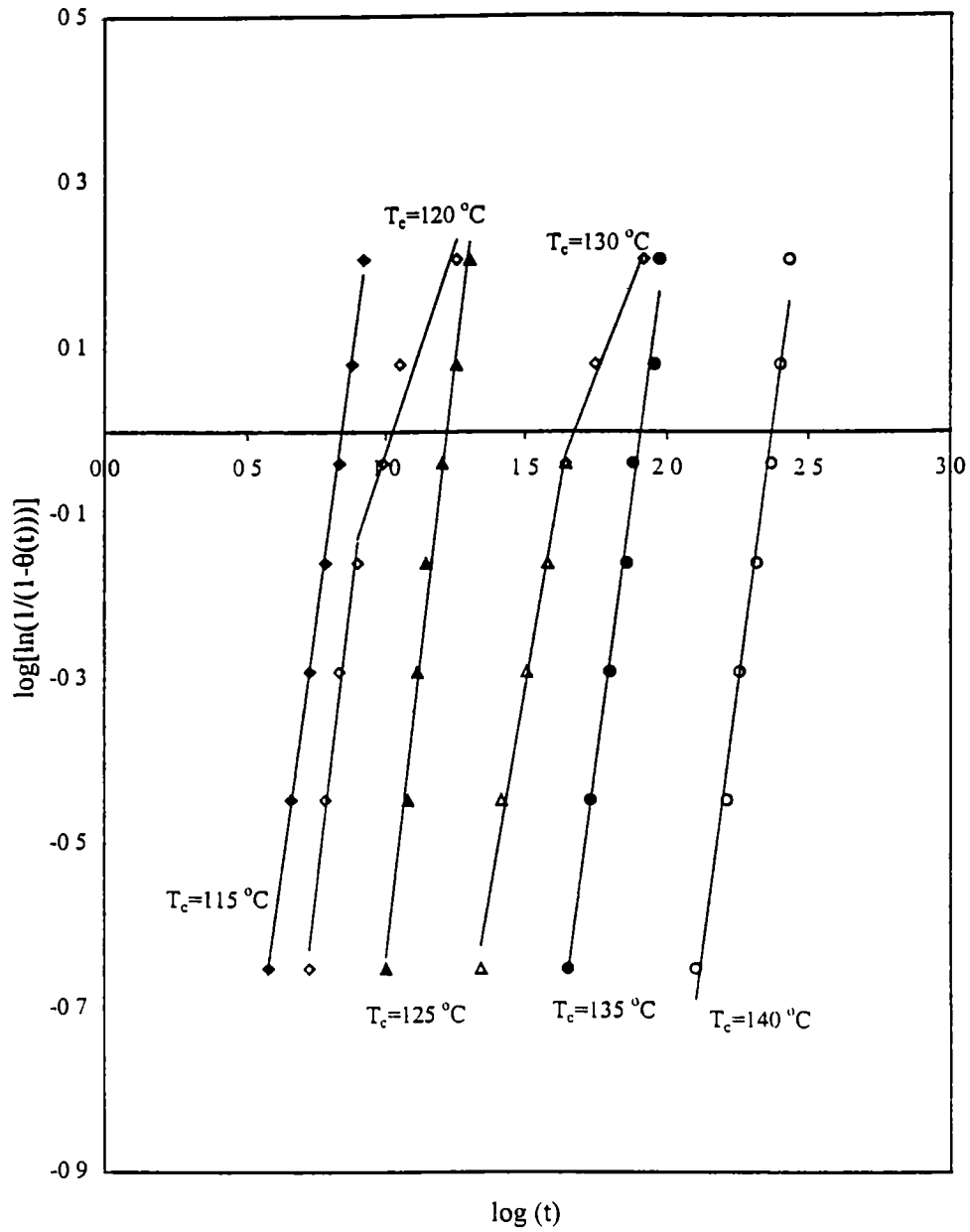
Figure 21: Plot of $\log\left[\ln\left(\dfrac{1}{1-X(t)}\right)\right]$ versus $\log(t)$ for specimen X2.
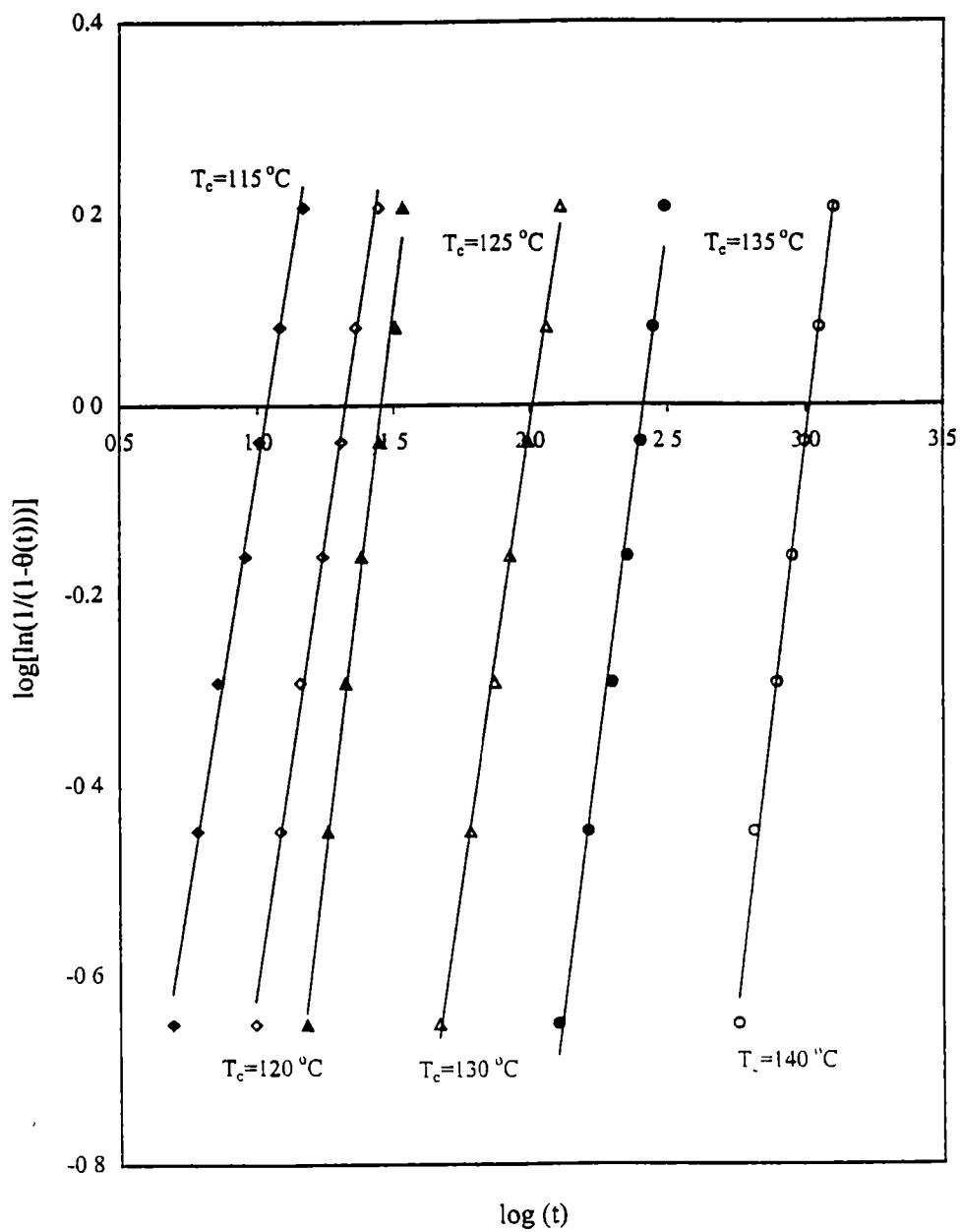
Figure 22: Plot of $\log\left[\ln\left(\dfrac{1}{1-X(t)}\right)\right]$ versus $\log(t)$ for specimen X3
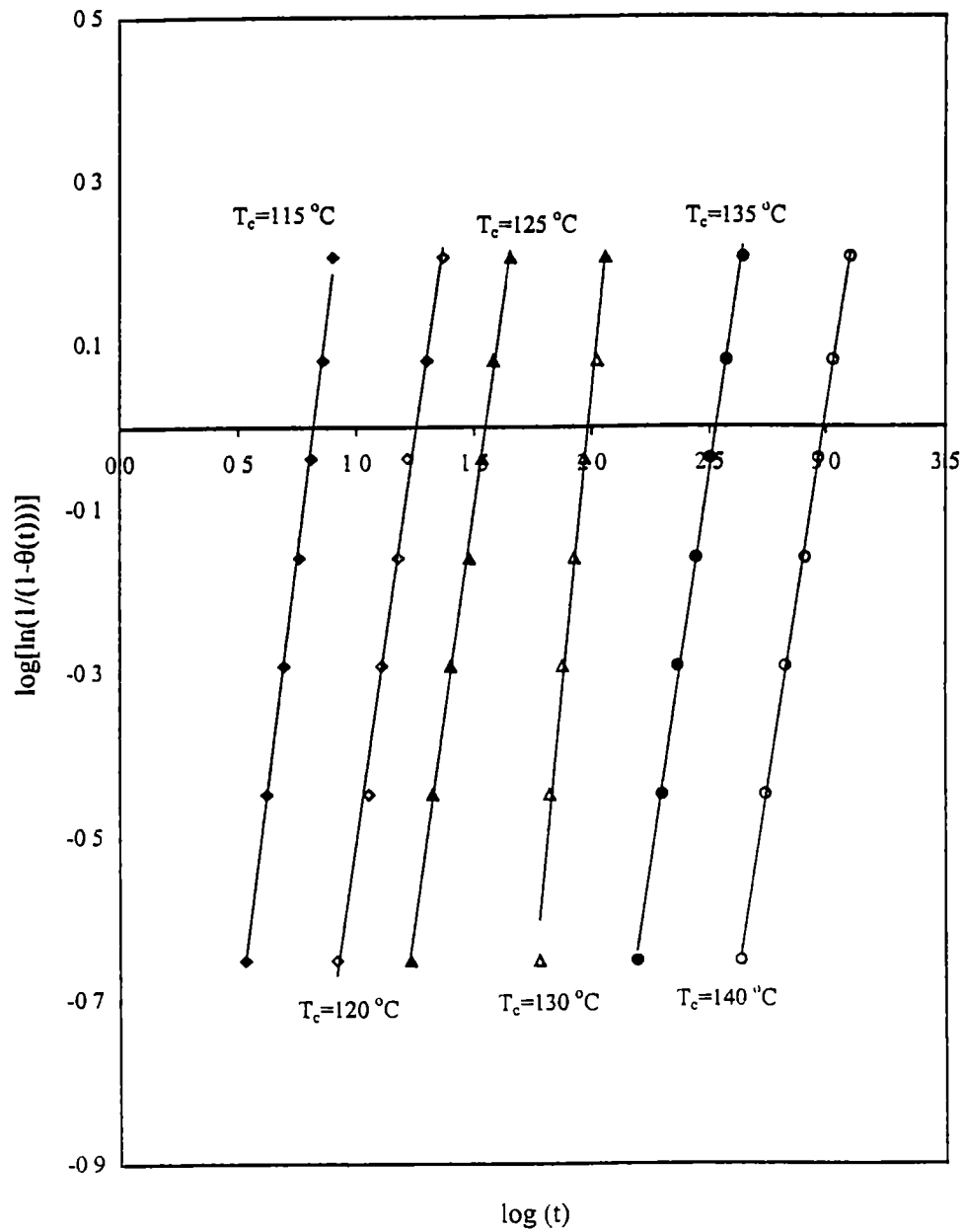
Figure 23: Plot of $\log\left[\ln\left(\dfrac{1}{1-X(t)}\right)\right]$ versus $\log(t)$ for specimen FINA.

Table 5: Avrami constants of the specimens at different crystallization temperatures.

T_c (°C)	X1 n	X1 k (sec^{-1})	X2 n	X2 k (sec^{-1})	X3 n	X3 k (sec^{-1})	FINA n	FINA k (sec^{-1})
115	2 5	$7.82e^{-3}$	2.2	$1\ 30e^{-2}$	1 8	$1.33e^{-2}$	2 9	$4\ 57e^{-3}$
120	1 8	$1\ 84e^{-2}$	2 8*	$2\ 14e^{-3}$	2 0	$2.33e^{-3}$	2 0	$3\ 08e^{-3}$
125	2 2	$5.01e^{-4}$	2.5	$9\ 45e^{-4}$	2 5	$2\ 46e^{-4}$	2 2	$3.90e^{-4}$
130	2.0	$2.66e^{-4}$	2.0*	$4\ 80e^{-4}$	2.0	$9\ 82e^{-5}$	2 9	$4\ 82e^{-6}$
135	2.2	$6.83e^{-6}$	2.9	$2.85e^{-6}$	2 2	$4\ 63e^{-6}$	1 8	$2\ 80e^{-5}$
140	2 2	$5\ 96e^{-7}$	2 5	$1.12e^{-6}$	2.5	$2\ 93e^{-8}$	2 0	$1\ 06e^{-6}$
AVG(n)	2.2		2 5		2.2		2.3	

* Indicates the value of the slope after subtracting the deviation at the end of the curves (please see figure 18) The Avrami constant for these deviations was n=1 0

is heterogeneous or homogeneous, respectively If a non-linear plot is obtained by this procedure, the opposite is true (Ross and Frolen, 1975) Figures 24 and 25 are plots of this nature and clearly show that the nucleation process is heterogeneous These nucleation processes will be discussed later

4.2 Results of Structural Studies Obtained by WAXD

In general, diffraction of any material results from the wavelength of the incident beam, λ, being of the same magnitude of the repeat distance between the particles scattering this energy Using the Bragg law (equation 11) it is possible to quantify the conditions upon which diffraction may occur for any given material

$$n\lambda = 2d \sin\theta \qquad \text{(equation 11)}$$

The variable n in this equation refers to the order of reflection and can be considered a constant in the case of constructive interference, since the rays scattered are completely in phase from all the atoms in the different planes. Therefore, these rays will reinforce one another to produce one diffracted beam in the direction θ The variable d corresponds to the distance of the spacings of the particles comprising the material Without going into detail, it will suffice to state that a specific material will have a unique spacing of its constituents within its unit cells and will produce scattering angles unique to its composition This will produce diffraction patterns that can be used to identify a material's constitution (Cullity, 1978)
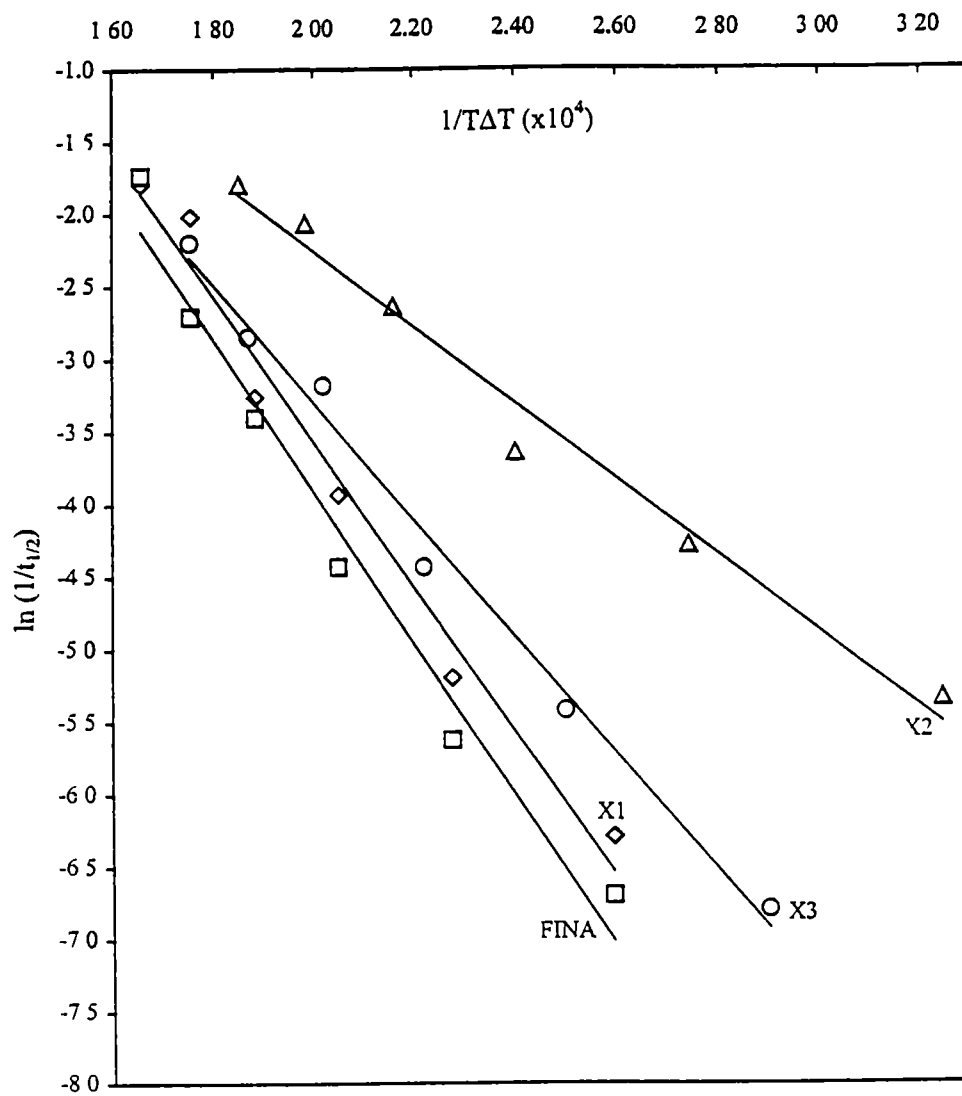
Figure 24: Plot of $\ln\left(\dfrac{1}{t_{1/2}}\right)$ versus $\dfrac{1}{T\Delta T}$ for all specimens.
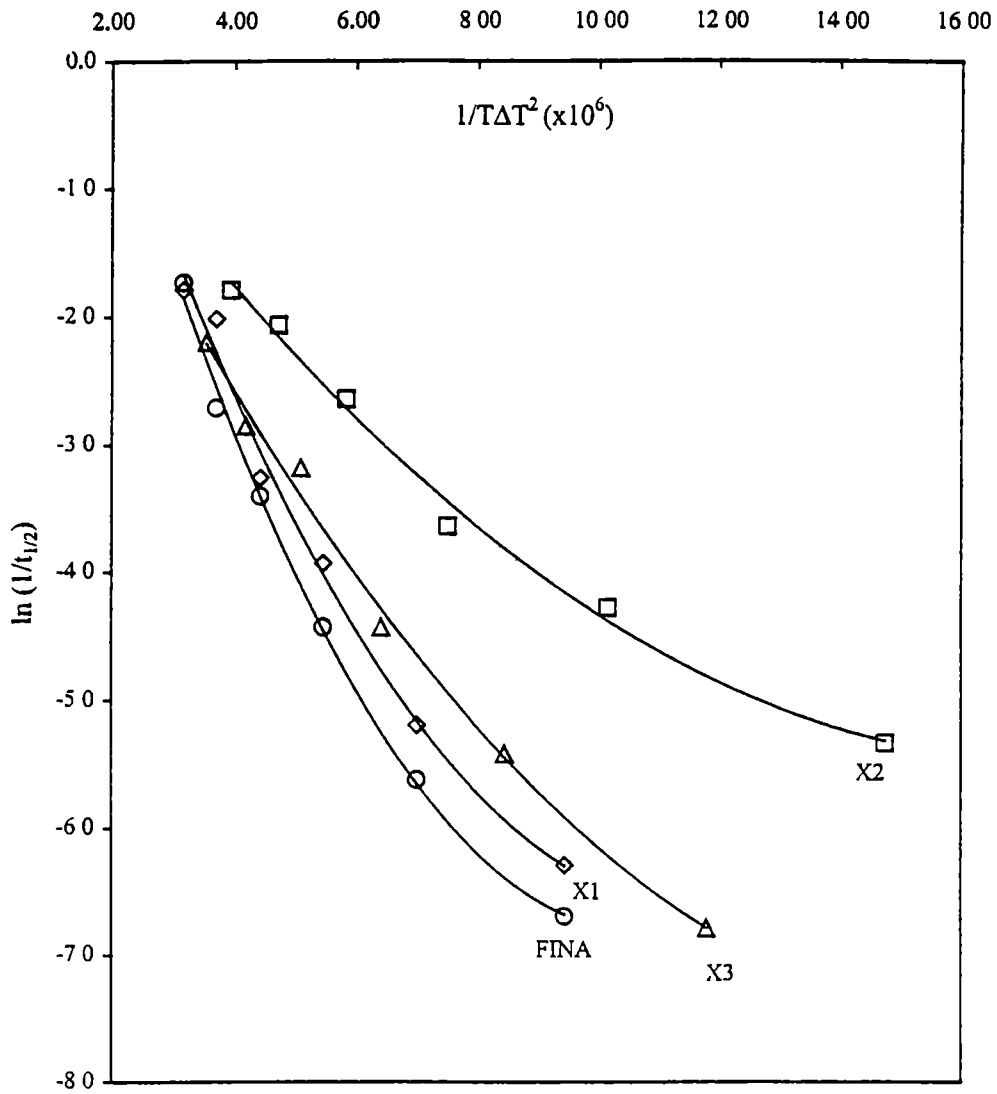
Figure 25: Plot of $\ln\left(\dfrac{1}{t_{1/2}}\right)$ versus $\dfrac{1}{T\Delta T^2}$ for all specimens.

4 2.1   <u>Structural Determinations</u>

The structure of the specimens was obtained through the reflection mode of a wide-angle x-ray diffractometer   Figures 26 through 29 are typical diffractograms of the four distinct forms of isotactic polypropylene and table 6 presents approximate 2θ peak positions that distinguish each polymorph from the others   Figures 30 through 33 are reflection mode diffraction patterns of specimens X1, X2, X3, and FINA, respectively. Using figures 26 through 29 as a general model, it is observed that all the specimens studied predominantly crystallize in the alpha form. However, some spectra for each specimen suggest there may indeed be other polymorphs present, i e. the beta and gamma forms To test if these forms are uniformly present throughout the material, x-ray diffractograms of the same samples were run, using the transmission mode Due to mechanical stresses placed on the samples when heat-pressed, or when any procedure involving stress is used, polymorphs of i-PP can be produced on the surface of the specimen that are not present in its interior, even though the specimen in question is a thin film (Krestev et al , 1989)

In the reflection mode, surface orientations are more pronounced in the spectrum than in the transmission mode. Therefore, by running a series of experiments in both reflection and transmission modes a clear picture of the sample as a whole can be envisioned Figures 34 through 37 are transmission spectra of specimens X1, X2, X3, and FINA, respectively
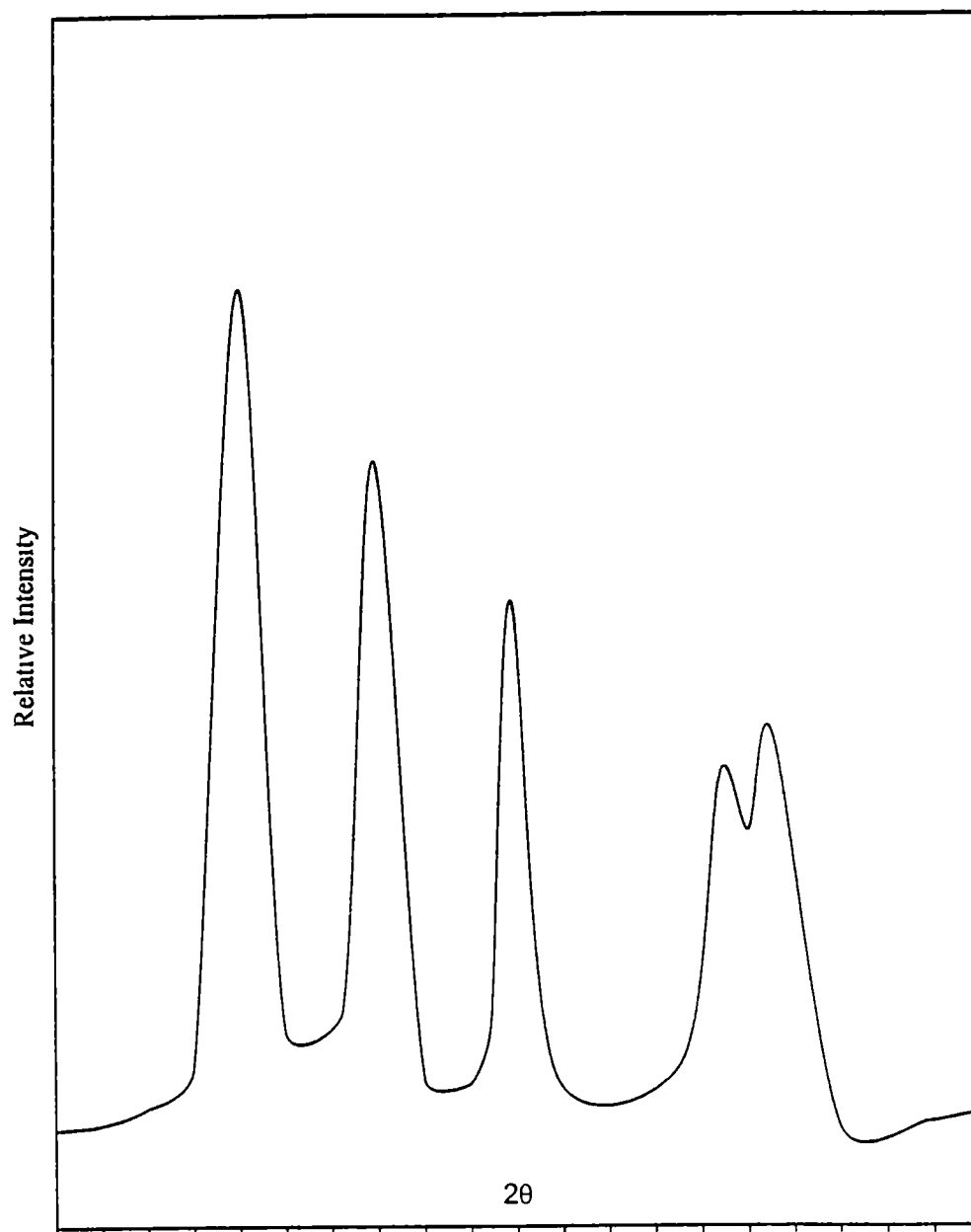
Figure 26: Typical diffraction pattern of the alpha modification of isotactic polypropylene.
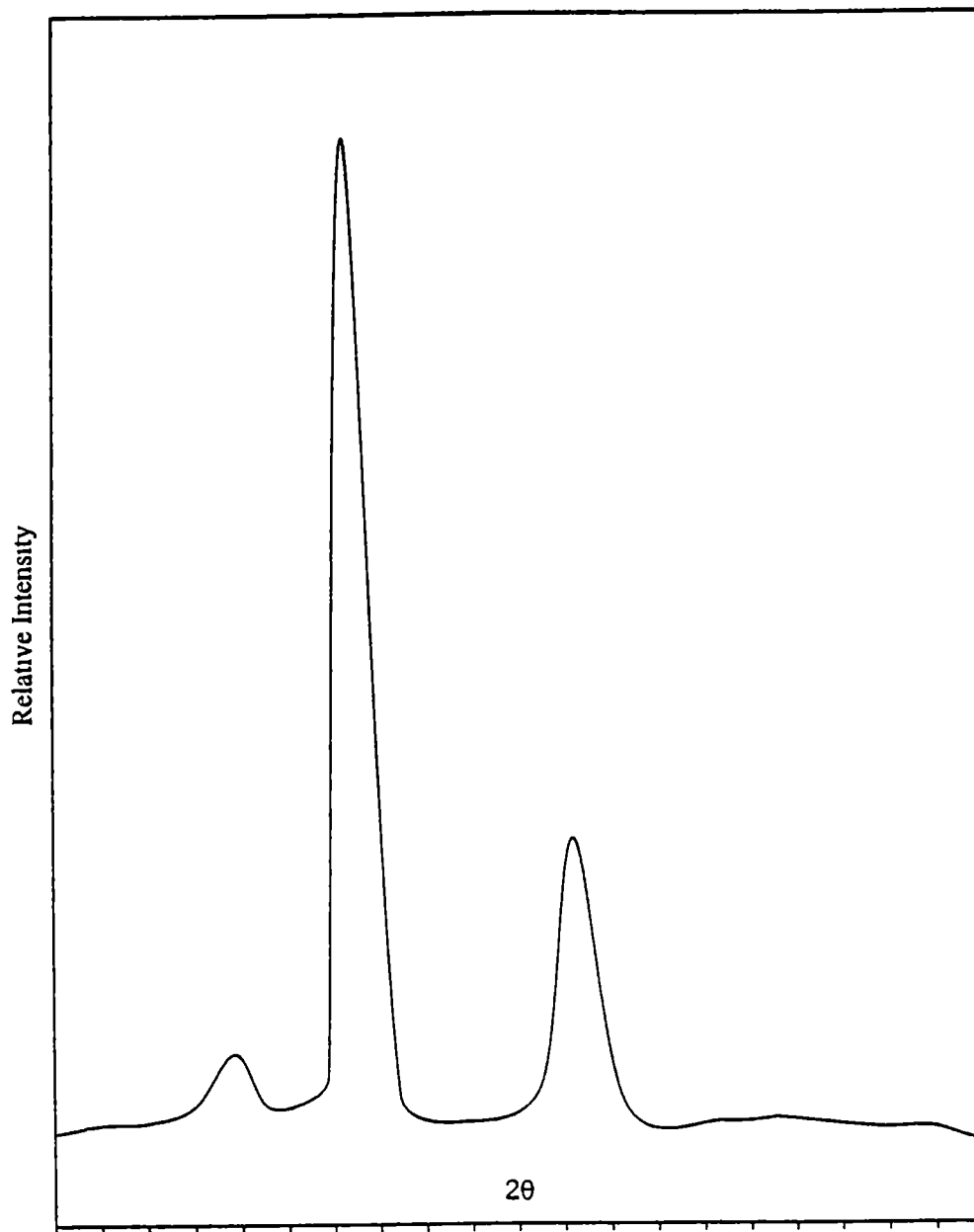
Figure 27: Typical diffraction pattern of the beta modification of isotactic polypropylene.
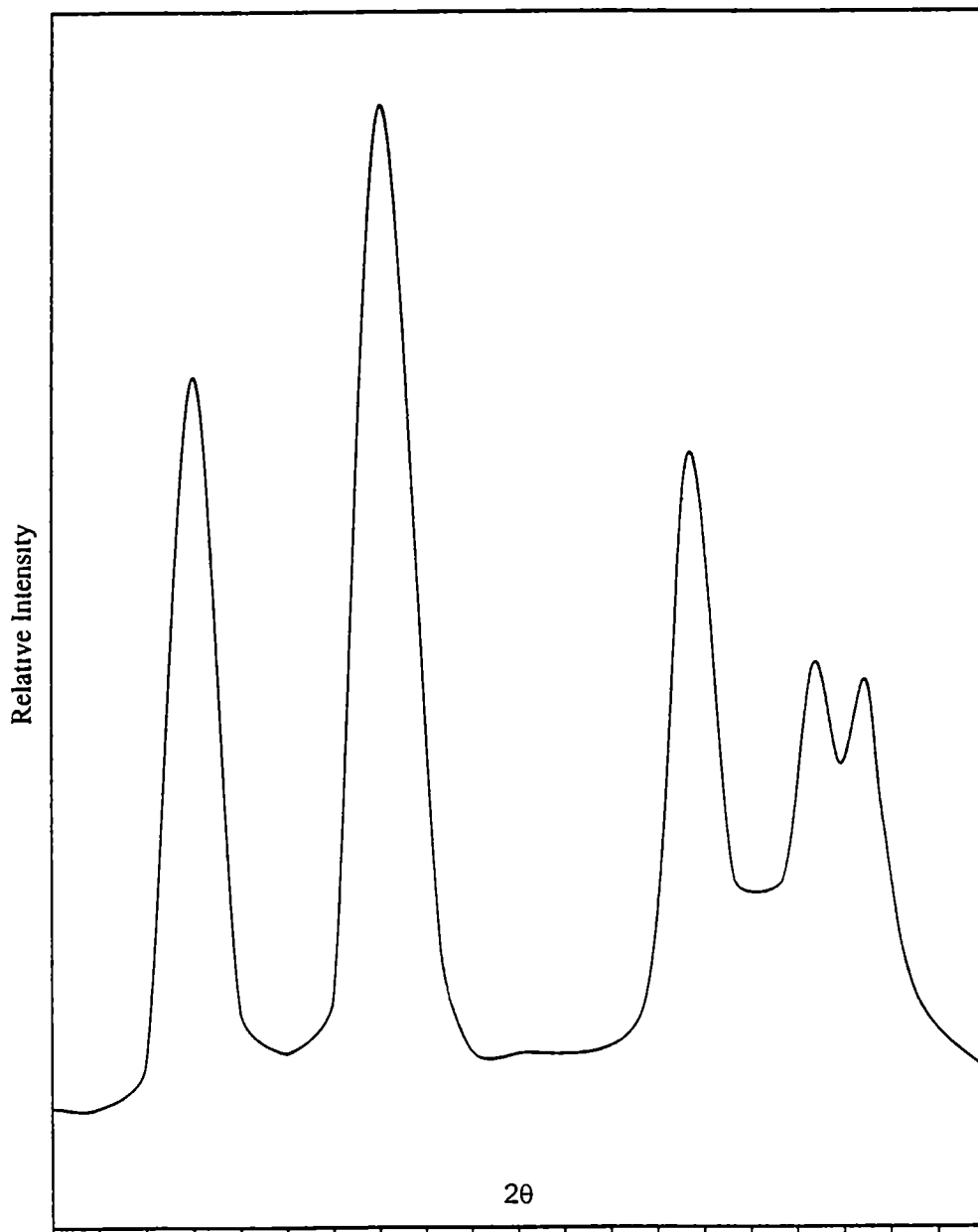
Figure 28: Typical diffraction pattern of the gamma modification of isotactic polypropylene
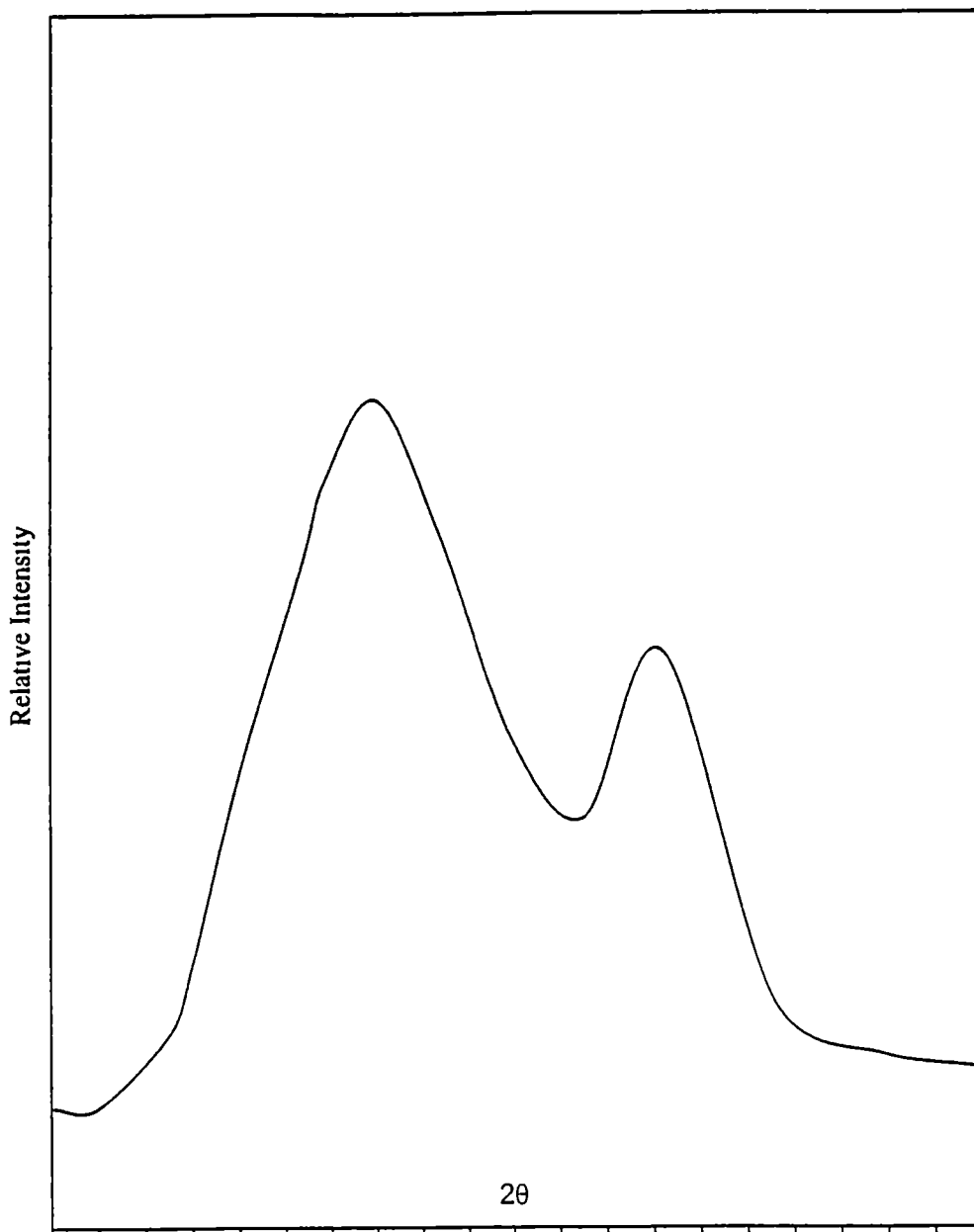
Figure 29: Typical diffraction pattern of the smectic modification of isotactic polypropylene.

Table 6: Some approximate (CuKα) 2θ peak positions for alpha, beta and gamma modifications of isotactic polypropylene.

Alpha Form 2θ°	Beta Form 2θ°	Gamma Form 2θ°
14 0	16 0	13.8
16 8	21 0	16 7
18 3		20 0
21 0		21 2
21 8		22.0
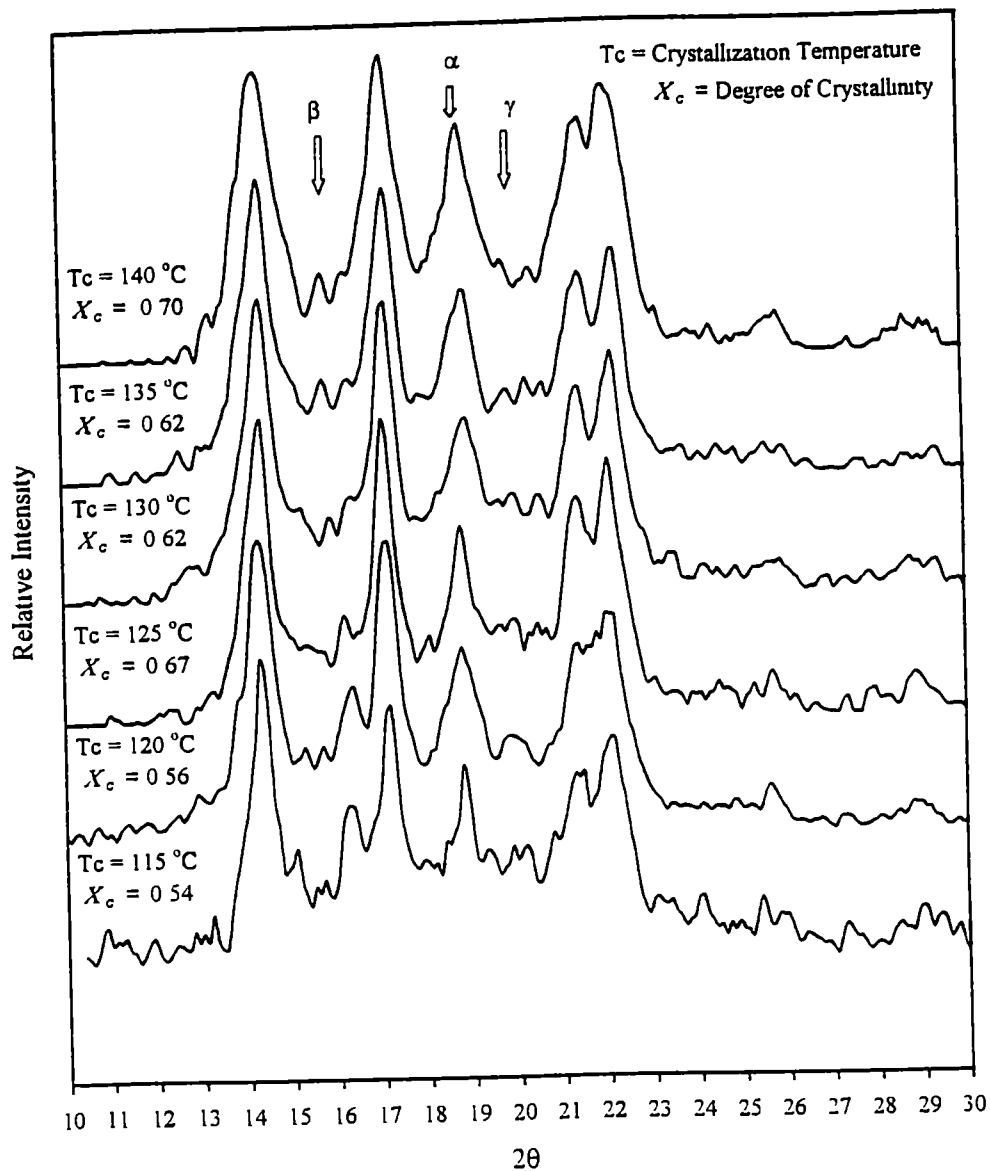
Figure 30: WAXD pattern of specimen X1 taken in reflection mode.
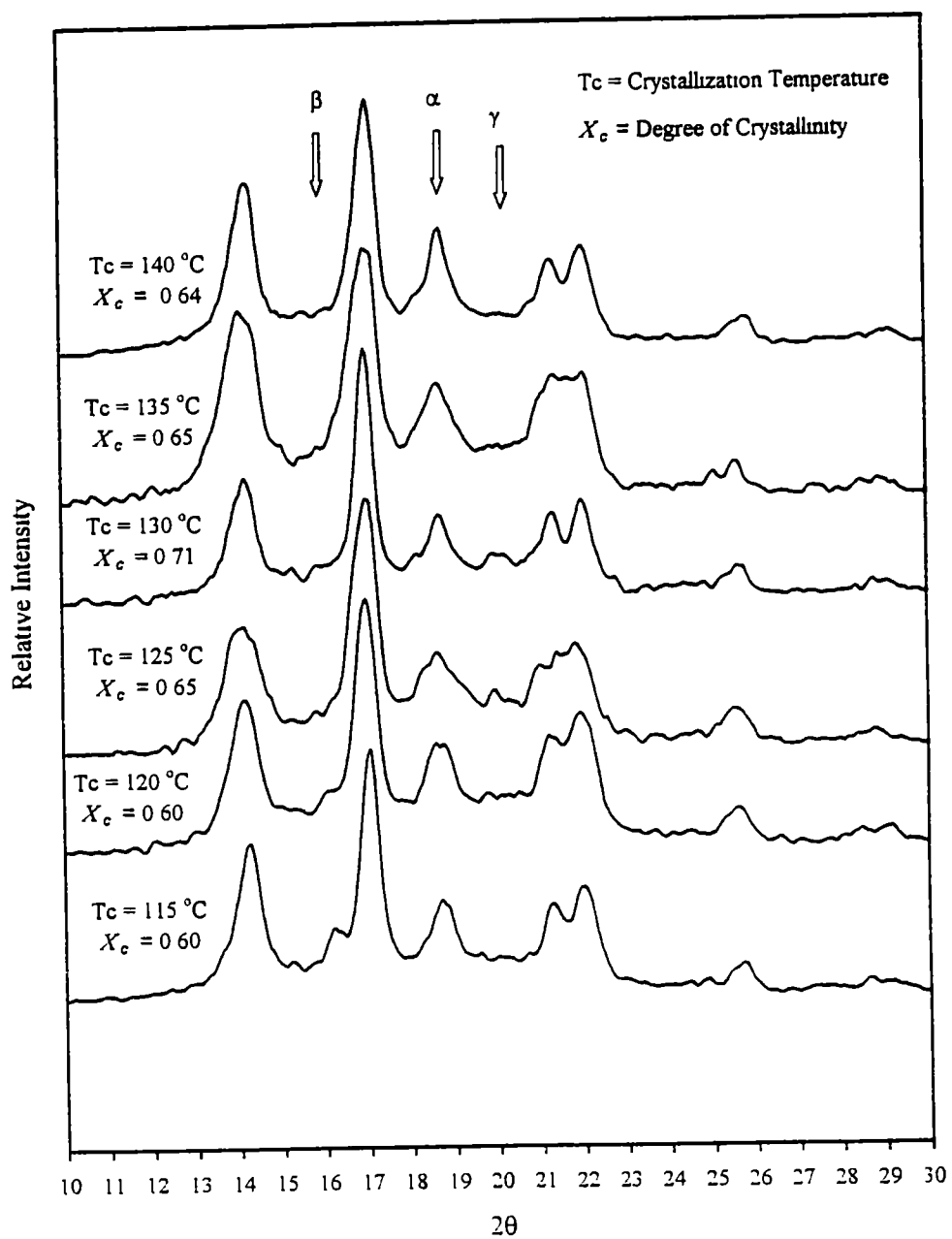
Figure 31: WAXD pattern of specimen X2 taken in reflection mode
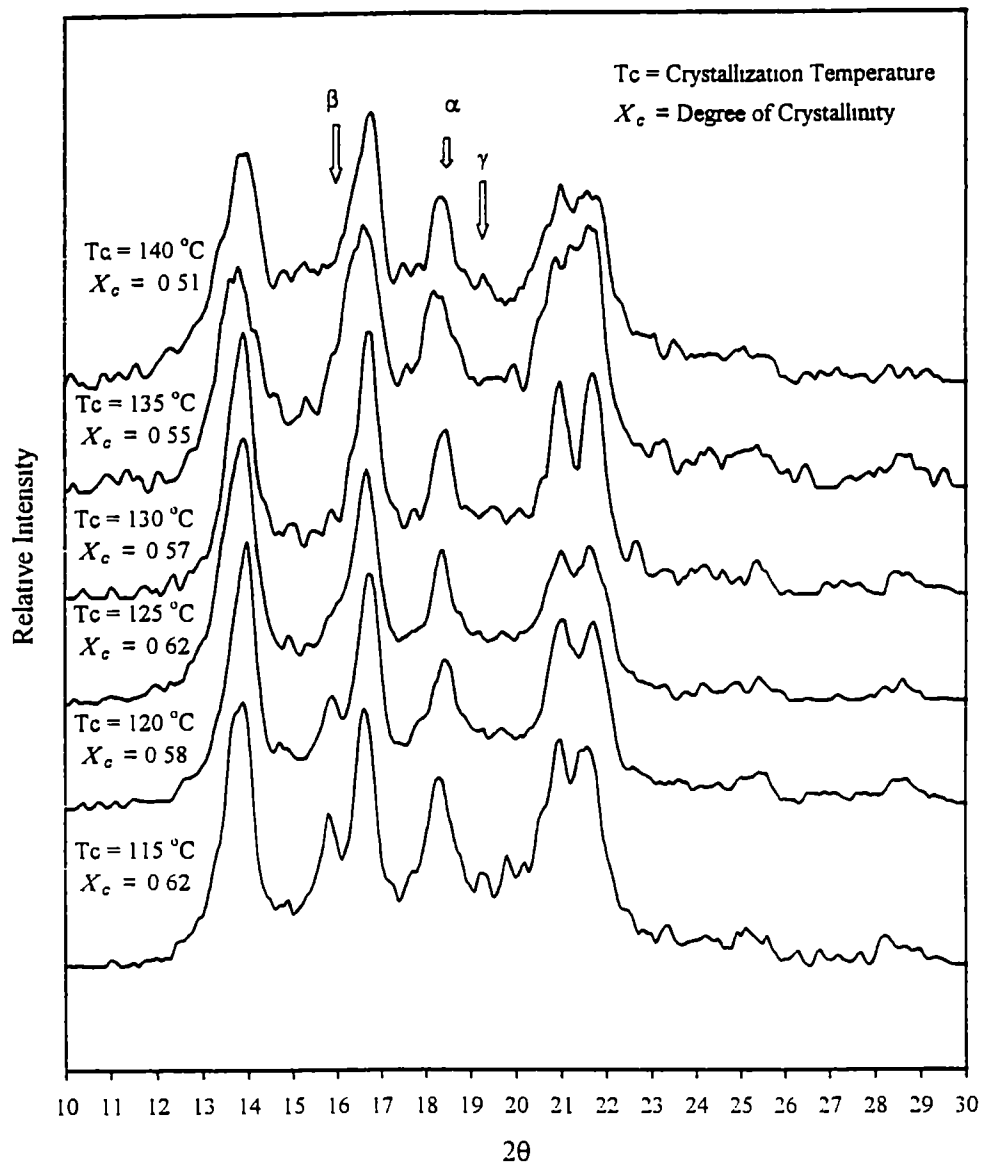
Figure 32: WAXD pattern of specimen X3 taken in reflection mode.
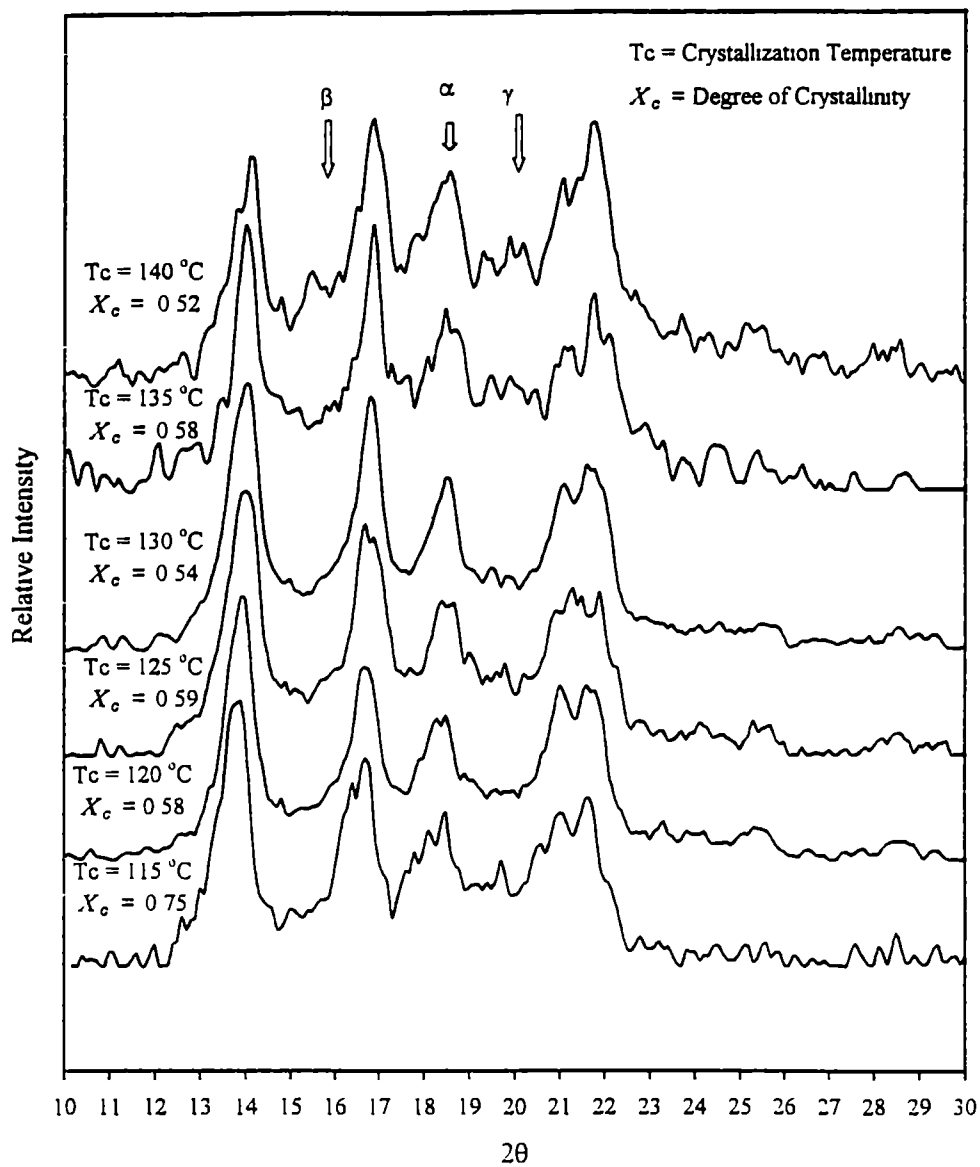
Figure 33: WAXD pattern of specimen FINA taken in reflection mode
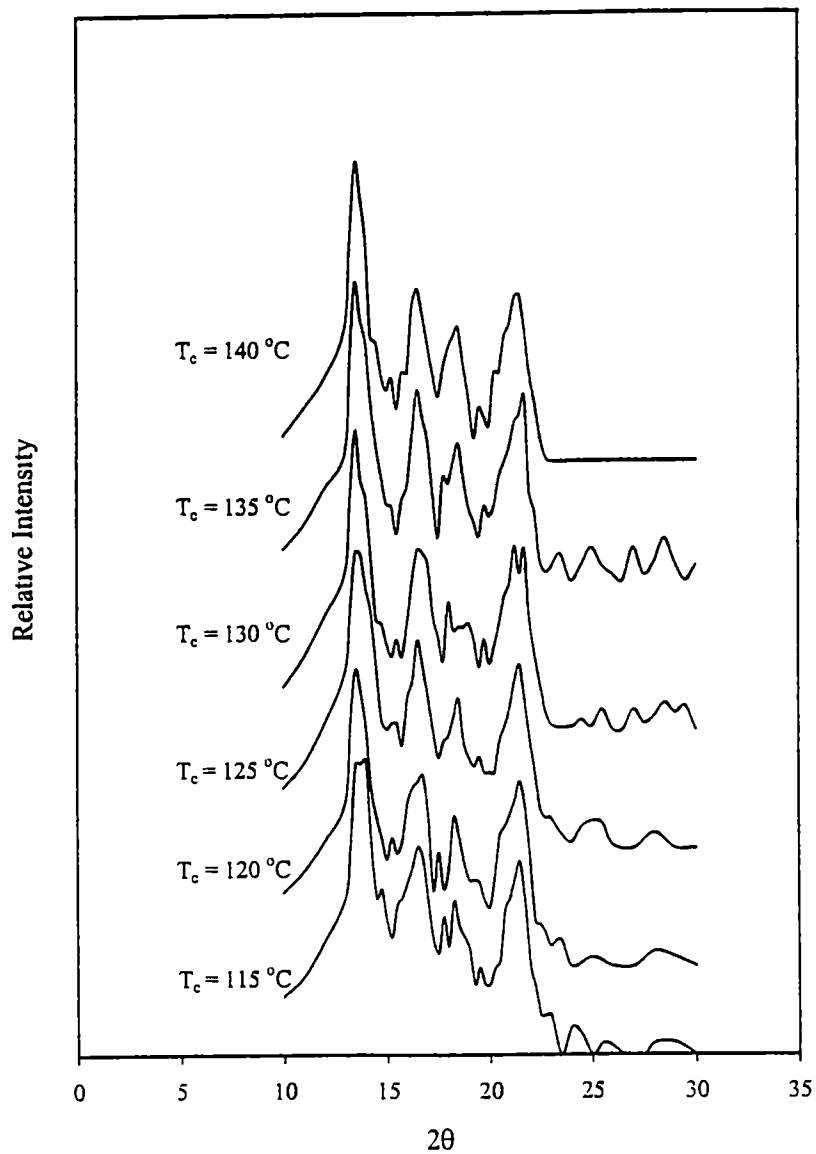
Figure 34: WAXD pattern of specimen X1 taken in transmission mode
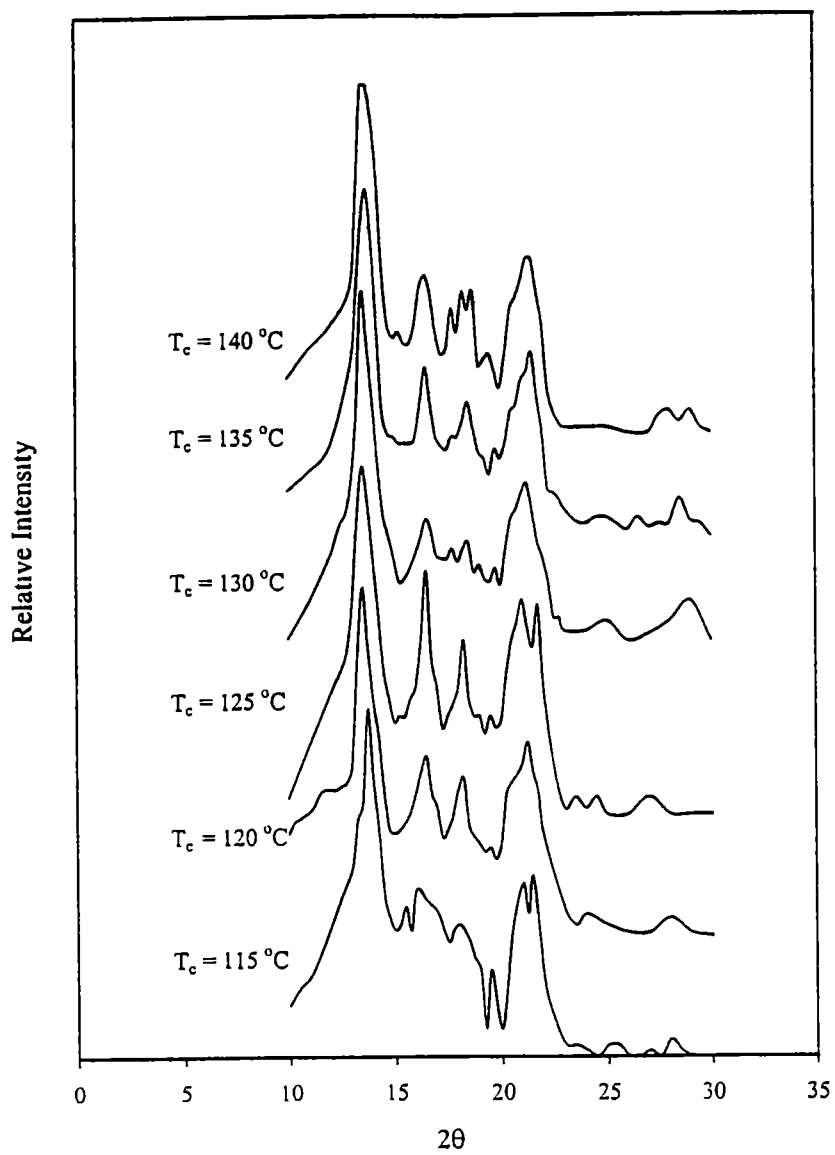
Figure 35: WAXD pattern of specimen X2 taken in transmission mode
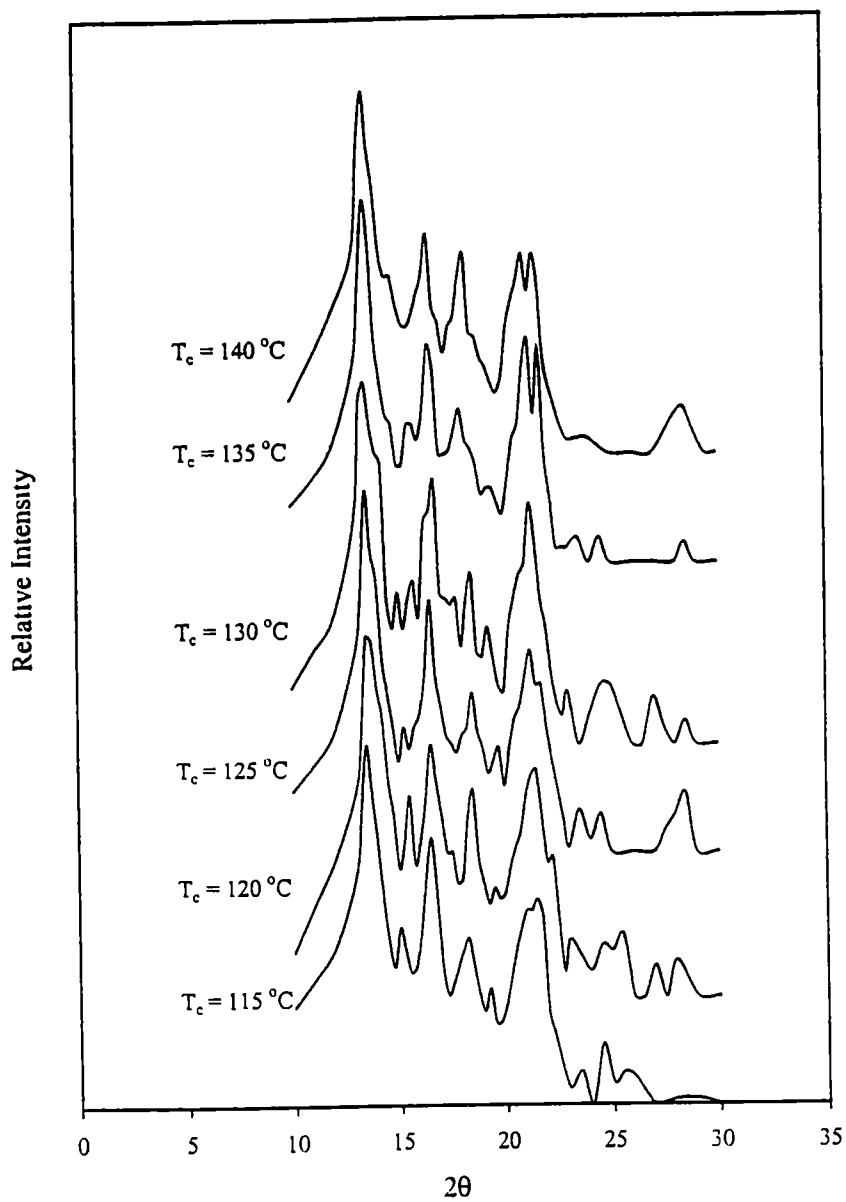
Figure 36: WAXD pattern of specimen X3 taken in transmission mode
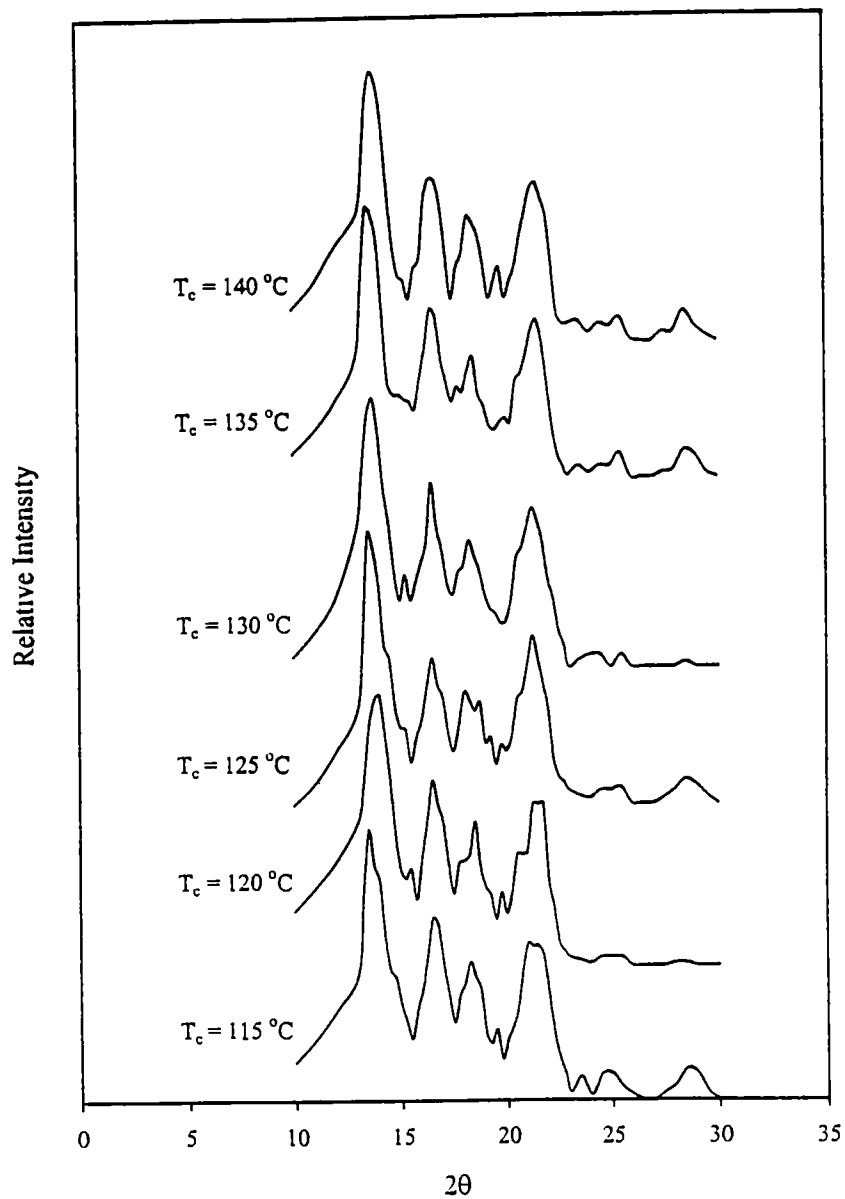
Figure 37: WAXD pattern of specimen FINA taken in transmission mode.

It was observed in the diffraction patterns taken in the reflection mode that the intensity of the peak $2\theta = 15°$ in many of the samples of the overwhelmingly alpha nature was less than the ones at $2\theta = 17°$ This was especially true for the X2 specimens. This condition could suggest that the irradiation and/or thermo-mechanical processes somehow interfered with the structure at the crystal lattice level Observing the transmission spectra, it was concluded that this phenomenon was due to surface orientations produced by stresses during specimen preparation It was further noticed that the transmission spectra were not well defined for some of the specimen This could have been a result of the films being so thin that pieces had to be placed on top of each other, sometimes four layers thick, in order to produce any patterns.

4 2.2   Degree of Crystallinity

The method of crystallinity determination by the Hermans and Weidinger approach follows three assumptions. The first is that the total diffraction pattern can be divided into crystalline peaks resulting from scattering by crystallites and amorphous peaks from the scattering produced by non-crystalline regions The second assumption follows closely to the first in that the total scattering produced from the sample is the effect from the resolved crystalline and amorphous regions. The third assumption states that the areas under these peaks are proportional to the mass of the material The degree of crystallinity can be calculated by the following equation

$$\chi_c = \frac{A_c}{A_c + KA_{am}}$$
(equation 12)

where A_c and A_{am} are the areas of the crystalline and amorphous peaks, respectively, and K is a constant set to unity for comparative purposes (Spruiell and Clark, 1980)

A general model simulating the procedure used in determining the amorphous and crystalline regions for isotactic polypropylene is shown in figure 38. The reflection mode diffraction patterns produced by the specimens were segregated into crystalline and amorphous parts by use of a computer program and in accordance with the procedure of figure 38   A cubic spline trendline drawn from $2\theta = 10°$ to $30°$, with the peak of the line touching the second peak of the diffraction patterns, was used to outline the amorphous halo   From there the computer calculated the areas of the crystal and amorphous peaks, respectively. These area values were manipulated by equation 12 to produce the degree of crystallinity of each specimen at differing crystallization temperatures and subsequentially multiplied by 100 to give the percent crystallinity   Table 7 presents the crystallinity values at different crystallization temperatures for specimens X1, X2, X3, and FINA, respectively. These values are also referenced in figures 30 through 33.
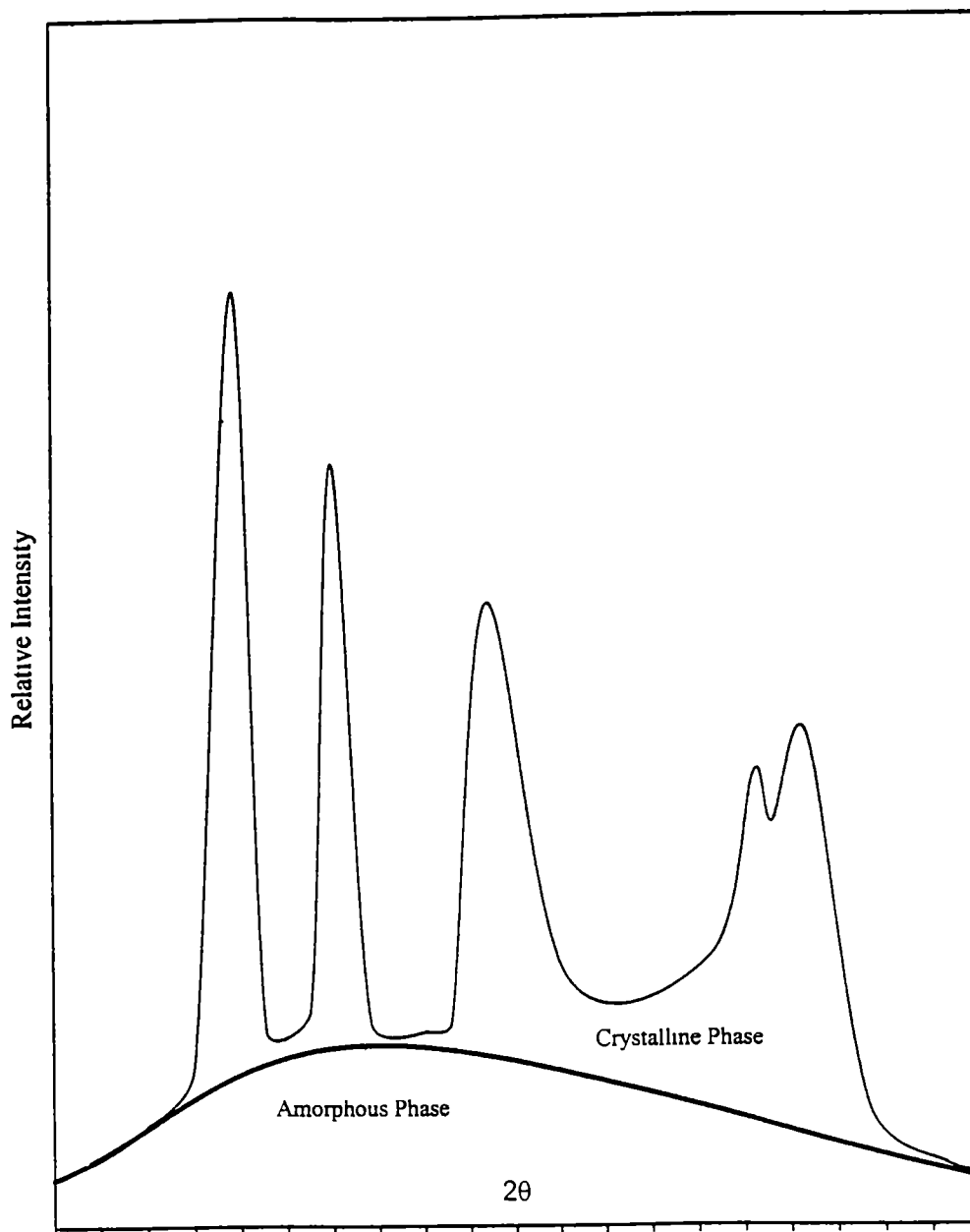
Figure 38: General model simulating the procedure for segregating the crystalline from amorphous phases of isotactic polypropylene.

Table 7: Percent crystallinity values for the specimens at different crystallization temperatures as determined by WAXD

T_c (°C)	X1	X2	X3	FINA
115	54.0	60 0	62 0	75 0
120	56.0	60.0	58.0	58.0
125	67.0	65.0	62.0	59 0
130	62.0	71.0	57 0	54 0
135	62.0	65 0	55 0	58.0
140	70 0	64 0	51 0	52.0

4.3 Results of Melting Studies by DSC and LDM

The onset and end of melting experiments were conducted on a Perkin-Elmer DSC-7 differential scanning calorimeter and the LDM apparatus mentioned above. The equilibrium melting point experiments were conducted on the DSC. The specimens used were the same samples used in the LDM crystallization studies and WAXD studies The specimens used in the LDM melting experiments were from the original powder samples

4 3 1 Equilibrium Melting Point Determinations by DSC

The equilibrium melting points of each specimen were obtained from the DSC endothermic curves by taking the temperature at which the highest peak was observed and the points where the curves returned to the baseline These temperatures were then used in the Hoffman-Weeks extrapolation method. The DSC endotherms for each sample taken at the different crystallization times are given in figures 39 through 42, while the Hoffman-Weeks plots of the peak and return to baseline values are presented in figures 43 and 44, respectively In some of the endotherms, a smaller peak at lower melting temperatures can be seen. These are the peaks from the melting of the beta modification, being the first structures to melt. This research is only concerned with the properties of the total specimen, therefore, the larger peaks, the ones belonging predominantly to the alpha modification, and the return to the baseline temperatures are used to
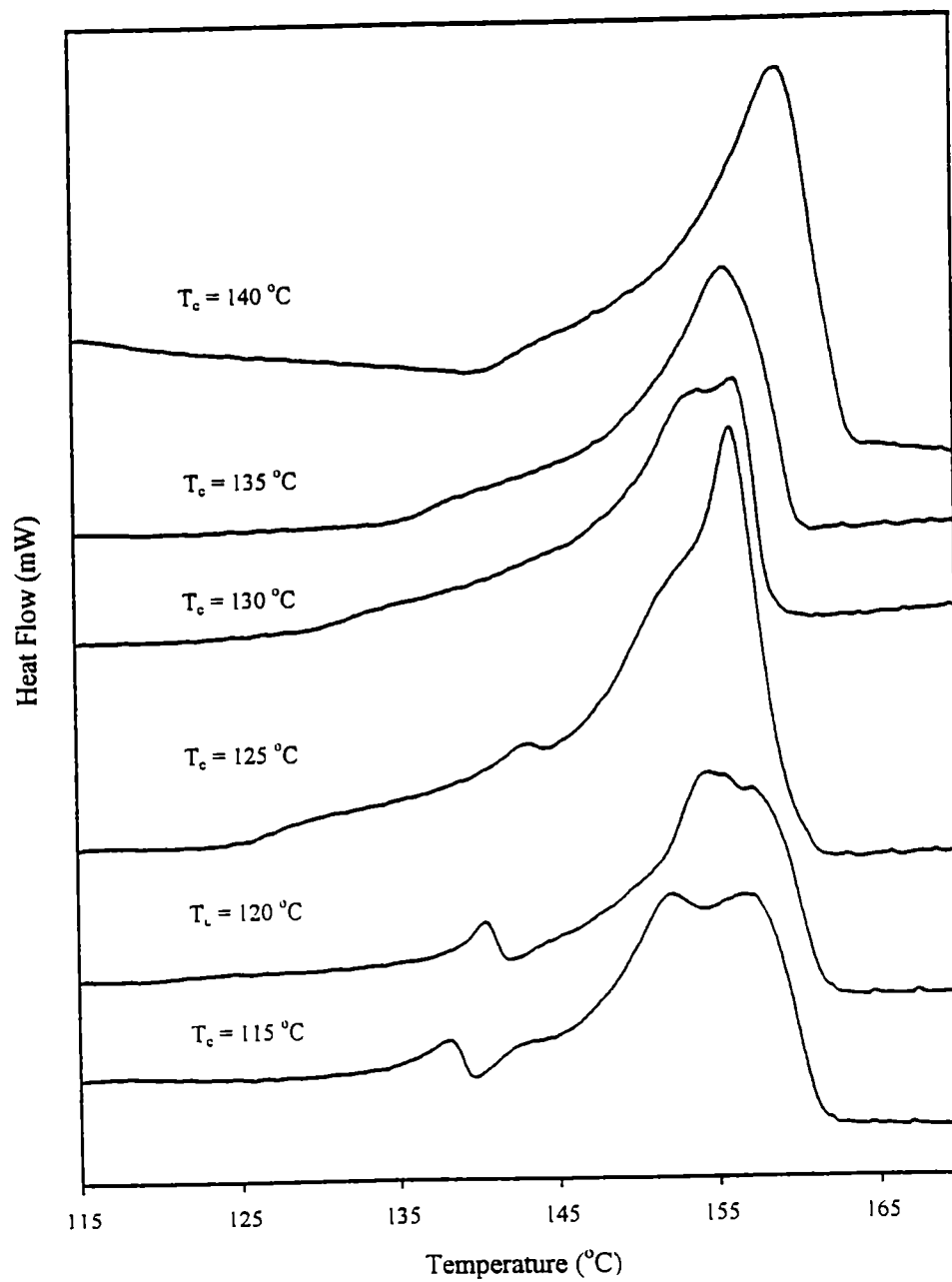
Figure 39: Melting endotherms for specimen X1 at different crystallization temperatures, T_c.
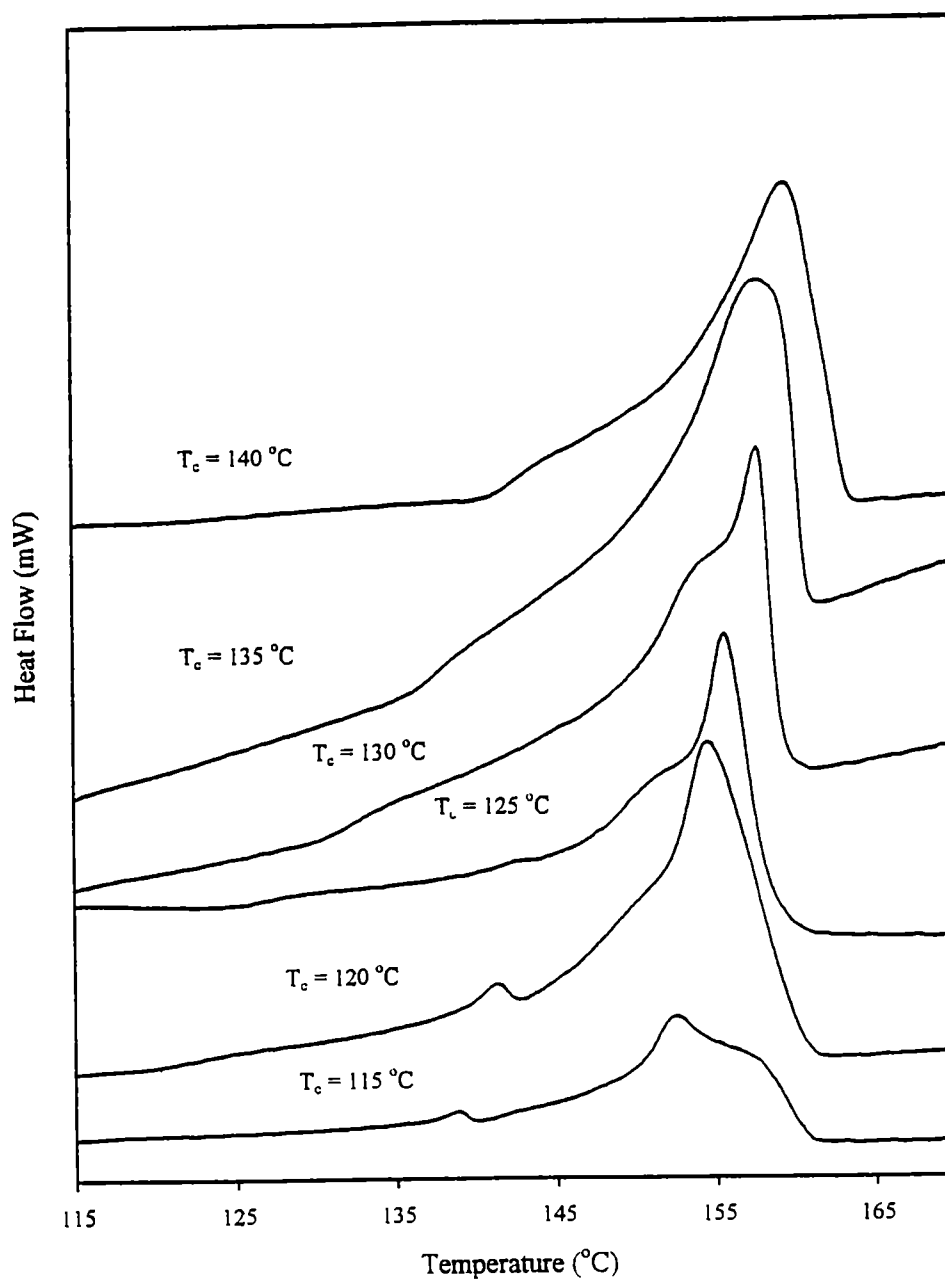
Figure 40: Melting endotherms for specimen X2 at different crystallization temperatures, T_c.
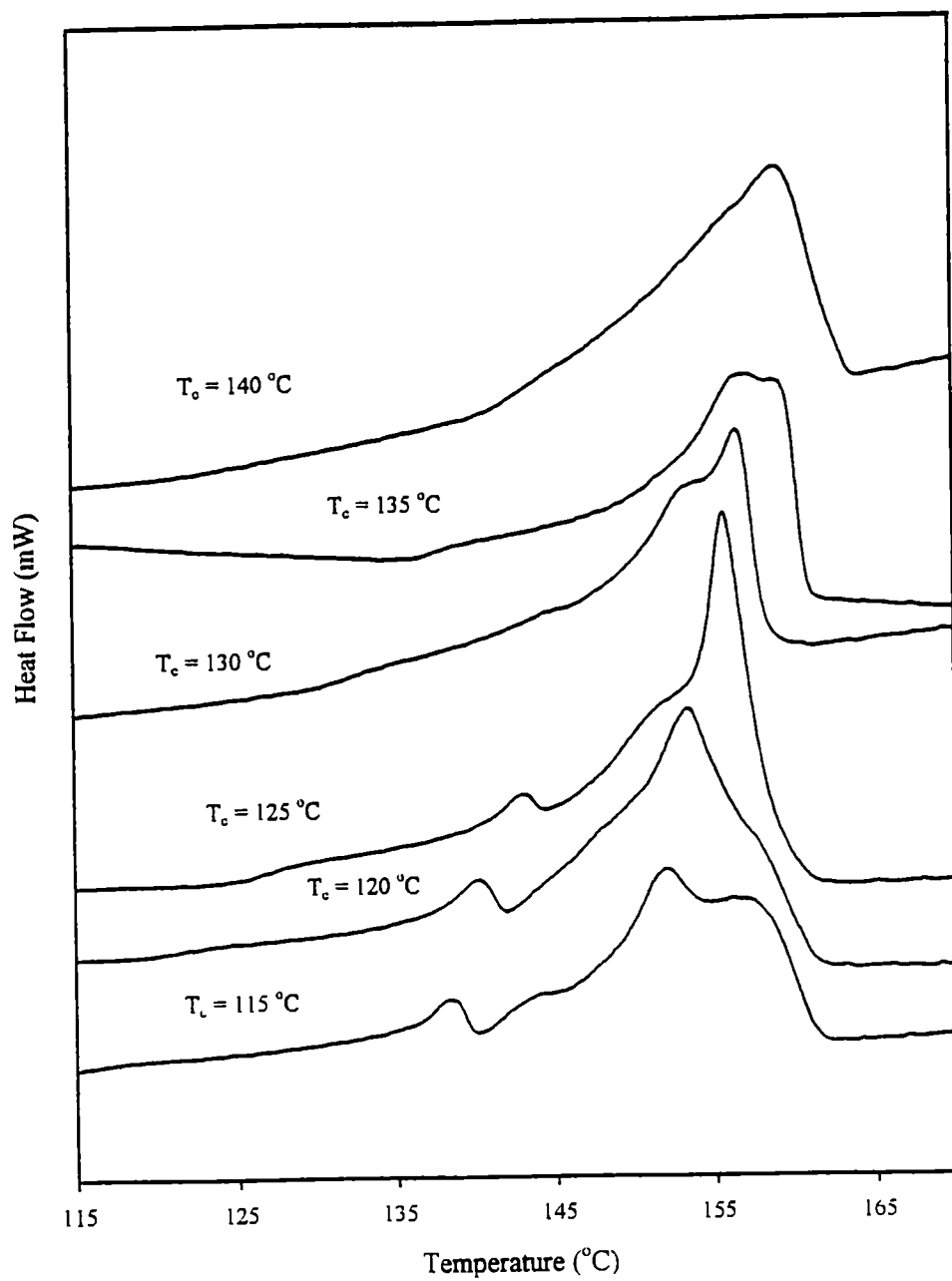
Figure 41: Melting endotherms for specimen X3 at different crystallization temperatures, T_c
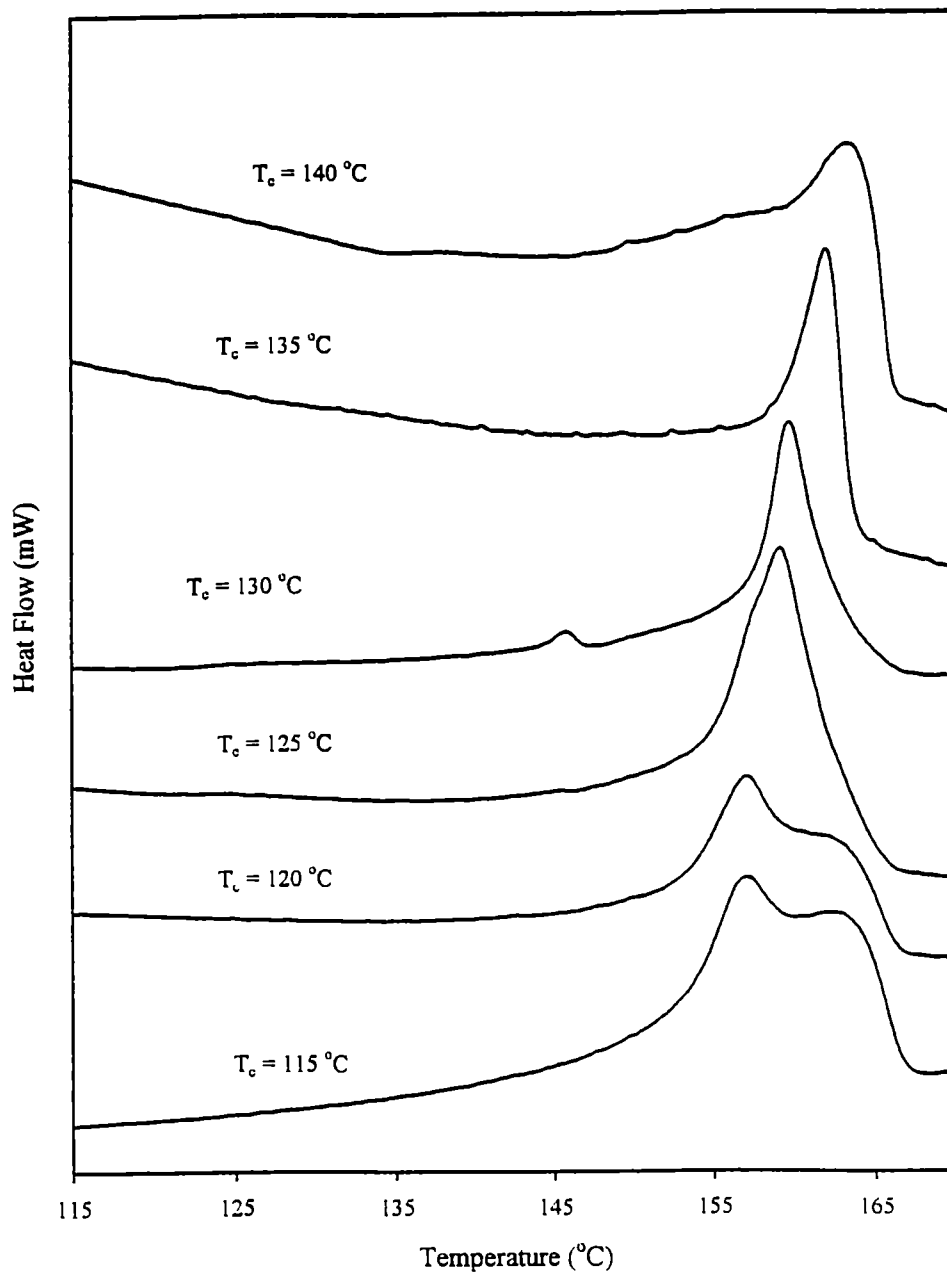
Figure 42: Melting endotherms for specimen FINA at different crystallization temperatures, T_c.
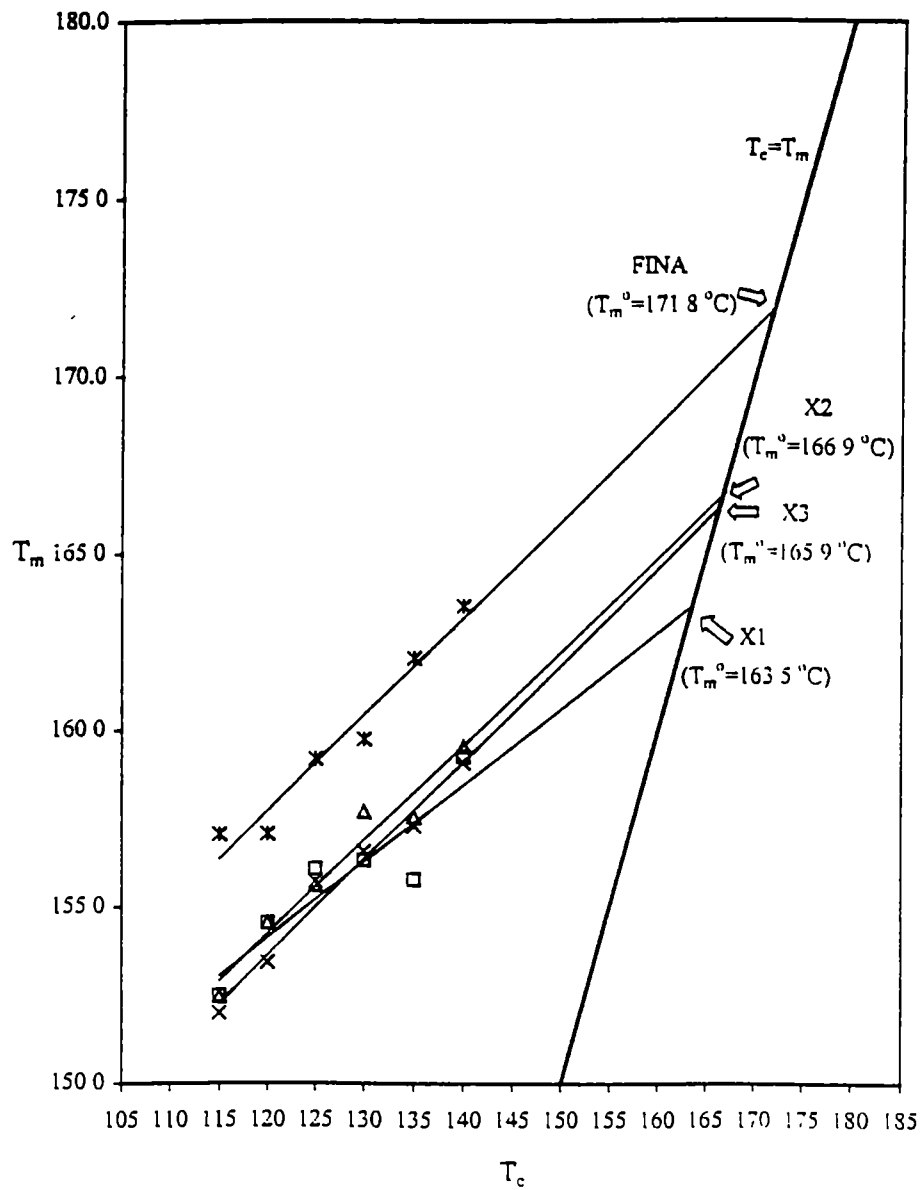
Figure 43: Hoffman-Weeks plots of X1, X2, X3, and FINA specimens from DSC peak values. T_m^o is the equilibrium melting point

Figure 44: Hoffman-Weeks plots of X1, X2, X3, and FINA specimens from DSC return to baseline values. T_m^0 is the equilibrium melting point.

determine the melting points   Equilibrium melting points for each specimen are given in figures 43 and 44 while the DSC melting peak and return to baseline (end of melting) temperatures are presented in tables 8 through 11

4 3 2   Determination of the Onset and End of Melting by DSC

The onset of melting points of the alpha modification for each specimen was determined using the extrapolation method shown in figure 14 on page 61. This was necessary due to the melting of the less stable and imperfect crystals interfering with the more perfect isothermally grown structures   This can be seen in the endotherms as "tailing" at temperatures between the peak melting points of the beta and alpha forms.   Therefore the extrapolation method attempts to measure the onset of melting of the more stable α crystals

The initial onset of melting was taken at that point where the heating curve began to deviate upwardly from the baseline.   These temperatures were taken as the start of melting for the total samples and used to determine the melting ranges The end of melting was taken as that point where the curve returned to the baseline   The onset and end of melting temperatures are presented in tables 8 through 11, along with the temperature difference, ΔT_{DSC} (initial and α peak), used to determine the melting ranges and compare broadness between the α peaks

Table 8: Information from melting studies conducted on specimen X1.

T_c (°C)	DSC Peak (°C)	Initial Onset of Melting (°C) (DSC)	Onset of α peak Melting (°C) (DSC)	End of Melting (°C) (DSC)	ΔT_{DSC} (°C) (Initial)	ΔT_{DSC} (°C) (α peak)	End of Melting (°C) (LDM)	ΔT_{LDM} (°C) (Initial)	ΔT_{LDM} (°C) (α peak)
115	151 5	131 5	145 0	162 0	30 5	17 0	159.0	27.5	14.0
120	154 5	134 2	148 0	162 0	27 8	14 0	160 0	25.8	12.0
125	156 1	125 5	150 0	161 0	35.5	11 0	159 0	33.5	9.0
130	156 3	130 0	145 0	160 0	30 0	15 0	160.0	30 0	15.0
135	155 8	135 0	146 0	161.0	26 0	15.0	163 0	28.0	17.0
140	159 3	141 0	150 0	163 0	22 0	13 0	164.0	23.0	14.0

Table 9: Information from melting studies conducted on specimen X2.

T_c (°C)	DSC Peak (°C)	Initial Onset of Melting (°C) (DSC)	Onset of α peak Melting (°C) (DSC)	End of Melting (°C) (DSC)	ΔT_{DSC} (°C) (Initial)	ΔT_{DSC} (°C) (α peak)	End of Melting (°C) (LDM)	ΔT_{LDM} (°C) (Initial)	ΔT_{LDM} (°C) (α peak)
115	152 5	120 0	148 0	161 0	41 0	13.0	160.0	40.0	12.0
120	154 6	121 5	149 0	162 0	40.5	13.0	162.0	40.5	13.0
125	155 6	126 9	152 0	162 0	35.1	10 0	161.0	34.1	9.0
130	157 7	131 2	153 0	162 0	30 8	9 0	161.0	29.8	8.0
135	157 6	135 5	149 0	162 0	26 5	13 0	162.0	26.5	13.0
140	159 6	141 0	151 0	164 0	23 0	13 0	163.0	22.0	12.0

Table 10: Information from melting studies conducted on specimen X3

T_c (°C)	DSC Peak (°C)	Initial Onset of Melting (°C) (DSC)	Onset of α peak Melting (°C) (DSC)	End of Melting (°C) (DSC)	ΔT_{DSC} (°C) (Initial)	ΔT_{DSC} (°C) (α peak)	End of Melting (°C) (LDM)	ΔT_{LDM} (°C) (Initial)	ΔT_{LDM} (°C) (α peak)
115	152 0	124 0	146 0	162 0	38 0	16 0	161.0	37.0	15.0
120	153 4	132 0	146 0	162.0	30 0	16 0	160.0	28.0	14.0
125	155 7	126 0	152 0	162 0	36 0	10 0	159.0	33.0	7.0
130	156 6	130 0	150 0	161 0	31 0	11.0	159.0	29.0	9.0
135	157 3	136 0	149 0	162 0	26 0	13 0	161.0	25.0	12.0
140	159 1	140 0	148 0	164 0	24 0	16 0	166 0	26.0	18.0

Table 11: Information from melting studies conducted on specimen FINA

T_c (°C)	DSC Peak (°C)	Initial Onset of Melting (°C) (DSC)	Onset of α peak Melting (°C) (DSC)	End of Melting (°C) (DSC)	ΔT_{DSC} (°C) (Initial)	ΔT_{DSC} (°C) (α peak)	End of Melting (°C) (LDM)	ΔT_{LDM} (°C) (Initial)	ΔT_{LDM} (°C) (α peak)
115	157.1	134 4	151 0	168 0	33.6	17.0	174.0	39.6	23.0
120	157 1	139 8	151 0	167 0	27.2	16.0	174.0	34.2	23.0
125	159 2	140 0	153 0	166 0	26 0	13.0	172.0	32.0	19.0
130	159 8	141 0	156 0	166 0	25.0	10 0	174.0	33.0	18.0
135	162 0	145 0	157 0	165 0	20.0	8.0	172.0	27.0	15 0
140	163 5	147 0	155 0	168 0	21.0	13.0	174 0	27.0	19.0

4.3 3 Determination of the End of Melting by LDM

The end of melting points for each specimen were taken as that point of the melting curve that returned to the baseline as observed from the plot taken by the LDM apparatus. These curves are presented in figures 45 through 48 Tables 8 through 11 also present the end of melting points for each specimen, along with ΔT_{LDM} (initial and α peak) The ΔT_{LDM} was determined as the difference between the return to the baseline points taken from LDM and the initial and α peak melting onsets By this procedure, the melting ranges obtained from the LDM apparatus was compared with the ranges from the DSC
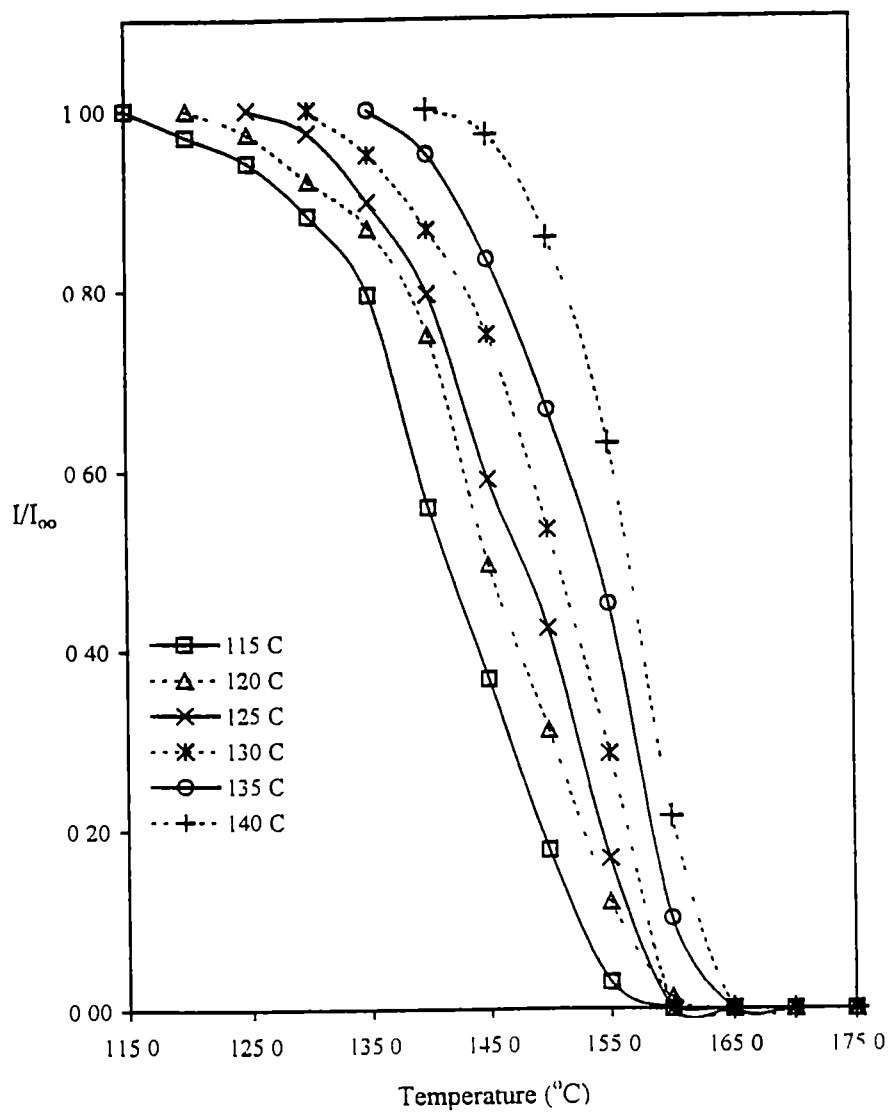
Figure 45: Melting curves of specimen X1 obtained by LDM
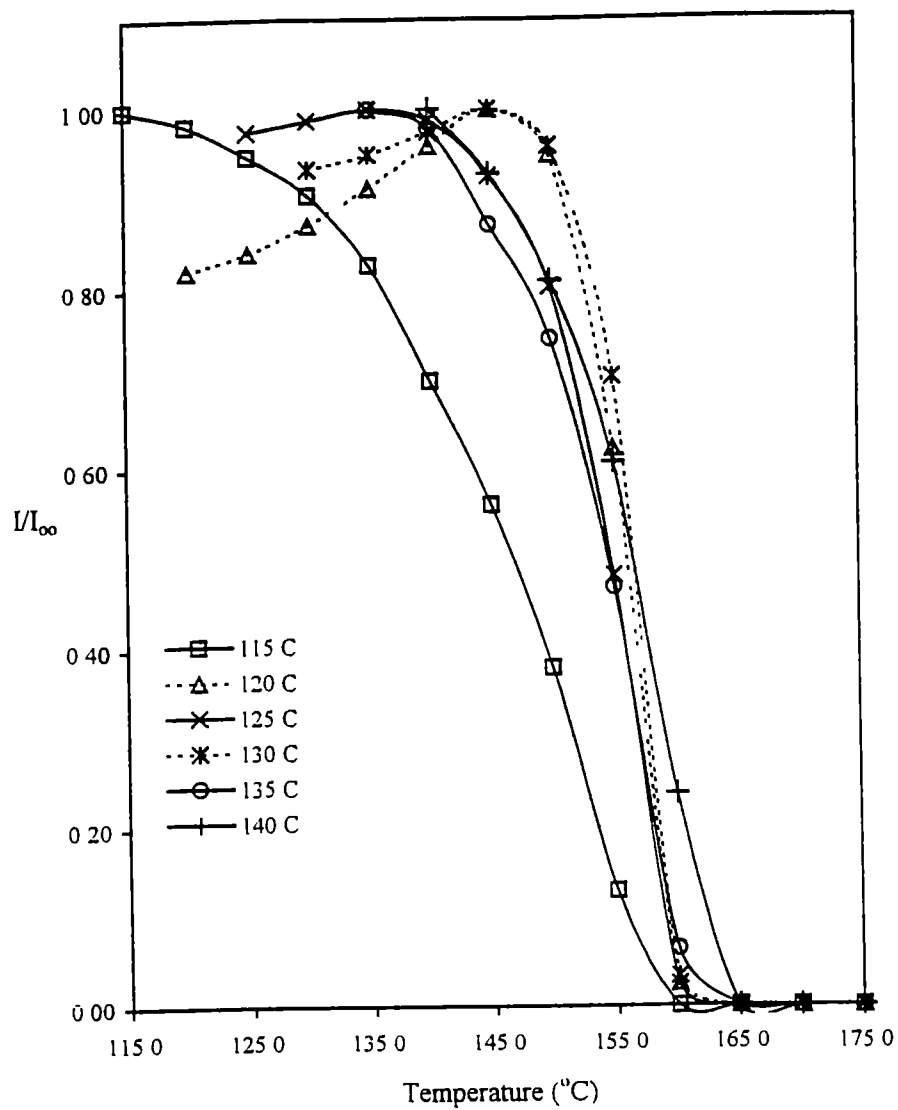
Figure 46: Melting curves of specimen X2 obtained by LDM.
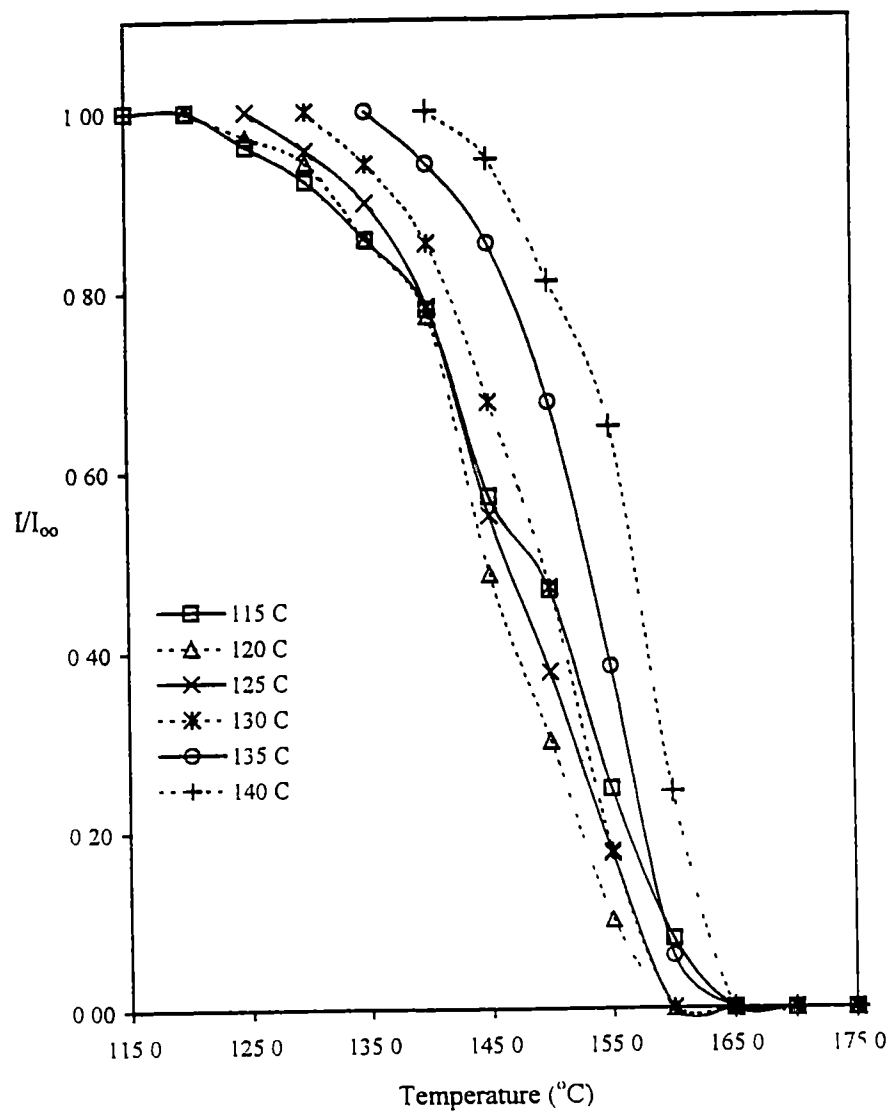
Figure 47: Melting curves of specimen X3 obtained by LDM
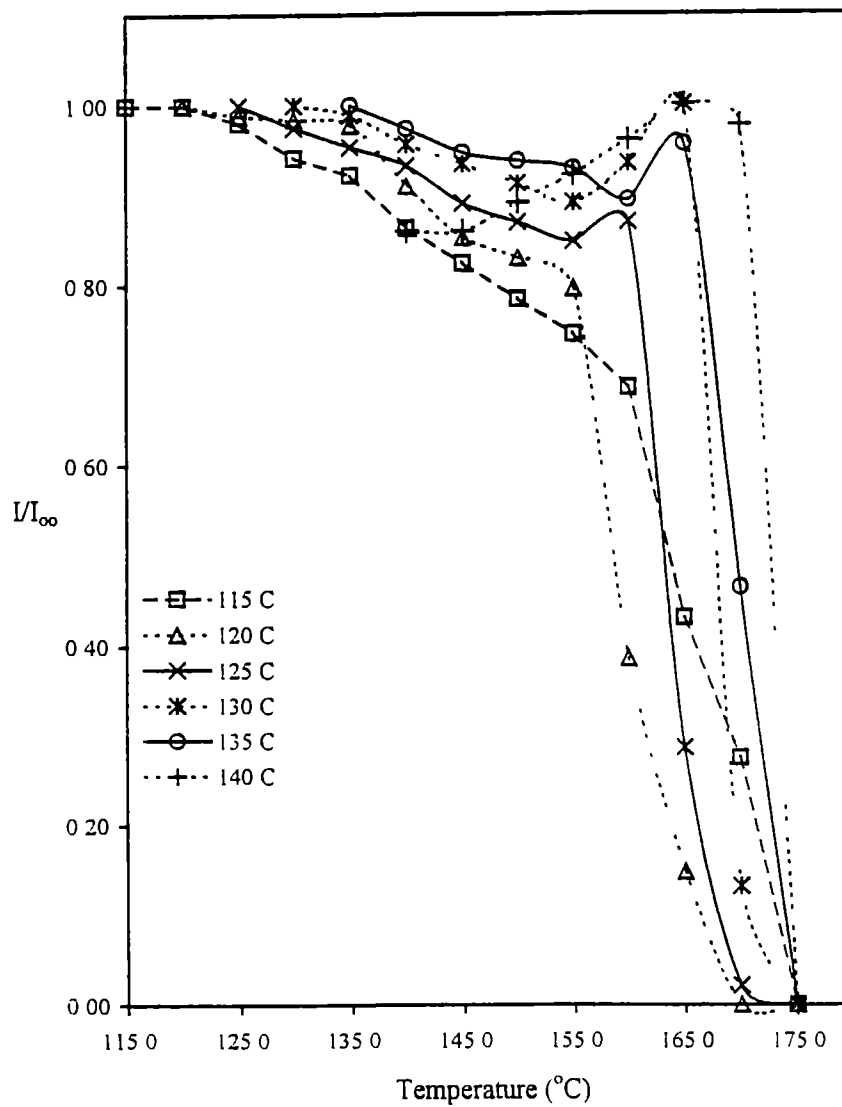
Figure 48: Melting curves of specimen FINA obtained by LDM.

Chapter 5

<u>Discussion</u>

5.1   <u>The Effects of Branching on the MFR Values</u>

Specimen information provided by the manufacturer was in the form of melt flow rates, MFR, taken before and after irradiation In the case of the FINA comparative specimen, only one MFR value was provided This information is contained in table 3 on page 56

The MFR is the measure of the extrusion rate of a molten polymer through a die The measurements are carried out under a constant temperature and load The die is of a specific length and the material is extruded through the barrel of the apparatus by a piston moving at a constant velocity. The amount of extrudant within a certain time period is taken as the rate of flow of the resin and is usually given in units of decagrams per 10 minutes (ASTM D 1238-98, 1998). Therefore, MFR can be thought of as the rate at which a certain mass of material in a molten polymer flows and, in a qualitative sense, can be considered inversely proportional to viscosity. For linear polymers, an increase in the molecular weight will produce a decrease in the MFR value while increasing the viscosity value. Conversely, a lower molecular weight specimen will have a higher MFR and a lower viscosity (R Phillips, 1999).

Adding branches onto a linear polymer chain would seemingly increase the molecular weight of the polymer, thus decreasing the MFR and increasing viscosity. For the X1, X2 and X3 specimens, and branched specimens via

irradiation paths studied previously, this is not the case. As seen in table 3, MFR values are higher for the final product when compared to the virgin material. The effects of this phenomenon have been extensively studied (Charlesby, 1955; Shultz et al , 1956, Black and Lyons, 1957, Zimm and Kilb, 1959, Kilb, 1959; Black and Lyons, 1959; Salovey and Dammont, 1963; Marans and Zapas, 1967)

When irradiating isotactic polypropylene with low levels of radiation and in certain environments, both chain scissions and branching take place simultaneously. This is true up to the gel point where cross-linking predominates It is generally observed that the degree of branching increases with radiation dose until the specimen reaches the gel point and, as per Black and Lyons (1959), could be reached at a dose of about 50 Mrad.

The phenomenon of decreasing intrinsic viscosity, $[\eta]$, and, consequentially, increasing MFR due to increasing branching may be explained by the following scenario, with the assumption that the original specimen consists of linear polymer chains. At the lowest radiation doses, the predominant reaction is that of main chain scissions with some branching. The slight decrease in $[\eta]$ is the result of the decrease in the weight average molecular weight and small amount of branches being added to some of the original linear chains. As the dosage gradually increases, the degree of scissions and branching becomes greater leading to further molecular weight reduction until the overall molecular weight begins to increase due to branching becoming the predominant reaction. Although the molecular weight is now increasing, the viscosity still tends to decrease This can be explained in terms of free volume.

In a polymer sample with predominantly linear chains, the packing of the chains will be much greater than with chains having branches. Steric hindrances produced by branches will cause the chains of these macromolecules to pack more loosely, lowering its density. Therefore the free volume in a volumetric segment of the linear sample will be much less than an equivalent segment of the branched sample. This would lead to more polymer chains per volume in the linear specimen than the branched one. Since viscosity is affected by the amount of mass in a volume of the solution, it would seem reasonable that due to more efficient packing, the linear chain sample would entail more mass, or chains, per volume than a branched sample similar in molecular weight. Thus, due to the greater amount of free volume, the branched specimen would have a lower [η]. The MFR would be increased because the amount of molten resin passing through the die per unit time would be greater simply due to the increasing freedom of flow produced by an increasing amount of free volume created by the branches. The study by DiNicola et al. (1992) of the effects of radiation on isotactic polypropylenes with varying initial molecular weights seems to support this theory.

According to table 3, the MFR values of the specimens studied increase in the following order X2 < X1 < X3, with X3 having the highest final MFR. The FINA sample has a MFR of 8 dg/10 min. This high MFR value is due to it being a lower molecular weight sample, since lower molecular weight specimens will have a faster flow rate. It should also be noted that the X2 specimen seemed to

have a yellowish discoloration This is indicative of a polypropylene being irradiated in an atmosphere where oxygen is present Oxygen enhances main chain degradation, therefore, the X2 specimen is considered the more degraded of all the samples tested The assumption will also be made that since no visible discoloration of the X1 and X3 samples was observed, these samples were irradiated in an atmosphere where the oxygen content was low enough to have a minimal degradation effect. Isotactic polypropylene irradiated by e-beams are usually treated in a nitrogen atmosphere to reduce oxidative degradation (Scheve et al., 1990)

5.2 Half-time of Crystallization Values, Mode of Nucleation, and Avrami Analysis

Below is a discussion of the results obtained through crystallization studies.

5 2 1 Half-time of Crystallization Values

As mentioned above, the half-time of crystallization, $t_{1/2}$, of a polymer crystallized from the melt can be manipulated through equation 10 to obtain the growth rate constant, k, of the spherulite at a given crystallization temperature In a truly comparative study the reciprocal of $t_{1/2}$ can be taken as the crystallization rate without knowing the value of the Avrami constant n.

The half-time of crystallization values for the specimens are given in table 4 and figure 49 is a plot of $\ln(t_{1/2})$ versus the crystallization temperature, T_c Examination of the data indicates that at the highest supercooling, $T_c = 115\ ^\circ C$, the crystallization half-times tend to be approximately the same for each specimen. It has been shown through numerous studies that increasing the supercooling, within a certain range of temperatures, will increase the nucleation density With the increase in primary nucleation, the time for impingement of the nuclei will be shorter, thus decreasing the time of growth in the radial direction This is obviously the effect seen at the lower temperatures Figure 49 also shows that at the higher crystallization temperatures a marked increase in $t_{1/2}$ occurs, albeit at different magnitudes for each sample Of all the specimens, it seems that $t_{1/2}$ for X2 is smaller than the rest, while X3 seems to have half-time values similar to the non-irradiated FINA sample The X1 specimen has greater half-time values than X2 but less than the other two specimens.

The vast differences in the $t_{1/2}$ values can be explained in terms of nucleation density Figures 50 through 53 are photographs of the specimens' spherulites after complete crystallization at 120 $^\circ C$. Measurements were taken of the various structures by use of a slide micrometer with divisions of 0 01 mm. The average diameters of the spherulites are as follows X1-0 0558 mm, X2-0 0529 mm, X3-0 0689 mm, and FINA-0 1310 mm The diameter ranges are as follows· X1-0.0400 to 0 0700 mm, X2-0 0400 to 0 0650 mm, X3-0 0500 to
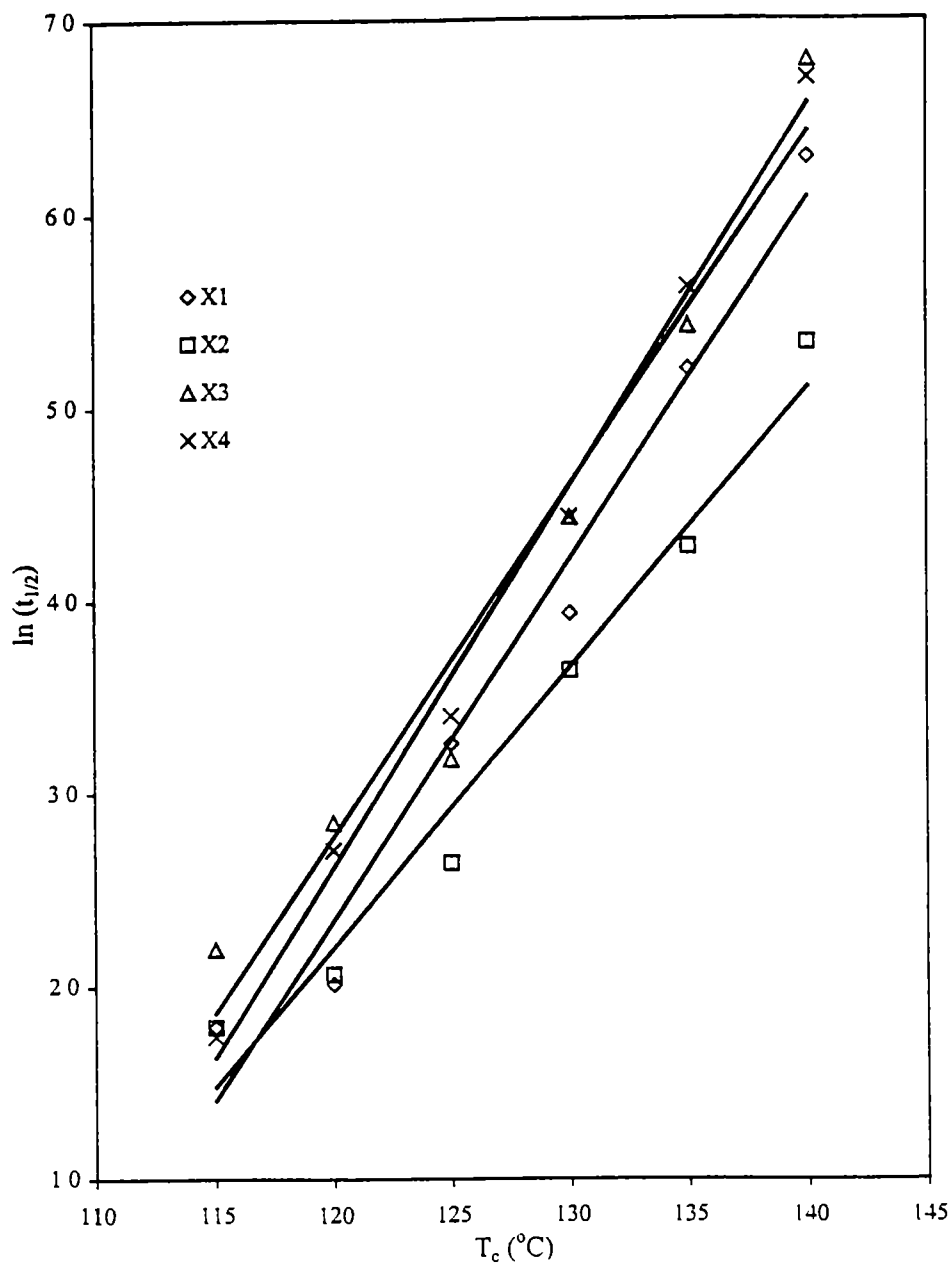
Figure 49: Plot of ln ($t_{1/2}$) versus crystallization temperature (T_c) for each specimen.
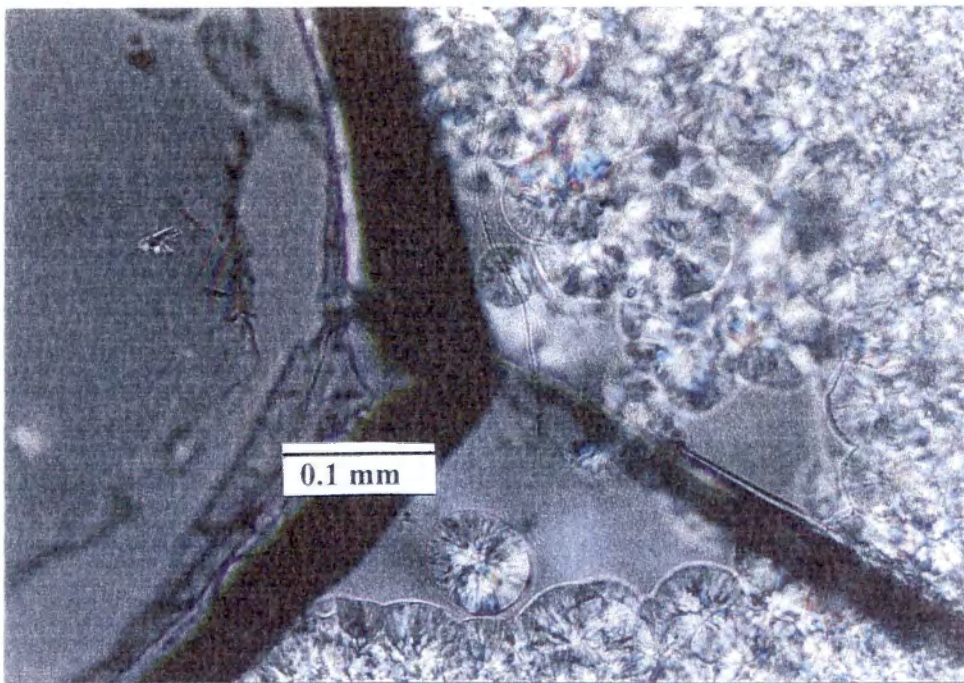
Figure 50: Photograph of spherulites from the X1 specimen (20X).
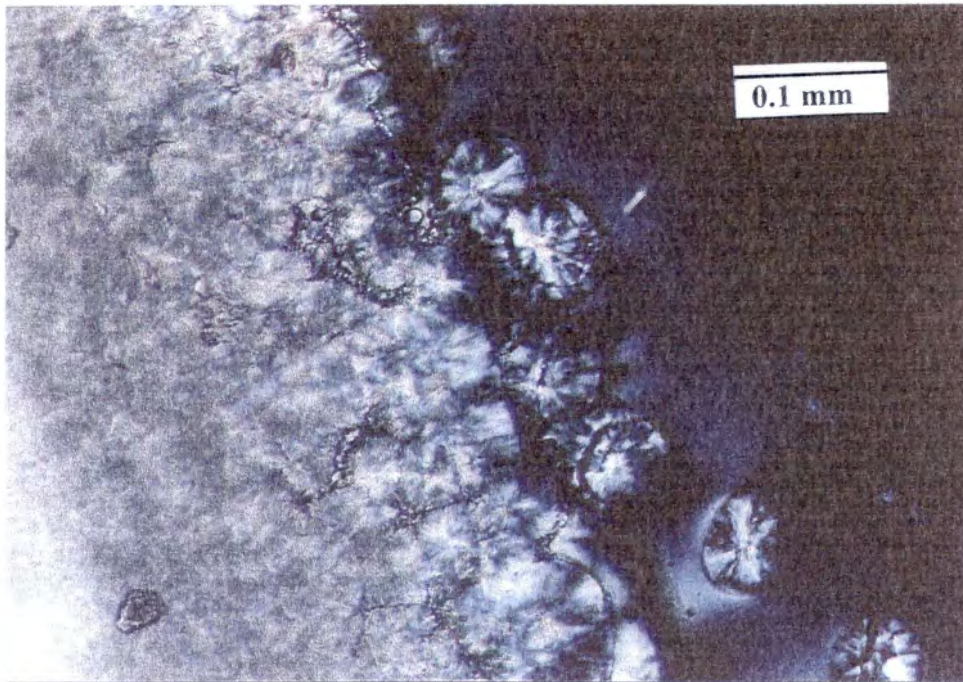
Figure 51: Photograph of spherulites from the X2 specimen (20X).

Figure 52: Photograph of spherulites from the X3 specimen (20X).
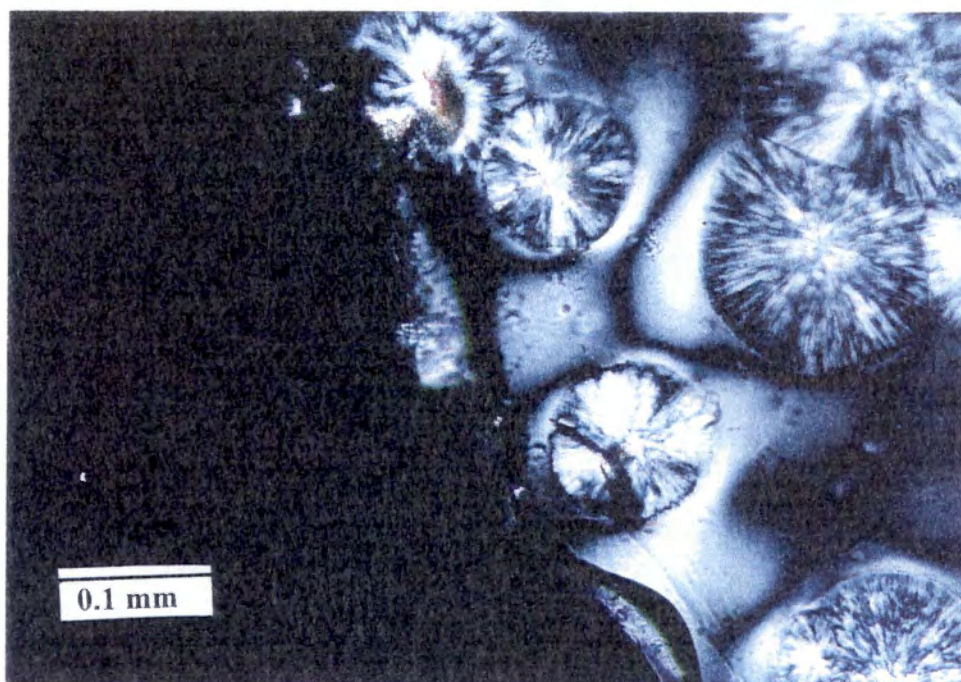
Figure 53: Photograph of spherulites from the FINA specimen (20X).

0.0900 mm, and FINA-0.1000 to 0.1900 mm. It can be postulated that the size of the spherulites will determine the nucleation density in a given area of material Therefore the specimen with the lowest nucleation density is the untreated FINA sample and the X2 specimen appears to have the highest density. The nucleation density increases as follows· FINA<X3<X1<X2

From studies conducted by Nedkov and his colleagues (Nedkov et al, 1991), an increase in radiation dose produced an increase in primary nucleation, as a result of scission reactions, hence increasing the nucleation density. On the other hand, a study by Cheung (Cheung et. al., 1996) suggested that branching in iPP had a negative effect on nucleation, decreasing the nucleation rate, ultimately decreasing the nucleation density. In light of these two studies it would seem that the X2 specimen has the least amount of branching X1 has slightly greater average spherulite diameters, suggesting that it may have a branched to linear chain ratio greater than in X2. Of all the irradiated samples, X3 appears to have the least nucleation density, suggesting that the number of branches is greater than in the other two specimens and is affecting the rate of nucleation. The FINA sample had average spherulite diameters roughly one order of magnitude larger than the treated specimens. This would suggest that the nucleation density is far less than in the other samples

Wunderlich (1976) theorized that during crystallization from the melt polymer spherulites undergo segregation, where the larger molecules crystallize first. The smaller molecular species are rejected and will crystallize later in the process. Bartczak (Bartczak et al., 1986) suggested that the rejection of lower

molecular weight species depressed the growth rate of the spherulite considerably Irradiating a polymer will produce chains with varying molecular weights due to random scission of the main chains and random placements of branches of varying lengths Therefore, it would seem that the distribution of molecular weights is narrower in X2 than in either X1 or X3 because the $t_{1/2}$ values are smaller. With increasing branching, the distribution broadens, slowing down the crystallization rate. This would suggest that the branching in X3 is much greater than in X1, since the $t_{1/2}$ values are greater. The $t_{1/2}$ values for the FINA specimen could be due solely to the fact that the fewer nuclei will have a greater distance to travel during growth to reach impingement, thus increasing crystallization times

5 2 2   Mode of Nucleation

The mode of primary nucleation in polymers is of two types, being classified as either homogeneous or heterogeneous In homogeneous nucleation the rate of nuclei formation is not constant resulting in the formation of new crystals growing at different times throughout the isothermal crystallization. Heterogeneous nucleation occurs from preexisting surfaces in the melt and is characterized as having a constant number of nuclei giving rise to a constant number of spherulites growing in a certain temperature range Studies, such as the one on nucleated iPP by Binsbergen and De Lange (1970), have shown that the heterogeneous mode of primary nucleation is the rule for polypropylene

Furthermore, Wunderlich (1976) points out that heterogeneous nuclei occur approximately between 10 °C to 70 °C under the melting point, while below this range the homogeneous mode is dominant.

The isothermal crystallization temperatures used for the samples in this research were within the range specified by Wunderlich as being optimal for heterogeneous nucleation Examination of figures 24 and 25 tend to support this notion The plot of ln $(t_{1/2})$ versus $\frac{1}{T\Delta T}$ shows the curves of all the specimens to be linear while the plot of ln $(t_{1/2})$ versus $\frac{1}{T\Delta T^2}$ shows these curves to be non-linear. According to the Ross and Frolen method mentioned above, this proves that the mode of nucleation for these samples within this specific range of temperatures is of the heterogeneous type

5.2 3   The Avrami Constants

Figures 15 through 18 are the crystallization curves obtained from each specimen at the specified crystallization temperature With the exception of the X2 sample at $T_c = 120$ °C and 130 °C, these plots show the typical S shaped curve obtained through isothermal crystallization studies by the LDM method. Furthermore, these curves may be superimposed by a mere shift in the T_c axis Figures 20 through 23 were used to find the Avrami constant, n, values given in table 5 These values range from a low of 1 0 to a high of 2 9 Average values for the specimens are as follows 2 2 for specimens X1 and X3, 2 3 for the FINA specimen, and 2 5 for sample X2

An n value of 3 0 is the theoretically correct value for the three dimensional growth geometry of a sphere in the heterogeneous nucleation mode An n value of 2 is the correct value for disks, while 1 represents growth of rods Therefore, the values obtained in this paper seem to suggest that the crystal structures grew in the shape of disks Many studies using the LDM or dilatometry methods yield values in the range of 3 to 4 However, studies taken by DSC have been known to give values in the 2 0 range A DSC experiment by Bogoeva-Gaceva (Bogoeva-Gaceva et al , 1998) gave n values in the range of 1 93 to 4 39 for iPP specimens with a degree of crystallinity from 41% to 48 9% Godovsky and Slonimsky (1974) also found different values using different methods The reason for the low n values obtained from these specimens could be due to the fact that the spherulites were grown between two glass slides, "flattening" the structures during their evolution If this hypothesis were correct, the thin films would have a thickness much less than the diameters of the species Therefore, the film thicknesses were measured by use of a micrometer The measurements showed that the thickness of these films were comparable to the diameters, meaning the structures should indeed have n values of 3 However, it was observed in photographs taken of the spherulites that the crystal structures were lying on top of each other in layers. It was impossible to make the films so thin as

to be one layer thick. This would suggest that film thickness could be caused by multi-layers of spherulites, not from individual spherulites growing in spherical geometries Therefore, other theories must be investigated

Other reasons for the low n values obtained from the specimens are related to radiation effects and/or structure of the chain. Wenxiu and Shui (1993) found that irradiating a sample of iPP lowered the Avrami exponent value from 3.36 to 2 36 They theorized that the increasing crosslinks, or branches, resulting from the treatment retarded the growth, leading to the lower value. Janimak, et al (1992) presented data suggesting that the isotacticity of the polymer may affect the n value Their study showed a decrease in n as the isotacticity increased They believed this to indicate that the three dimensional development of the crystal texture was influenced by the stereoregularity of the specimens This could certainly be reconciled with the data taken from the specimens in this research, since the degree of isotacticity was found to be greater than 99% for all samples studied.

Still another factor affecting the Avrami exponent could be the phenomenon of secondary crystallization. This is the process of the crystallization of the stereoirregular molecules and chains of lower molecular weight trapped in the melt between the radially growing crystals This process happens after the radial growth of the spherulite is complete In Janimak's study mentioned above (Janimak, et al , 1992) the slopes of the curves taken from the plots of log $[\ln(1-\chi(t))]$ versus log t for some samples drastically decreased at higher T_c's Recalling the deviation from the typical S shape of specimen X2 at

T_c's of 120 °C and 130 °C, figure 21 does show a drastically decreasing slope This is clearly due to secondary crystallization and is probably not observed in the other specimens because the growth rates of the spherulites were slow enough that the phenomena was not observed by the apparatus It is recalled that the time for the X2 spherulites to reach impingement was extremely fast when compared to the other specimens Impingement effectively ends the radial growth of the spherulite and if there is an amount of material between these crystals they will grow in the transverse direction. The speed at which the radial crystals of the spherulite reached impingement made allowance for the crosshatched portion to be observed This could also be the reason why the n values for the other specimens are lower than in other literature Although not distinguishable, possibly due to the sensitivity of the system and the slower rate of crystal growth, secondary crystallization must be taking place if there is an appreciable amount of the α or γ modification in the samples.

5.2 4   Spherulite Growth Rate Constants

Tables 12 through 15 present the growth rate constants, k, calculated using the n values from this research, the theoretical value of $n = 3$, and using only the value of the reciprocal of the half-time of crystallization Where applicable, equation 10 was used It is observed that k for all the specimens tend to decrease with decreasing supercooling, possibly due to the decrease in the number of nuclei It is also noticed that k using the extrapolated n and theoretical n are in

Table 12: Spherulite growth rate constants for the X1 specimen

T_c ($^\circ$C)	k (n extrapolated)	k (k = $1/t_{1/2}$)	k (n=3)
115	7 83e^{-3}	1 66e^{-1}	3 21e^{-3}
120	1 84e^{-2}	1 33e^{-1}	1 64e^{-3}
125	5 01e^{-4}	3 85e-^{2}	3 94e^{-5}
130	2.66e^{-4}	1 96e^{-2}	5 23e^{-6}
135	6 83e^{-6}	5 56e^{-3}	1.19e^{-7}
140	5 96e^{-7}	1.85e^{-3}	4 40e^{-9}

Table 13: Spherulite growth rate constants for the X2 specimen

T_c (°C)	k (n extrapolated)	k (k = $1/t_{1/2}$)	k (n=3)
115	$1\,30e^{-2}$	$1\,66e^{-1}$	$3\,21e^{-3}$
120	$2\,14e^{-3}$	$1\,27e^{-1}$	$1\,41e^{-3}$
125	$9\,45e^{-4}$	$7\,14e^{-2}$	$2.53e^{-4}$
130	$4.80e^{-4}$	$2\,63e^{-2}$	$1\,26e^{-5}$
135	$2\,85e^{-6}$	$1.39e^{-2}$	$1.86e^{-6}$
140	$1\,12e^{-6}$	$4\,83e^{-3}$	$7\,81e^{-8}$

Table 14: Spherulite growth rate constants for the X3 specimen

T_c (°C)	k (n extrapolated)	k (k = $1/t_{1/2}$)	k (n=3)
115	$1\ 33e^{-2}$	$1\ 11e^{-1}$	$9\ 51e^{-4}$
120	$2.33e^{-3}$	$5\ 78e^{-2}$	$1\ 34e^{-4}$
125	$2\ 46e^{-4}$	$4.17e^{-2}$	$5\ 01e^{-5}$
130	$9\ 82e^{-5}$	$1\ 19e^{-2}$	$1\ 17e^{-6}$
135	$4\ 63e^{-6}$	$4.44e^{-3}$	$6\ 09e^{-8}$
140	$2.93e^{-8}$	$1\ 12e^{-3}$	$9\ 80e^{-10}$

Table 15. Spherulite growth rate constants for the FINA specimen

T_c (°C)	k (n extrapolated)	k (k = $1/t_{1/2}$)	k (n=3)
115	$4\ 57e^{-3}$	$1.75e^{-1}$	$3\ 74e^{-3}$
120	$3.08e^{-3}$	$6\ 67e^{-2}$	$2.05e^{-4}$
125	$3\ 90e^{-4}$	$3.33e-^2$	$2\ 57e^{-5}$
130	$1\ 82e^{-6}$	$1\ 19e^{-2}$	$1.17e^{-6}$
135	$2\ 80e^{-5}$	$3\ 62e^{-3}$	$3\ 30e^{-8}$
140	$1\ 06e^{-6}$	$1\ 23e^{-3}$	$1\ 30e^{-9}$

much closer agreement than using only the reciprocal half-time This confirms that there is indeed a dependence on n for crystal growth and that the reciprocal half-time values should only be used in a qualitative manner.

5.3   Structural Analyses and Degree of Crystallinity

The following is a discussion of results obtained through WAXD in the reflection and transmission modes

5 3 1   Structural Analyses

Figures 30 through 33 are the WAXD diffratograms of the specimens studied in the reflection mode. These show that the predominant crystal structural is of the α type However, the β form of iPP shows up in the spectra of the X1 and X3 samples, mostly in the 115 °C to 125 °C degree range. The γ structure seems to be more prevalent in the X1 and FINA samples. Degrees of disorder in a crystalline material can be observed from x-ray patterns by the lack of "smoothness" of the pattern lines This could be caused by degradation of the thermal or radiational types, or a consequence of branching Increasing disorder in materials has been known to produce patterns of increasing "jagged" nature. The x-ray patterns seem to show amounts of disorder in the increasing order X2<X1<X3<FINA. The FINA sample, since assuming it to be a non-irradiated specimen, could possibly attribute its degradation to that of the thermal nature, while the other specimens may exhibit varying amounts of scission and branching due to the different doses of radiation received

The beta modification has been known to be relegated to the surface of a thin film isothermally crystallized from the melt (Krestev et al, 1988). Therefore, WAXD patterns were run in the transmission mode to determine if the β spherulites resided on the surface, being a product of surface orientation created by the thin film production process, or if it was in the sample through and through Since the samples were so thin that individual sections had to be placed one on another, the results may be suspect With this in mind, figures 34 and 36 may show some β modifications being formed at some of the crystallization temperatures. Figures 54 through 56 are photographs of the various spherulite types observed under a polarizing microscope.

Another benefit of running the samples in the transmission mode is to determine the reason the peaks at approximately $2\theta = 14.5°$ were consistently lower than the ones at approximately $2\theta = 17.5°$, as shown in the reflection patterns In the ideal alpha isotactic polypropylene the former should have a higher intensity than the latter. The transmission spectra do show the correct pattern, meaning that the reflection patterns were a product of surface orientation and not a change in any structural factors as a consequence of irradiation

5.3.2 Degree of Crystallinity

The reflection mode of the WAXD was used to determine the degree of crystallinity of each specimen at the specified crystallization temperatures and are given in figures 30 through 33. These values were compared to observe the effects branching had on the crystalline phase of the polymers The
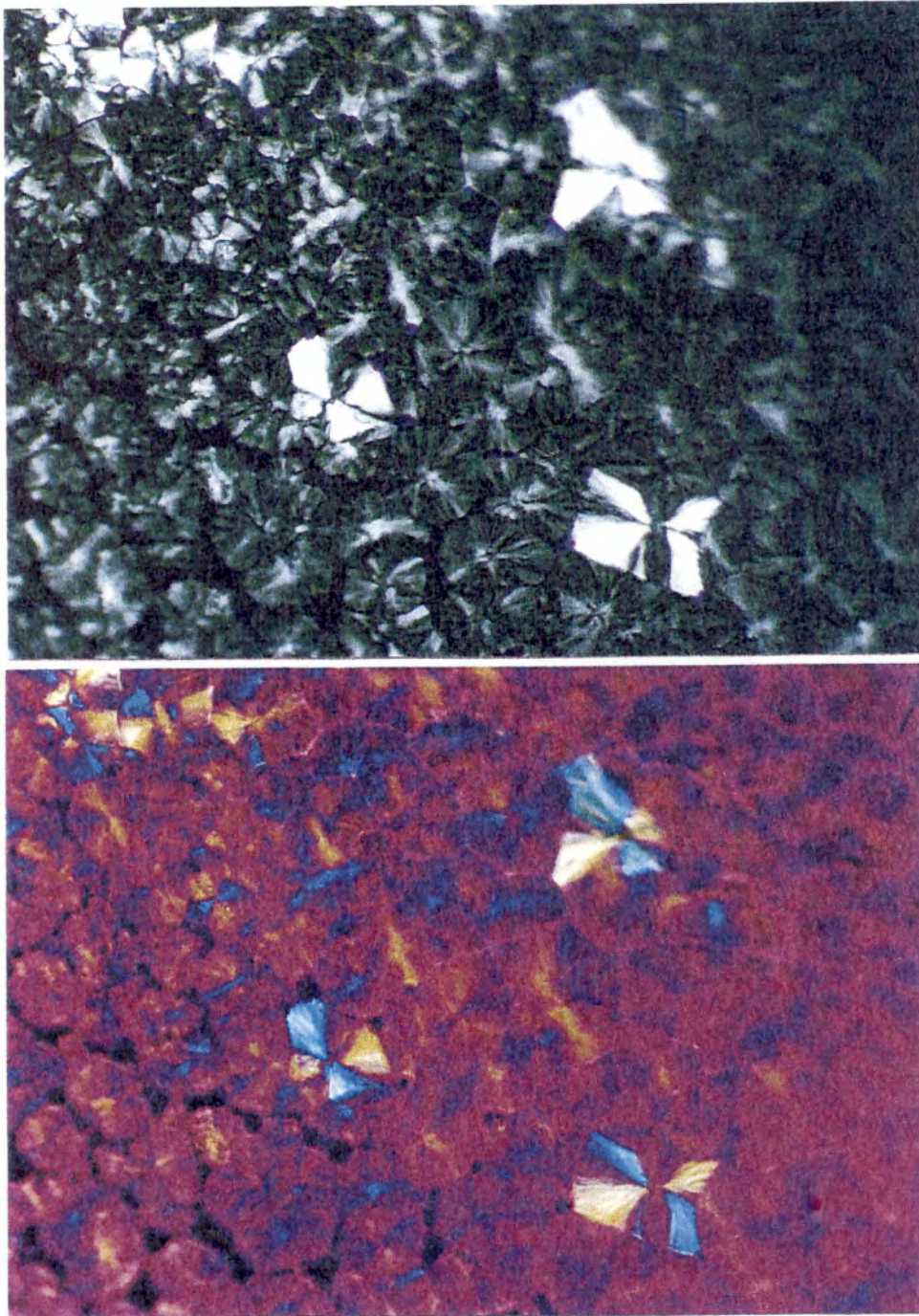
Figure 54: Photograph of the beta spherulites amongst the predominantly mixed alpha spherulites of the X1 specimen.
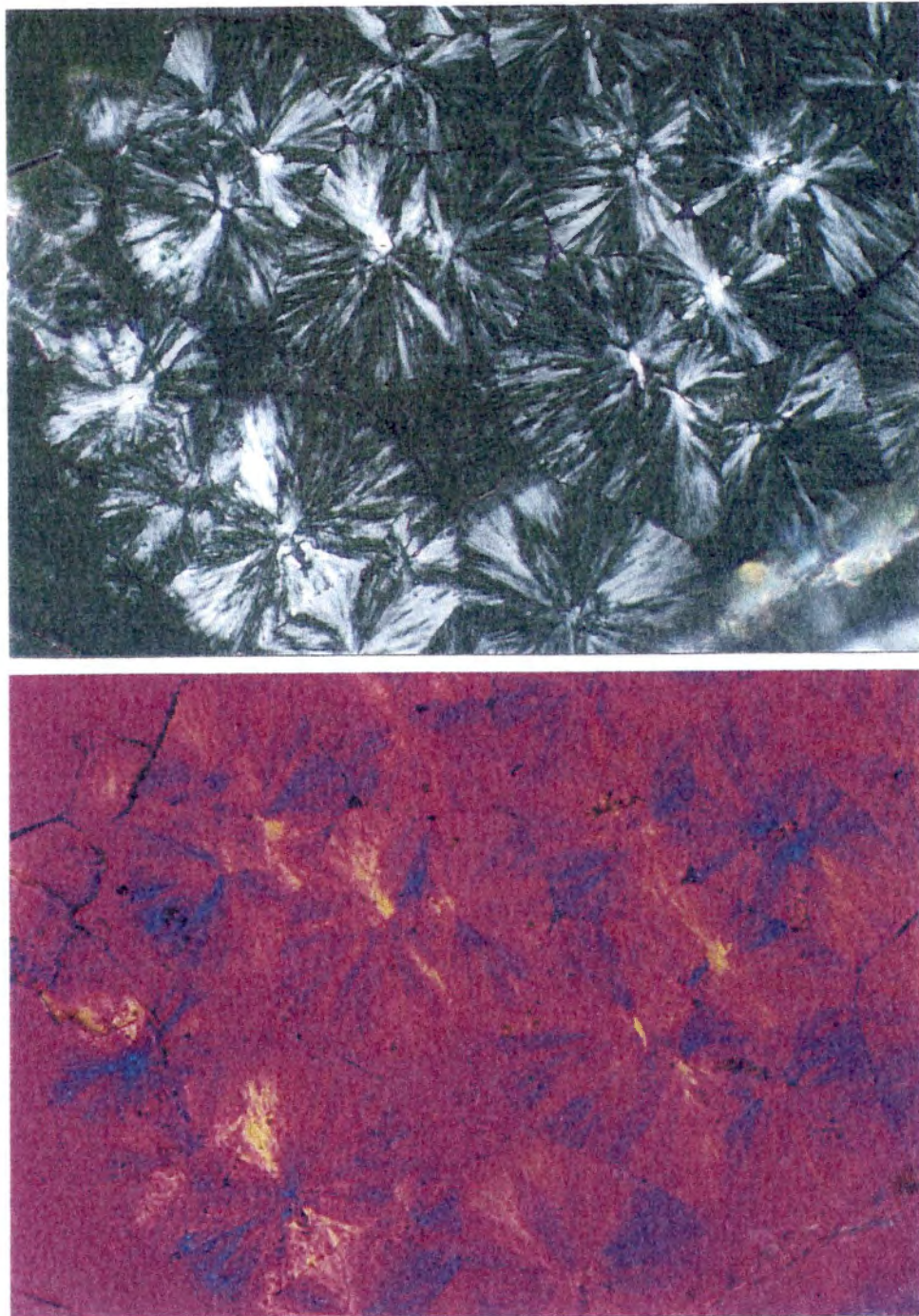
Figure 55: Photograph of the predominantly mixed alpha spherulites of the X2 specimen.
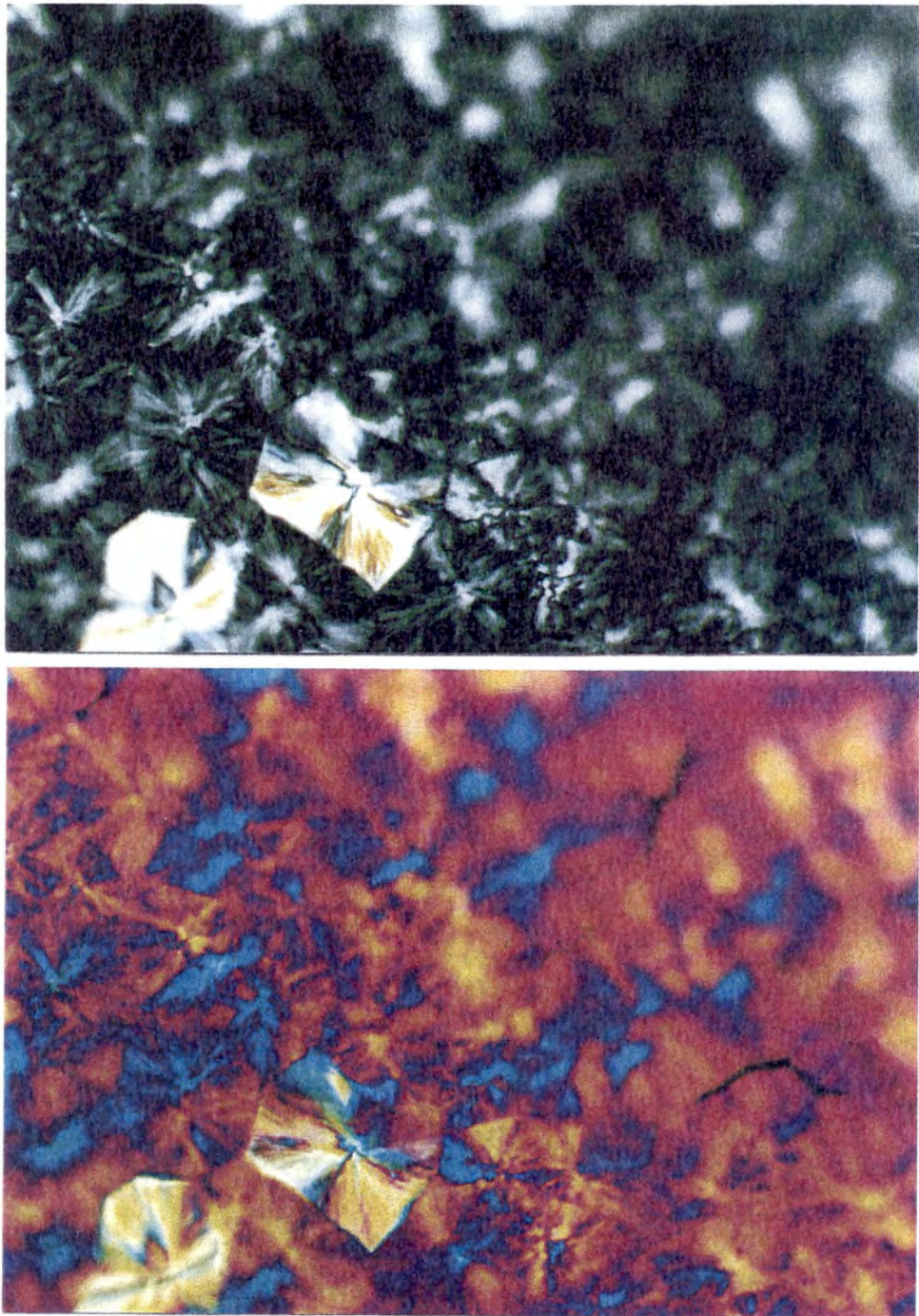
Figure 56: Photograph of the beta spherulites amongst the predominantly mixed alpha spherulites of the X3 specimen.

percent crystallinity in increasing order follows X3<FINA<X1<X2. With the knowledge that branches, cross-links, and other "defects" are relegated to the amorphous part of a semi-crystalline polymer, this tends to suggest that specimen X2 has the least amount of branching, followed by X1, while X3 has the greatest amount of branches on its linear chains. The low percent crystallinity value of the FINA sample might be attributable to thermal degradation producing an amount of low molecular weight species being rejected by the crystals The unusually high crystallinities at the lower crystallization temperatures observed for some of the specimens were disregarded, attributed to errors in crystalline phase segregation due to the disordered nature of the patterns

5.4   Melting Studies and Equilibrium Melting Point Determination

The following is a discussion of results obtained from the DSC and LDM studies.

5 4 1   Melting Studies Obtained by DSC

Figures 39 through 42 are the endotherms of the specimens at the specified T_c's The small peaks around the 140 °C to approximately 145 °C are attributed to the melting of the β modification (Mezghani and Phillips, 1995) These peaks can be seen in the X1 and X3 specimens crystallized at T_c = 115 °C through 125 °C and for the X2 specimen crystallized at 115 °C and 120 °C Since these samples are highly nucleated, the β modification is probably a consequence of the nucleating agent(s) used The small peak observed in the FINA sample at T_c =

130 °C is also probably due to the β modification This sample was assumed to not be highly nucleated, therefore the β peak is most likely due to stresses induced in the sample when making the thin films and probably resides only on the surface (Krestev et al., 1989) The transmission WAXD patterns seem to confirm this

At the highest supercoolings, broad and twinned peaks are observed When the twinned peaks are observed, the first melting peak is the one corresponding to the actual crystal formed under isothermal conditions, while the second peak is due to the melting of crystals recrystallized from the melt This recrystallization is a process increasing the order in spherulites, making them more stable (Tigani et al, 1996) Broadening of the peaks can be attributed to less perfect crystals, varying in size and stability, melting at temperatures lower than the more stable structures.   Burfield and Kashiwa (1985) found similar results from LLDPE and Brady and Thomas (1988) found that the melting peak breadths increased as the branch content increased in LLDPE. Yoshii and his colleagues (Yoshii et al., 1995) found that melting peaks broadened due to considerable degradation The endotherms coresponding to the α peak of specimens X1 and X3 seem to show, on the average, broader peaks than the α peak of X2, which itself gave a broader peak than the FINA sample Therefore it is postulated that specimens X1 and X3 have more crystal defects, such as branches, and the broadening of the alpha peak in the X2 and FINA samples is the result of degradation, by scission and thermal processes Tables 8 through 11 present the temperature ranges between the onset and end of melting points for each α peak and the specimen as a whole. The ΔT_{DSC} (α peak) values are used to

compare the peak widths, while the Δ T$_{DSC}$ (Initial) values are used as an indicator of the melting range for the specimens as a whole   The broadening of the α peaks has been discussed above. Therefore, the following discussion will be limited to the melting range of the samples   All samples treated with e-beam radiation melt within the range of 145 °C to 164 °C   The untreated FINA specimen's range shifted upwardly in the range of 151 °C to 168 °C. These results show that along with depressed melting points, melting ranges are broadened by degradation and branching. The average temperature differences within the melting ranges are as follows: X1 (ΔT=28 6 °C), X2 (ΔT=32 8 °C), X3 (ΔT=30.8 °C), and FINA (ΔT=25.5 °C)   Again, the broadening of the melting ranges for the X1 and X3 specimens are attributed to the degree of branching, while degradation by scission reactions and heat are responsible for the ranges of X2 and FINA, respectively

5.4.2   Equilibrium Melting Points

Tables 8 through 11, pages 103-106, give the DSC peak and return to baseline temperatures used to determine the equilibrium melting points given in figures 43 and 44   For reasons alluded to above, the first of the twinned peaks, when using peak height data, are used as the isothermally crystallized peaks in the determinations. The data clearly shows that degradation and branching have the effect of lowering the equilibrium melting points   The FINA had the highest melting point in both methods used, while the irradiated specimens' melting points decreased in the following order X2>X3>X1 (peak height data) and X3>X1>X2 (return to baseline data)   It is observed through studies of branched

polymers that the equilibrium melting points are depressed with branching frequency and oxidative degradation (Karbashewski et al , 1992, Yoshii et al., 1995) Nedkov and Krestev (1990) also observed a decrease in the melting point with increase in radiation dose The three irradiated samples have equilibrium melting points too close to one another to conclusively comment on the quantity of branches and degree of degradation related to each specimen It can only be speculated that the FINA sample has a lower melting temperature than ones reported in other studies of iPP, most probably due to thermal degradation and lower molecular weight The irradiated specimens' lower melting temperatures are a result of the varying degrees of branching and radiation induced degradation

5 4 3   Melting Studies from LDM

Tables 8 through 11, pages 103-106, give the end of melting temperatures (return to baseline) for all the specimens. ΔT_{LDM} (Initial and α peak) values are obtained by taking the difference of the LDM end of melting and DSC (Initial and α peak) values These values are in basic agreement with the ones taken by the DSC. The melting curves of the X2 and FINA specimens, figures 46 and 48, show a rise in light intensity for the specimens at certain crystallization temperatures. This is clearly the result of the melting of the crystals in the transverse directions, i e. epitaxial branching of the α modification When all these crystals have melted, the radially oriented crystals begin to melt, thus a decrease in the intensity curve is observed The crystals oriented in the transverse direction tend to have the effect of lowering the intensity because of their more

positive refractive nature. When these crystals melt, the observed light intensity becomes greater until all the crystals producing the lower birefringence have been melted. The subsequent decreasing in intensity after the epitaxially deposited crystals have melted out is due to the radially oriented crystals decreasing in number until all crystal structures have melted resulting in zero light intensity. With this, it is possible to calculate the percent of transversely oriented crystals remaining in a bulk sample at certain melting temperatures. Figure 57 details the method used and table 16 presents the data obtained from some of the melting curves.

The rise in light intensity is not observed in the X1 or X3 specimens, and in many of the X2 samples. Photographs of the crystal structures clearly show that the predominant modifications are of the mixed alpha type. It could be that the negative components of these spherulites "cancel out" the effects of the tangential, positive birefringent crystals. If this were the case, the negative and positive components in the crystals would have to melt simultaneously. The lack of the rise in the curves may also be due to branching affecting the crystallizing mechanism of the cross-hatching structure. The cause(s) behind the phenomenon of cross-hatching being observed in some X2 specimen and not the others, along with no patterns seen in the X1 and X3 specimen, is not at all clear and needs to be investigated further.

Melting Temperature (°C)
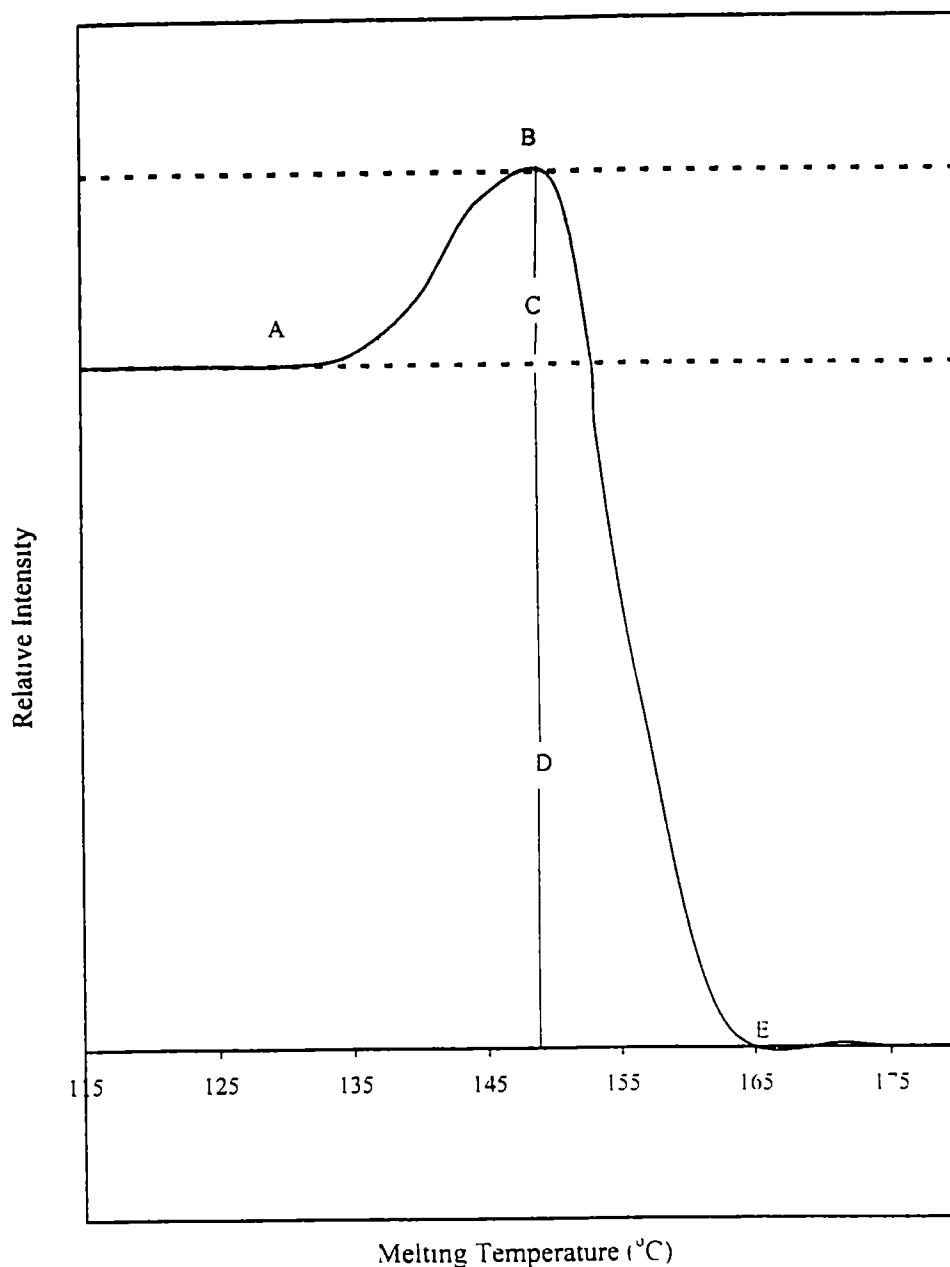
Figure 57: Typical melting curve showing the melting of transversly oriented lamellae. Point A is the beginning of melting and point B signifies the end of melting for these crystals. The area between points A and B is related to the amount of tangential lamella, decreasing as the curve increases. Lines C and D, added together, are related to the radially growing lamellae. Point E is the detectable end of melting point.

Table 16: Percent of crosshatched branching remaining at the indicated temperatures for some specimens at the given T_c

% Crosshatch Remaining	X2 T_c=120°C	X2 T_c=130°C	FINA T_c=125°C	FINA T_c=130°C	FINA T_c=135°C	FINA T_c=140°C
100	120.0 °C	130.0 °C	154 9 °C	154.8 °C	160.3 °C	145.2 °C
80	127.4 °C	133.3 °C	155 4 °C	158.3 °C	161 2 °C	150.1 °C
60	133.2 °C	136.7 °C	156.1 °C	160 9 °C	161 9 °C	156 0 °C
40	138.0 °C	139 2 °C	156.9 °C	161 8 °C	162 7 °C	158 7 °C
20	141.6 °C	141.9 °C	157 2 °C	162 6 °C	163 1 °C	163.0 °C
0	147 4 °C	148.0 °C	159 5 °C	165.1 °C	164.2 °C	168 6 °C

Chapter 6

<u>Conclusion</u>

The investigation of the structure, isothermal crystallization, and melting of three high melt strength isotactic polypropylenes prepared by electron beam irradiation, along with an untreated iPP, was conducted and has led to some interesting observations Through these observations a qualitative comparison of the samples as to the degree of degradation and branching was accomplished

Wide angle x-ray experiments were performed to determine what affects branching and degradation had on the structural integrity and degree of crystallization of the specimens. Although the predominant structure found was of the α modification, some β crystals were observed These were due to nucleating agent(s) used, and in the case of the untreated specimen, it was concluded that the modification was the result of stresses applied in the preparation of the specimen From transmission x-ray studies, the degree of irradiation was found to have no effect on the structure at the crystal lattice level. This was evident due to the intensities of the diffraction patterns matching the ones of normal patterns Intensity of peaks depends on the position of the chains in the unit cell. If these chains were not in the correct position, as determined by structural factor calculations using the unit cell indices, the peak intensity patterns would be different from the normally observed patterns.

Through the degree of crystallization obtained by WAXD it was concluded that as the branching increased the percent crystallinity decreased. This was a result of the amount of defects in the crystal. It was also noted that the increased "jagged" nature between individual x-ray patterns was a result of increased disorder resulting from degradation (thermal and radiation induced scission) and branching. It was also observed that some percentages at the lower T_c's could be in error, and thus disregarded. Since the patterns exhibited some degree of disorder, another method of percent crystallization determination might have produced more reliable results.

Crystallization studies showed that the amount of branching affected the rate of spherulitic growth in the radial direction. The increase of branching generally had a negative effect on primary nucleation, decreasing the nucleation density. Therefore, the time for impingement was greater making the half-times of crystallization longer. The growth geometry of the spherulite seemed to be affected by the degree of branching in that lower values were found as the branching increased.

Melting studies performed indicated a broadening of the melting range for the specimens with increased chain scissions and branching. The melting temperatures, along with the ranges, tended downward as compared to the un-irradiated specimen. It was thus concluded that the presence of branches on the linear backbone of the chains and increased amounts of chain scissions lowered the melting points. It was also concluded that another method of equilibrium melting point determination might have given more reliable results. It was clear

that the use of the end of melting to determine these points was not a dependable method, due to the amount of scattering of the points and the fact that only three points could be used to produce a reasonable trend line. Because of the branching effects on the crystal lamellae, the determination of the equilibrium melting points by the DSC peak method also showed considerable scatter, and, although more reliable than the end of melting determinations, may not have been as trustworthy a method for branched specimens.

The melting of tangentially oriented crystals was observed in some of the melting curves of the X2 specimens and almost all of the FINA samples studied. The melting could not be seen in the other treated specimens It was concluded that branching somehow interfered with the cross-hatching pattern seen in the alpha crystals and should be investigated further.

With the evidence presented, it was determined that the X2 specimen had the least amount of branching of the three specimens. It also suffered from oxidative degradation, as evidenced by the yellow discoloration. The X1 specimen was determined to have a greater amount of branching than the X2 sample, although less than the X3 material. This was proved by it having a degree of crystallinity less than the X2 specimen but greater than X3 Of all the treated specimens, the X3 sample, by far, had the greatest amount of branching as evidenced by the "after treatment" MFR values and its low percent crystallinity values found from x-ray studies. The lower melting points, crystallization times, Avrami constants, and lower, broader melting ranges indicated that chain scission degraded structures and branching were present However, these were not totally

conclusive in regards to the determination of degrees of branching and scissions, as all these parameters were too close to one another. Clearly these samples need to be characterized as to the amount and nature of the branching

Chapter 7

Suggestions for Further Study

7.1 Zero Shear Rate Viscosity, n_o

A material with a high value of zero shear rate viscosity, n_o, will generally exhibit a high melt strength As recalled, this property is dependent on the degree of branching and molecular weight distribution in that it increases with both Therefore, it can be determined which material will have the highest melt strength and would be more suitable in applications such as blow molding

7.2 Tensile Properties

Branching has been shown to affect the mechanical properties of polymers For example, the tensile strength and stiffness will decrease with increased branching iPP will show a decrease in modulus with increasing radiation dose below the gel point. By performing tensile tests it can be determined which specimens have been exposed to greater doses of electron beams and the effects irradiation has on the mechanical properties of the material.

7.3 Molecular Characterizations

A detailed study of weight-average molecular weight, molecular weight distribution, level of branching, and molecular shapes and sizes needs to be performed. The weight-average molecular weight and molecular shapes and sizes can be determined by small angle light scattering measurements To obtain the

molecular weight distribution, fractionation of the specimens may be achieved by temperature rising elution fractionation (TREF). The eluted fractions can be characterized by either IR or NMR methods. NMR methods are also effective in the determination of the level of branching

References

Addink E J , and Beintema J , *Polymer*, 2 (1962) 185.

ASTM Standards, Designation D 1238-98 (1998)

Avrami M , *J Chem Phys* , 7 (1939) 1103.

Avrami M , *J Chem. Phys* , 8 (1940) 212

Avrami M., *J Chem Phys* , 9 (1941) 177.

Bartczak Z , Galeski A , and Parcella M., *Polymer*, 27 (1986) 537.

Billmeyer F. W , Jr., "Textbook of Polymer Science, 2nd edition", Wiley-Interscience, New York, (1971).

Black R. M , and Lyons B J , *Nature*, 180 (1957) 1346

Black R. M., and Lyons B. J , *Proc. R Soc London*, A253 (1959) 322

Bogoeva-Gaceva G., Janevski A., and Grozdanov A., *J Appl Polym Sci* , 67 (1998) 395.

Boye C A , Jr , Watson M. T , and Patton H. W , *J Polym Sci* , 39 (1959) 534

Bradley M B., and Phillips E M , *Plast Eng* , March (1991) 82

Brady J M , and Thomas E L., *J Polym Sci* , B26 (1988) 2385.

Bruckner S., and Meille S V , *Nature*, 340 (1989) 455

Bruckner S., Meille S V , Sozzani P., and Giangiacomo T , *Makromol Chem , Rapid Commun* , 11 (1990) 55

Burfield D R , and Kashiwa N., *Makromol Chem* , 186 (1985) 2657

Calhoun L R , Thomas A. J., Shaffer H. L , Sullivan G M., and Williams C B , "Electron Beam Systems for Medical Device Sterilization", Titan Corp Publication (1999)

Chapiro A., "Radiation Chemistry of Polymeric Systems", Interscience Publishers, New York (1962)

Chapiro A , in "Irradiation of Polymers", Gould R. F (ed), ACS Publications, Washington, D C (1967).

Charlesby A , *J Polym Sci* , 17 (1955) 379

Charlesby A , in "Irradiation of Polymers", Gould R F (ed.), ACS Publications, Washington, D. C (1967).

Cheung L. K , Chul B. P., and Behravesh A H., *ANTEC '96*, (1996) 1941

Clark E. J., and Hoffman J. D., *Macromol.*, 17 (1984) 878.

Corradini P , De Rosa C., Guerra G , and Petraccone V , *Polym Commun* , 30 (1989) 281

Cullity B D , "Elements of X-Ray Diffraction, 2nd ed.", Addison-Wesley Publishing Company, Inc., Reading, MA, (1978).

DeNicola A. J., Galambos A F., and Wolkowicz M D , *ACSPMSE*, 67 (1992) 106

Friedlander G., Kennedy J W , and Miller J. M., "Nuclear and Radiochemistry, 3rd ed ", Wiley-Interscience, Inc., New York, (1981).

Fatou J G., *Europ Polym. J* , 7 (1971) 1057.

Geil P H , *J Appl Phys* , 33 (1962) 642

Geil P H , "Polymer Single Crystals", Krieger Publishing, Huntington, NY, (1973)

Godovsky Y. K , and Slonimsky G. L , *J. Polym Sci., Polym Phys Ed* , 12 (1974) 1053.

Gomez M A , Tanaka H , and Tonelli A. E., *Polymer*, 28 (1987) 2227

Hermans P. H , and Weidinger A , *Makromol Chem* , 44-46 (1961) 24

Hiemenz P. C., "Polymer Chemistry The Basic Concepts", Marcel Dekker, Inc , New York (1984)

Hikosaka M , and Seto T , *Polym J* , 2 (1973) 111.

Hoffman J. D., and Lauritzen J. L., Jr., *J Res NBS*, 65A (1961) 297

Hoffman J D , and Weeks J J , *J Res NBS*, 66A (1962) 13

Horng P., and Klemchuk P , *Plast Eng* , April (1984) 35

Hosemann R., *Acta Cryst* , 4 (1951) 520

Jacoby P , Bersted B. H., Kissel W. J., and Smith C. E , *J Polym Sci* , B24 (1986) 461.

Janimak J J., Cheng S Z D., Zhang A., and Hsieh E T , *Polymer*, 33 (1992) 728

Karbashewski E., Kale L., Rudin A , Tchir W. J., Cook D. G., and Pronovost J. O , *J Appl. Polym Sci* , 44 (1992) 425.

Kardos J.L., Christiansen A. W., and Baer E., *J Polym Sci , A-2*, 4 (1966) 777

Keith H D , Padden F. J., Jr., Walter N. M , and Wyckoff H. W., *J Appl Phys* , 30 (1959) 1485.

Khoury F , *J Res NBS*, 70A (1966) 29.

Kilb R W , *J Phys Chem* , 63, (1959) 1838

Klee D., Gribbin D., and Kirch D , *Angew Makromol Chem* , 131 (1985) 145

Kojima M , *Polym Lett* , 5 (1967) 245.

Kojima M., *J Polym. Sci , A-2*, 6 (1968) 1255.

Kondo M , and Dole M , *J Phys. Chem* , 70 (1966) 883.

Krestev V , Dobreva B , Krestev M , Minkova L., and Nedkov E., *Bulg J Phys* , 15 (1989) 265

Krigbaum W. R., and Uematsu I, *J Polym Sci* , A3 (1965) 767

Lacoste J., Vaillant D., and Carlsson D J., *J Polym Sci* , A31 (1993) 715.

Lambert W S , M S Thesis, University of Tennessee, Knoxville (1988)

Lauritzen J I , Jr and Hoffman J. D , *J Appl Phys* , 44 (1973) 4430

Leugering H J , *Makromol Chem* , 109 (1967) 204

Lotz B , Graff S., and Wittmann J C , *J Polym. Sci* , B24 (1986) 2017

Lotz B., and Wittmann J. C., *J Polym Sci* , B24 (1986) 1541.

Luongo J P , *J Appl Polym Sci* , 3 (1960) 302.

Magill J H , *Nature*, 187 (1960) 770.

Magill J H , *Polymer*, 2 (1961) 221

Marans N. S., and Zapas L. J , *J Appl Polym Sci* , 11 (1967) 705

McAllister P B., Carter T J., and Hinde R M., *J Polym Sci , Polym Phys Ed* , 16 (1978) 49

Meille S V., Brückner S , and Porzio W., *Macromol* , 23 (1990) 4114

Mencik Z , *J Macromol Sci , Phys* , B6 (1972) 101

Mezghani K , Campbell R. A , and Phillips P J., *Macromol* , 27 (1994) 997

Miller R. L , *Polymer*, 1 (1960) 135.

Miller R.L and Seeley E G , *J Polym Sci , Polym Phys Ed* , 20 (1982) 2297

Monasse B. and Haudin J M , *Colloid Polym Sci* , 263 (1985) 822

Montell Polyolefins, "High Melt Strength Polypropylene (HMS)", Montell Polyolefins Publication (1997).

Moore G. R and Kline D E., "Properties and Processing of Polymers for Engineers", Prentice-Hall, Inc., Englewood Cliffs, NJ, (1984)

Morrow D R , *J Macromol Sci , Phys* , B3 (1969) 53.

Morrow D. R. and Newman B. A., *J. Appl Phys* , 39 (1969) 4944

Natta G , *Nuovo Cimento, Suppl* , 15 (1960) 3.

Natta G and Corradini P , *Nuovo Cimento, Suppl* , 15 (1960) 9.

Natta G and Corradini P , *Nuovo Cimento, Suppl* , 15 (1960) 40

Natta G , Peraldo M , and Corradini P , *Rend Accad Naz Lincei*, 26 (1959) 14.

Nedkov E and Krestev V , *Colloid Polym Sci* , 268 (1990) 1028.

Nedkov E , Stoyanov A., and Krestev V , *Radiat Phys Chem* , 37 (1991) 299

Nikitina T S., Zhuravskaya E V , and Kuzminsky A S., "Effect of Ionizing Radiation on High Polymers", Gordon and Breach Science Publishers, Inc , New York (1963)

Nishimoto S., Kitamura K , Watanabe Y , and Kagiya T , *Radiat Phys Chem* , 37 (1991) 71.

Norton D R and Keller A., *Polymer*, 26 (1985) 704

Padden F. J and Keith H. D., *J Appl Phys*, 30 (1959) 1479

Padden F. J. and Keith H D., *J Appl. Phys*, 44 (1973) 1217.

Pae K D, *J Polym Sci, A-2*, 6 (1968) 657

Pae K D, Morrow D. R, and Sauer J A, *Nature*, 211 (1966) 514.

Phillips P. J, *ACSPMSE*, 20 (1979) 438.

Phillips P. J, *Rep Prog Phys*, 53 (1990) 549.

Phillips P J, Private Communication, University of Tennessee, Knoxville (1999)

Phillips P. J and Mezghani K, in " Polymeric Materials Encyclopedia",
      Salamone J C (ed.), CRC Press, Inc., Boca Raton (1996)

Phillips R, Private Communication, Montell Polyolefins (1999)

Rånby B. and Carstensen P., in "Irradiation of Polymers", Gould R F (ed), ACS
      Publications, Washington, D. C. (1967)

Ross G S and Frolen L. J, *J Nat Bur Std*, 79A (1975) 701.

Salovey R and Dammont F R., *J Polym Sci*, A1 (1963) 2155

Samuels R. J and Yee R. Y., *J Polym Sci., A-2*, 10 (1972) 385.

Sarcinelli L, Valenza A., and Spardaro G, *Polymer*, 38 (1997) 2307

Sauer J. A. and Pae K D, *J Appl Phys*, 39 (1968) 4959.

Scheve B J, Mayfield J W, DeNicola A J., Jr, United States Patent 4,916,198
      to Himont Inc. (1990)

Seymour R B, "Introduction to Polymer Chemistry", McGraw-Hill, Inc,
      New York (1971)

Shultz A R, Roth P I, and Rathmann G. B, *J Polym Sci*, 22 (1956) 495

Sperling L H., " Introduction to Physical Polymer Science, 2nd ed ", John Wiley
      and Sons, Inc., New York (1992)

Spruiell J. E., Private Communication, University of Tennessee, Knoxville (1999)

Spruiell J. E and Clark E S., *Methods Experm Phys*, 16B (1980) 1

Tidjani A and Watanabe Y., *J Appl Polym. Sci*, 60 (1996) 1839.

Tiganis B E, Shanks R A., and Long Y, *J Appl. Polym Sci*, 59 (1996) 663

Turner-Jones A., Aizlewood J M., and Beckett D. R., *Makromol Chem*, 75 (1964) 134

Turner-Jones A. and Cobbold A. J., *Polym Lett*, 6 (1968) 539

Vittoria V., Olley R H, and Bassett D C, *Colloid Polym Sci*, 267 (1989) 661

Wenxiu C. and Shui Y, *Radiat Phys Chem*, 42 (1993) 207

Williams J L. and Dunn T S., *Radiat Phys Chem*, 22 (1983) 209

Williams J L, Dunn T. S., and Stannett V. T., *Radiat Phys Chem*, 19 (1982) 291

Williams J L, Dunn T. S., Sugg H. and Stannett V. T., *Radiat Phys Chem*, 9 (1977) 445

Wilson J W., "Radiation Chemistry of Monomers, Polymers, and Plastics", Marcel Dekker, Inc, New York (1974)

Wunderlich B., "Macromolecular Physics. Volume 1", Academic Press, New York (1973).

Wunderlich B, "Macromolecular Physics Volume 2", Academic Press, New York (1976).

Yoshii F, Makuuchi K., Kikukawa S, Tanaka T, Saitoh J, and Koyama K, *J Appl Polym Sci*, 60 (1996) 617

Yoshii F, Meligi G., Sasaki T., Makuuchi K., Rabie A M., and Nishimoto S, *Polym Degrad Stab*, 49 (1995) 315

Zimm B H and Kilb R. W, *J Polym Sci*, 37 (1959) 19

<u>Vita</u>

Michael J. Trapp was born in Smithville, Tennessee on June 11, 1964. He graduated from DeKalb County (Tennessee) High School in May of 1982 He entered Middle Tennessee State University the following September, receiving his Bachelor of Science degree in Biology in 1986 and Bachelor of Science degree in Chemistry in 1991. He began his studies at the University of Tennessee, Knoxville in September 1996 and received his Master of Science degree in Polymer Engineering in August 2000